Optical Activity and Optical Anisotropy in Chiral Photomechanical Crystals Using Generalized High-Accuracy Universal Polarimeter

キラルフォトメカニカル結晶の Generalized High-Accuracy Universal Polarimeter による光学活性と光学的異方性

February 2017

Waseda University
Graduate School of Advanced Science and Engineering
Department of Advanced Science and Engineering,
Research on Life Science and Medical Bioscience

Akifumi TAKANABE
高鍋　彰文

Contents

Glossary

ρ	Optical rotatory power
ε	Permittivity
ε_0	Electric constant
ε_r	Dielectric constant in real part
$\Delta\varepsilon$	Molar circular dichroism
ω	Angular frequency
$\mathbf{k}$	Wavevector
θ	Azimuth angle of polarizer from an arbitrary origin
θ_0	Extinction position angle of polarizer from the arbitrary origin
θ'	Azimuth angle of polarizer from θ_0
Y	Azimuth angle of analyzer from the crossed Nicols position
δY	Error angle attributed to the displacement of the crossed Nicols configuration
Y'	Azimuth angle of analyzer from δY
λ	Wavelength
λ_j	Wavelength of transition from the ground state to the excited state j
C	Capacitane
c	Concentration of a solution
S	Area of a crystal surface
d	Thickness of a sample
V	Volume
F	Farads
T	Temperature
T_c	Temperature of phase transition
p	Systematic error originating from parasitic ellipticity of polarlizer
q	Systematic error originating from parasitic ellipticity of analyzer
I	Intensity of transmitted light

I_0 Intensity of incident light

Γ The ratio of I and I_0

N Difference of θ_0 from its absolute value

n Refractive index

m Absorption coefficient

Δ Phase difference

Δ_r Recorded phase difference

E Total linear dichroism

k Ellipticity of the eigen polarization derived from circular birefringence

k' Ellipticity of the eigen polarization derived from circular dichroism

μ Absorbance coefficient

$\Delta\mu$ Absorbance difference between right and left circularly polarized light

α Specific optical rotation

g Dissymmetry parameter

Chapter 1

General Introduction

1.1 Photochromism

Photochromism is defined as a reversible photoisomerization between two chemical species that have different colors (Figure 1.1). Fritsche first reported photochromism in tetracene compound in 1867[1] and since then, there have been a large number of studies on photochromic crystals. Photochromism is a fascinating phenomenon due to its potential applications in photochromic ophthalmic lenses[2], photooptical switching,[3] optical memory,[4] nonlinear optics,[5] displays,[6] and so on.

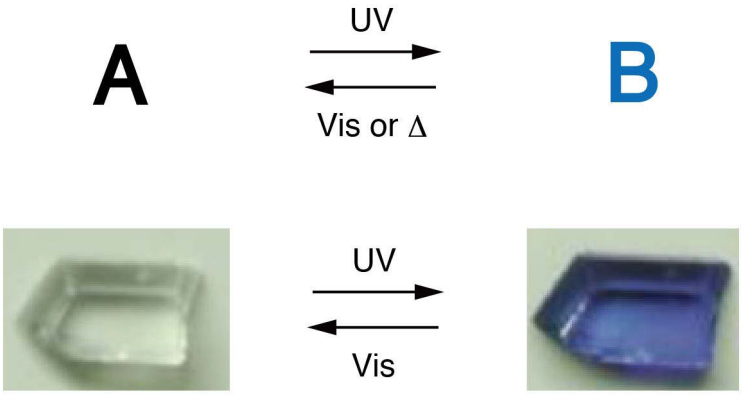

Figure 1.1. Reversible photochromic reaction and photochromism in a single crystal. Crystal photographs of this Figure is adapted with permission from "Photochromism of Diarylethene Molecules and Crystals: Memories, Switches, and Actuators" by Irie, M. Fukaminato, T.; Matsuda, K.; Kobatake, S. *Chemical Reviews* **2014**, 114, 12174–12277.[7] Copyright 2014 American Chemical Society.

1.2 Photomechanical Crystals*

Photomechanical motion in a single crystal is one of the functions of photochromism; specifically, photomechanical crystals show light-driven macroscale mechanical motion in a single crystal. Upon photoirradiation, molecular conformation or arrangement changes in the crystalline phase that occur through the excited state lead to macroscale mechanical motion. Photomechanical motion in crystals is a fascinating phenomenon from the viewpoint of both basic research and potential applications. Photomechanical motion involves the direct conversion of light energy to mechanical energy; thus, photomechanical crystals are beneficial for energy conversion. Such mechanical crystals can be operated by light irradiation without wire connections. For example, Irie et al. reported reversible photomechanical bending in rod-shaped diarylethene crystals.[8] Similarly, Bardeen et al. reported reversible and irreversible shape changes in rod-shaped anthracene nanocrystals.[9]

In the last decade, an increasing number of studies on the photomechanical motion of crystals, have broadened the scope of the field to examine various photomechanical crystals such as diarylethenes,[10–12] anthracenes,[13–15] azobenzenes,[16,17] furylfulgides,[18] salicylideneanilines,[19] 4-chlorocinnamic acid,[20] benzylidenedimethylimidazolinone,[21] 1,2-bis(4-pyridyl)ethylene salt,[22] and naphthalene diimides,[23] (Figures 1.2 and 1.3). Recently, reviews[7, 24–26] and a book[27] on photomechanical crystals have also been published. The development of new mechanical crystals with various characteristics is required to ensure that they meet their wide application potential as synthetic molecular machinery[28].

* This Section is partly reproduced with permission from "Optical Activity and Optical Anisotropy in Photomechanical Crystals of Chiral Salicylidenephenylethylamines" by Takanabe, A; Tanaka, M.; Johmoto, K.; Uekusa, H.; Mori, T.; Koshima, H.; Asahi, T. *Journal of the American Chemical Society* **2016**, *138*, 15066–15077.[29] Copyright 2016 American Chemical Society. Consent from all authors has been secured.

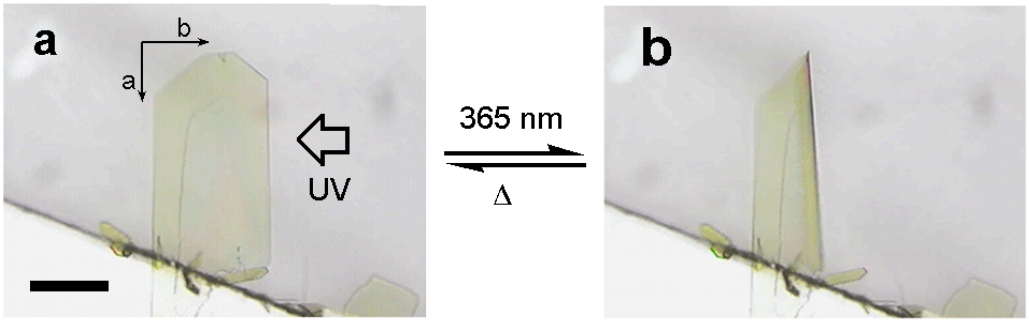

Figure 1.2. Photomechanical bending of azobenzene crystal (a) before and (b) after ultraviolet (UV) irradiation from the right rear. The scale bar is 200 μm. Reprinted with permission from "Mechanical Motion of Azobenzene Crystals upon Photoirradiation" Koshima, H. Ojima, N. and Uchimoto, H. *Journal of the American Chemical Society* **2009**, *131*, 6890–6891.[16] Copyright 2009 American Chemical Society.

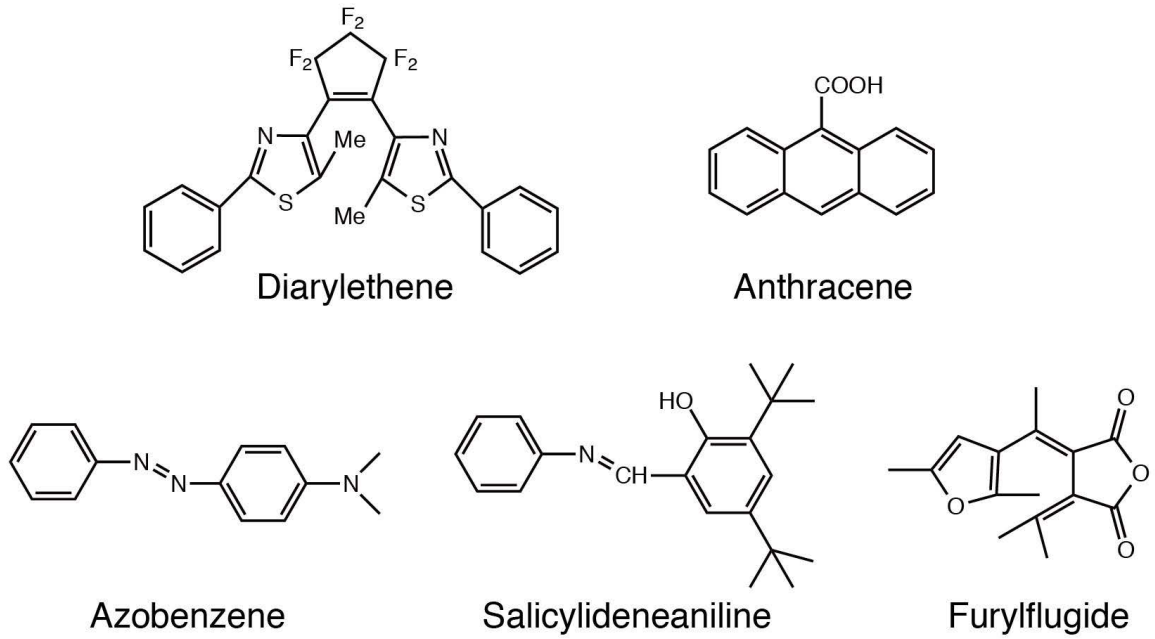

Figure 1.3. Typical photochromic compounds which show photomechanical bending in crystalline state.[8,9,16,18,19]

Chiral crystals usually show different photoreactivities from achiral crystals. The chiral environment is retained during reactions, and the motion of molecules is restricted in the crystal lattice.[30] Further, there have been reports of photoinduced twisting motions of chiral diarylethene crystals in a left- and right-handed helical manner.[12b] Taniguchi et al. demonstrated that the chiral crystals of azobenzene derivatives exhibited photomechanical bending with twisting, while the racemic crystals bent very slightly without twisting. Such findings show that the photomechanical behavior of chiral crystals differs from that of racemic crystals (Figure 1.4).[31] Despite the fact that the plate-like chiral crystals of salicylidenephenylethylamines [enol-(*S*)-**1** and enol-(*R*)-**1**] (Scheme 1.1) exhibit photomechanical bending similar to that of the racemic crystals [enol-(*rac*)-**1**], the durability of repeated bending and physical properties, such as Young's modulus and stress, differ between the chiral and racemic crystals. Specifically, the Young's moduli are 0.76 GPa [enol-(*S*)-**1**] and 2.60 GPa [enol-(*rac*)-**1**], and the stress values are 0.68 MPa [enol-(*S*)-**1**] and 1.81 MPa [enol-(*rac*)-**1**].[32] The introduction of chirality is beneficial to increase diversification in photomechanical crystals.

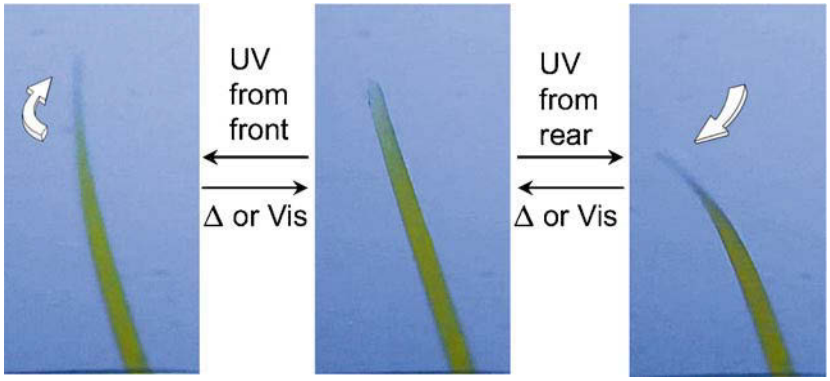

Figure 1.4. Photomechanical bending with twisting of chiral azobenzene crystal. Reprinted with permission from "Mechanical Motion of Chiral Azobenzene Crystals with Twisting upon Photoirradiation" Taniguchi, T.; Fujisawa, J.; Shiro, M.; Koshima H.; Asahi, T. *Chemistry—A European Journal* **2016**, *22*, 7950–7958.[31] Copyright 2016 John Wiley & Sons, Inc.

Scheme 1.1. Photoinduced hydrogen transfer reaction of salicylidenephenylethylamines enol-(*S*)-**1** and enol-(*R*)-**1**. Reprinted with permission from "Optical Activity and Optical Anisotropy in Photomechanical Crystals of Chiral Salicylidenephenylethylamines" by Takanabe, A; Tanaka, M.; Johmoto, K.; Uekusa, H.; Mori, T.; Koshima, H.; Asahi, T. *Journal of the American Chemical Society* **2016**, *138*, 15066–15077.[29] Copyright 2016 American Chemical Society.

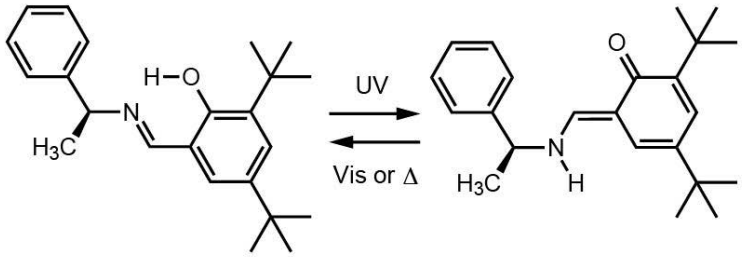

enol-(*S*)-**1** *trans*-keto-(*S*)-**1**

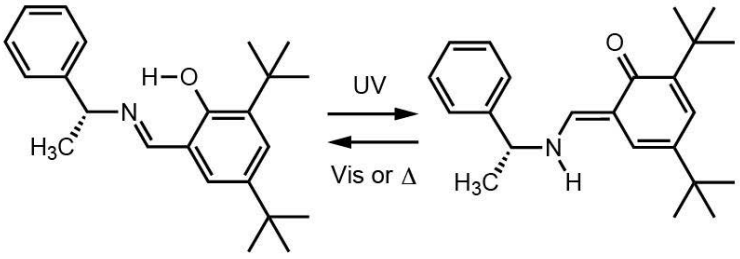

enol-(*R*)-**1** *trans*-keto-(*R*)-**1**

1.3 Chiroptical and Optical Anisotropic Properties of Single Crystals †

Every chiral organic crystal has inherent optical activity, exhibiting the chiroptical properties of circular birefringence (CB) and circular dichroism (CD).[33] CB is defined as the refractive difference between two crossed circularly polarized lights. In chemistry, optical rotatory power[33] (ORP; ρ, degree per 1 mm thickness) is used instead of CB (Figure 1.5). CD is defined as the absorption coefficient difference between two crossed circularly polarized lights. Moreover, many chiral and achiral crystals have optical anisotropy, such as linear birefringence (LB) and linear dichroism (LD). LB is defined as the refractive difference between two crossed linearly polarized lights and LD is defined as the absorption coefficient difference between two crossed linearly polarized lights.

From the viewpoint of electromagnetics, LB, LD, CB, and CD are defined by the second rank permittivity tensor:[34]

$$\epsilon_{\mathrm{ij}}(\omega,\mathbf{k}) = \epsilon'^{sym}_{ij}(\omega,\mathbf{k}) + \epsilon'^{an}_{ij}(\omega,\mathbf{k}) + i\left[\epsilon''^{sym}_{ij}(\omega,\mathbf{k}) + \epsilon''^{an}_{ij}(\omega,\mathbf{k})\right], \qquad (1.1)$$

where the superscripts *sym* and *an* represent the symmetric and antisymmetric components of $\varepsilon_{\mathrm{ij}}$, respectively; and the single and double primes represent the real and imaginary parts of $\varepsilon_{\mathrm{ij}}$, respectively; ω and $\mathbf{k}$ represent angular frequency and wavevector, respectively; and $\epsilon'^{sym}_{ij}(\omega,\mathbf{k})$, $\epsilon'^{an}_{ij}(\omega,\mathbf{k})$, $i\epsilon''^{sym}_{ij}(\omega,\mathbf{k})$, and $i\epsilon''^{an}_{ij}(\omega,\mathbf{k})$ represent LB, CD, LD, and CB, respectively. The second rank permittivity tensor depends on the ω, which means that the wavelength dependences of LB, LD, CB, and CD are informative. Moreover this tensor also depends on $\mathbf{k}$ (spatial dispersion[35,36]), which means that the measurement of LB, LD, CB, and CD along one specific direction, such as the crystal axis of a single crystal, is informative for relating these four optical properties to the molecular arrangement in a single crystal.

---

†This Section is partly reproduced with permission from "Optical Activity and Optical Anisotropy in Photomechanical Crystals of Chiral Salicylidenephenylethylamines" by Takanabe, A; Tanaka, M.; Johmoto, K.; Uekusa, H.; Mori, T.; Koshima, H.; Asahi, T. *Journal of the American Chemical Society* **2016**, *138*, 15066–15077.[29] Copyright 2016 American Chemical Society. Consent from all authors has been secured.

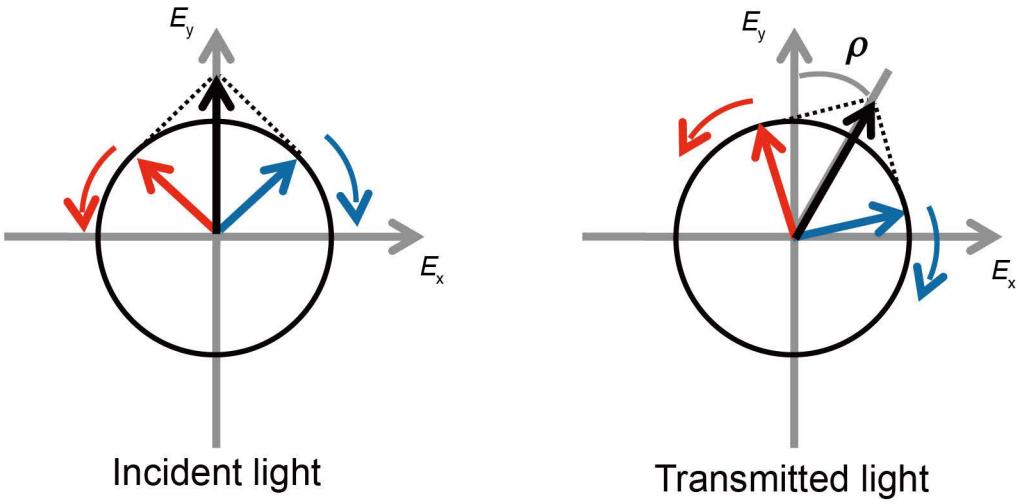

Figure 1.5. CB (ORP, ρ). The polarization direction of linearly polarized light is tilted after passing through a chiral medium. The polarization direction of linearly polarized light (black) from the viewpoint of an observer is composed of an addition of the right circularly polarized light (blue) and the left circular polarized light (red).

The simultaneous measurement of LB, LD, CB, and CD is necessary for evaluating the optical responses of chiral photomechanical crystals; however, such simultaneous measurement is extremely difficult to conduct. The CB and CD signals are overwhelmed by the LB and LD signals because the latter are 10^2–10^3 times larger than the former.[37] Hence, conventional polarimeters and CD spectrophotometers cannot be applied to accurately measure CB and CD, except in one specific case: along the optic axis.

The high-accuracy universal polarimeter (HAUP) was developed in 1983[38] to measure the LB and CB of various crystals, such as glutamic acid[39] and chiral cocrystals.[40] In the HAUP method, transmitted light intensities passing through a polarizer, sample, and then analyzer are measured as a quadratic function of the azimuth angles of the polarizer from an arbitrary origin (θ) and the analyzer from the crossed Nicols position (Y; Figure 1.6). The HAUP method has been extended to be used in the measurement of anisotropic colored materials, and has made possible the simultaneous measurement of LB and CB, as well as LD and CD.[41–45] Recently, the HAUP apparatus was generalized using a conventional Xe lamp and a monochromator to obtain ultraviolet (UV) and visible region spectra (300–680 nm).[46] The generalized HAUP (G-HAUP) was then applied to intercalated $K_4Nb_6O_{17}$ crystals with an azobenzene derivative,[46] and to laminated collagen membranes.[47] Chapter 3 describes the detailed principles of the HAUP method.

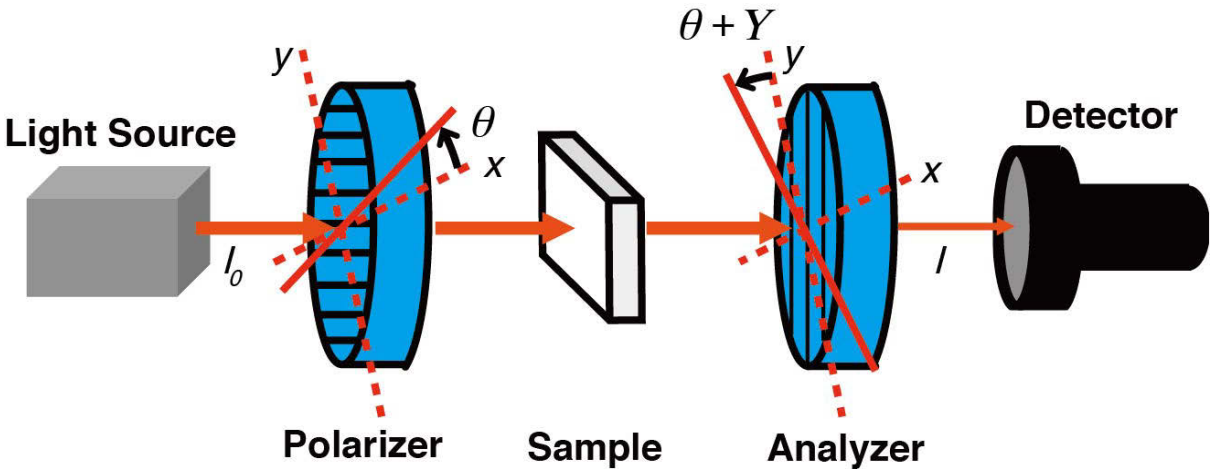

Figure 1.6. Optical system of high-accuracy universal polarimeter. Here, θ represents the azimuth angle of polarizer from an arbitrary origin and Y represents the deflecting angle of analyzer from the crossed Nicols position.

1.4 Scope of This Thesis

In Sections 1.1–1.3, I describe the importance of the measurement of the optical activity (CB, CD) and optical anisotropy (LB, LD) of chiral photomechanical crystals which show unique photomechanical motion, such as bending with twisting, upon UV irradiation. It is critically important to research the correlation between changes in the optical properties and changes in the crystal structures, accompanied by reaction in the chiral crystals. The purpose of this thesis is to simultaneously measure the chiroptical and optical anisotropic properties of chiral photomechanical crystals using G-HAUP before and under UV irradiation, and to relate these properties to the crystal structure. In order to accomplish this purpose, I investigated photomechanical motion, crystal structure, and the chiroptical and optical anisotropic properties of chiral photomechanical salicylidenephenylethylamine crystals (Scheme 1.1). I chose chiral salicylidenephenylethylamine crystals for my thesis because sufficient thin, wide, plate-like single crystal can be grown by gentle sublimation to enable HAUP measurements. The present thesis is the first study of the chiroptical properties of chiral photomechanical crystals, and changes in the chiroptical and optical anisotropic properties accompanied by reaction in chiral photomechanical crystals. By investigating optical activity and optical anisotropy using G-HAUP, a new useful strategy for the diversification of mechanical motion can be developed.

This doctoral thesis consists of 5 chapters. In Chapter 1, as a general introduction I describe the backgrounds of photochromism, photomechanical motion in a single crystal, the chiroptical and optical anisotropic properties of single crystals, and the scope of this thesis. In Chapter 2, I describe the photomechanical bending with twisting found in plate-like chiral enol-(*S*)-**1** crystal. Although photomechanical bending motions in plate-like enol-(*S*)-**1** and enol-(*R*)-**1** crystals have been already reported,[31] the twisting motion has not been reported due to the high aspect ratio (7:1) of plate-like crystals. Based on the calculated crystal

structure of enol-(*S*)-**1** and *trans*-keto-(*S*)-**1**, I propose a possible mechanism of the photomechanical bending with twisting. I also describe a reversible single-crystal-to-single-crystal (SCSC) phase transition of enol-(*S*)-**1** crystal. In Chapter 3, I describe the chiroptical and optical anisotropic spectra of chiral photomechanical enol-(*S*)-**1** and enol-(*R*)-**1** crystals on the (001) face before and under continuous UV light irradiation simultaneously measured using G-HAUP. I also discuss the correlation between the four optical properties and the crystal structure. In Chapter 4, to overcome the problem of decreasing specimen thickness under UV irradiation during HAUP measurements described in Chapter 3, I describe the development of a fast, high-accuracy universal polarimeter using a charge-coupled device (CCD) spectrometer (CCD-HAUP) and its performance and application. Finally, in Chapter 5, I present a summary of the thesis contents.

1.5 References

(1) Fritsche, M. *Comp. Rend. Acad. Sci.* **1867**, *69*, 1035–1037.

(2) Crano, J. C.; Flood, T.; Knowles, D.; Kumar, A.; Gemert, B. V. *Pure Appl. Chem.* **1996**, *68*, 1395–1398.

(3) *Molecular Switches*, Feringa, B. L., Eds.: Wiley-VCH, Weinheim, 2001, Chapter 2.

(4) *Electron Transfer in Chemistry*, Prasanna de Silva, A., Eds.: Wiley-VCH, Weinheim, 2001, vol. 5, Chapter 7.

(5) Bechinger, C.; Ferrer, S.; Zaban, A.; Sprague, J.; Gregg, B. A. *Nature* **1996**, *383*, 608–610.

(6) Delaire, J. A.; Nakatani, K. *Chem. Rev.* **2000**, *100*, 1817–1846.

(7) Irie, M. Fukaminato, T.; Matsuda, K.; Kobatake, S. *Chem. Rev.* **2014**, *114,* 12174**–**12277.

(8) Kobatake, S.; Takami, S.; Muto, H.; Ishikawa, T.; Irie, M. *Nature* **2007**, *446*, 778–781.

(9) (a) Al-Kaysi, R.O.; Mueller, A.M.; Bardeen, C. J. *J. Am. Chem. Soc.* **2006**, *128*, 15938–15939. (b) Al-Kaysi, R.O.; Bardeen, C. J. *Adv. Mater.* **2007**, *19*, 1276–1280.

(10) (a) Kuroki, L.; Takami, S.; Yoza, K.; Morimoto, M.; Irie, M. *Photochem. Photobiol. Sci.* **2010**, *9*, 221–225. (b) Morimoto, M.; Irie, M. *J. Am. Chem. Soc.* **2010**, *132*, 14172–14178. (c) Terao, F.; Morimoto, M.; Irie, M. *Angew. Chem. Int. Ed.* **2012**, *51*, 901–904.

(11) Uchida, K.; Sukata, S.; Matsuzawa, Y.; Akazawa, M.; de Jong, J. J. D.; Katsonis, N.; Kojima, Y.; Nakamura, S.; Areephong, J.; Meetsma, A.; Feringa, B. L. *Chem. Commun.* **2008**, *3*, 326–328.

(12) (a) Kobatake, S.; Hasegawa, H.; Miyamura, K. *Cryst. Growth Des.* **2011**, *11*, 1223–1229. (b) Kitagawa, D.; Nishi, H.; Kobatake, S. *Angew. Chem. Int. Ed.* **2013**, *52*, 9320-9322. (c) Kitagawa, D.; Kobatake, S. *J. Phys. Chem. C* **2013**, *117*, 20887–20892. (d) Kitagawa, D.; Kobatake, S. *Photochem. Photobiol. Sci.* **2014**, *13*, 764–769.

(13) (a) Zhu, L.; Agarwal, A.; Lai, J.; Al-Kaysi, R. O.; Tham, F. S.; Ghaddar, T.; Mueller, L.; Bardeen, C. J. *J. Mater. Chem.* **2011**, *21*, 6258–6268. (b) Zhu, L.; Al-Kaysi, R. O.; Bardeen, C. J. *J. Am. Chem. Soc.* **2011**, *133*, 12569–12575.

(14) Kim, T.; Al-Muhanna, M. K.; Al-Suwaidan, S. D.; Al-Kaysi, R. O.; Bardeen, C. J. *Angew. Chem. Int. Ed.* **2013**, *52*, 6889–6893.

(15) Koshima, H.; Uchimoto, H.; Taniguchi, T.; Nakamura, J.; Asahi, T.; Asahi, T. *CrystEngComm* **2016**, *18*, 7305–7310.

(16) (a) Koshima, H.; Ojima, N.; Uchimoto, H. *J. Am. Chem. Soc.* **2009**, *131*, 6890–6891. (b) Koshima, H.; Ojima, N. *Dyes Pigm.* **2012**, *92*, 798–801.

(17) (a) Bushuyev, O. S.; Singleton, T. A.; Barrett, C. *J. Adv. Mater.* **2013**, *25*, 1796–8000. (b) Bushuyev, O. S.; Tomberg, A.; Friščić, T.; Barrett, C. J. *J. Am. Chem. Soc.* **2013**, *135*, 12556–12559. (c) Bushuyev, O. S.; Corkery, T. C.; Barret, C. J.; Friščić, T. *Chem. Sci.* **2014**, *5*, 3158–3164.

(18) Koshima, H.; Nakaya, H.; Uchimoto, H.; Ojima, N. *Chem. Lett.* **2012**, *41*, 107–109.

(19) Koshima, H.; Takechi, K.; Uchimoto, H.; Shiro, M.; Hashizume, D. *Chem. Commun.* **2012**, *47*, 11423–11425.

(20) Kim, T.; Zhu, L.; Mueller, L. J.; Bardeen, C. J. *CrystEngComm* **2012**, *14*, 7792–7799.

(21) Naumov, P.; Kowalik, J.; Solntsev, K. M.; Baldridge, A.; Moon, J.-S.; Kranz, C.; Tolbert, L. M. *J. Am. Chem. Soc.* **2010**, *132*, 5845–5857.

(22) Sun, J.-K.; Li, W.; Chen, C.; Ren, C.-X.; Pan, D.-M.; Zhang, J. *Angew. Chem. Int. Ed.* **2013**, *52*, 6653–6657.

(23) Matsunaga, Y.; Goto, K.; Kubono, K.; Sako, K.; Shinmyozu, T. *Chem. Eur. J.* **2014**, *20*, 7309–7316.

(24) Kim, T.; Zhu, L.; Al-Kaysi, R. O.; Bardeen, C. J. *ChemPhysChem* **2014**, *15*, 400–414.

(25) Naumov, P.; Chizhik, S.; Panda, K. M.; Nath, K. N.; Boldyreva, E. *Chem. Rev.* **2015**, *115*, 12440–12490.

(26) Abendroth, J. M.; Bushuyev, O. S.; Weiss P. S.; Barrett, C. J. *ACS Nano* **2015**, *9*, 7746–7768.

(27) *New Frontiers in Photochromism*, Irie, M., Yokoyama, Y., Seki, T., Eds.; Springer, Heidelberg, 2013, Chapters 1 and 2.

(28) Garcia-Garibay, M. A. *Angew. Chem., Int. Ed.* **2007**, *46*, 8945–8947.

(29) Takanabe, A; Tanaka, M.; Johmoto, K.; Uekusa, H.; Mori, T.; Koshima, H.; Asahi, T. *J. Am. Chem. Soc.* **2016**, *138*, 15066–15077.

(30) *Chiral Photochemistry*, Inoue, Y., Ramamurthy, V., Eds.; Marcel Dekker, New York, 2004, Chapters 11–14.

(31) Taniguchi, T.; Fujisawa, J.; Shiro, M.; Koshima H.; Asahi, T. *Chem. Eur. J.* **2016**, *22*, 7950–7958.

(32) Koshima, H.; Matsuo, R.; Matsudomi, M.; Uemura, Y.; Shiro, M. *Cryst. Growth Des.* **2013**, *13*, 4330–4337.

(33) Lowry, T. M.; *Optical Rotatory Power*; Dover Publications, New York, 1964.

(34) *Introduction to Complex Mediums for Optics and Electromagnetics*, Wieglhofer, W. S., Lakhtakia, A., Eds.: SPIE press, Bellingham, 2003, Chapter 26.

(35) Agranovich, V. M., Ginzburg, V.; *Crystal Optics with Spatial Dispersion, and Excitons*; Springer-Verlag Berlin Heidelberg, Berlin and Heidelberg, 1984, Chapter 4.

(36) Landau, L.D.; Pitaevskii, L.P.; Lifshitz, E.M.; *Electrodynamics of Continuous Media*, Butterworth-Heinemann, Oxford, 1984, 2nd Eds., Chapter XII.

(37) Nye, J. F.; *Physical Properties of Crystals*; Oxford University Express, 1985.

(38) Kobayashi, J.; Uesu, Y. *J. Appl. Cryst.* **1983**, *16*, 204–211.

(39) Asahi, T.; Utsumi, H.; Itagaki, Y.; Kagomiya, I.; Kobayashi, Z. *Acta Crystallogr.* **1996**, *A52*, 766–769.

(40) Koshima, H.; Nagano, M.; Asahi, T. *J. Am. Chem. Soc.* **2005**, *127*, 2455–2463.

(41) Kobayashi, J.; Asahi, T.; Sakurai, M.; Takahashi, M.; Okubo, K.; Enomoto, Y. *Phys. Rev. B* **1996**, *53*, 11784–11790.

(42) Moxon, J. R. L.; Renshaw, A. R. *J. Phys.: Condens. Matter* **1990**, *2*, 6807–6836.

(43) Moxon, J. R. L.; Renshaw, A. R.; Tebbutt, I. J. *J. Phys. D: Appl. Phys.* **1991**, *24*, 1187–1192.

(44) Dijkstra, E.; Meekes, H.; Kremers, M. *J. Phys. D: Appl. Phys.* **1991**, *24*, 1861–1868.

(45) Kremers, M.; Meekes, H. *J. Phys. D: Appl. Phys.* **1995**, *28*, 1212–1224.

(46) Tanaka, M.; Nakamura, N.; Koshima, H.; Asahi, T. *J. Phys. D: Appl. Phys.* **2012**, *45*, 175303 (8pp).

(47) Nakagawa, K.; Harper-Lovelady, H.; Tanaka, Y.; Tanaka, M.; Yamato, M.; Asahi, T. *Chem. Commun.* **2014**, *50*, 15086–15089.

Chapter 2

Photomechanical Motion of

Chiral Salicylidenephenylethylamine Crystals

2.1 Introduction

As described in Chapter 1, the introduction of chirality is beneficial to increase diversification in photomechanical crystals. I discovered that plate-like chiral crystals of enol-(*S*)-**1** (Scheme 1.1) exhibited photomechanical bending with twisting. Although photomechanical bending motions in plate-like enol-(*S*)-**1** and enol-(*R*)-**1** crystals have been already reported,[1] the twisting motion has not been reported due to the high aspect ratio (7:1) of the plate-like crystal. In this chapter, I describe this photomechanical bending with twisting. Based on the calculated crystal structure of enol-(*S*)-**1** and *trans*-keto-(*S*)-**1**, I propose a possible mechanism of the photomechanical bending with twisting. This part is reproduced with permission from "Optical Activity and Optical Anisotropy in Photomechanical Crystals of Chiral Salicylidenephenylethylamines" by Takanabe, A; Tanaka, M.; Johmoto, K.; Uekusa, H.; Mori, T.; Koshima, H.; Asahi, T. *Journal of the American Chemical Society* **2016**, *138*, 15066–15077.[2] Copyright 2016 American Chemical Society. Consent from all authors has been secured.

Additionally, I discovered the chiral enol-(*S*)-**1** crystal underwent a reversible SCSC phase transition. SCSC phase transition is defined as a micro-mutual transformation in crystal structure with no destruction of the crystal lattice. A reversible SCSC phase transition can occur when the changes in the molecular conformation and packing arrangement in the crystal are very small at the phase transition, so there are no cracks or breaks in the crystal. Hence, the reversible SCSC phase transition is a fascinating phenomenon. This reversible

SCSC phase transition is rare occurrence because it occurs between two enantiomorphic phases, which also mean noncentrosymmetric phases. The properties such as ferroelectricity, piezoelectricity, and second-order optical nonlinearlity are allowed in a noncentrosymmetric structure. In this chapter, I also describe the enantimorphic SCSC phase transition. Based on the crystal structure change, I propose a possible mechanism for the enantimorphic SCSC phase transition. This part is reproduced with a slight modification from "Reversible Single-Crystal-to-Single-Crystal Phase Transition of Chiral Salicylidenephenylethylamine" by Takanabe, A; Katsufuji, T.; Johmoto, K.; Uekusa, H.; Shiro, M.; Koshima, H.; Asahi, T. *Crystals* **2017**, *7*, 7,[3] which is an open access article distributed under the terms and conditions of the Creative Commons Attribution (CC-BY) license (http://creativecommons.org/licenses/by/4.0/). Copyright 2016 by the authors; licensee MDPI, Basel, Switzerland. Consent from all authors has been secured.

2.2 Experimental Section

2.2.1 Sample Preparation

The compounds enol-(*S*)-**1** and enol-(*R*)-**1** were synthesized according to a published protocol.[4] The melting points of both enol-(*S*)-**1** and enol-(*R*)-**1** were identical (92–93 °C). Thin, plate-like single crystals of enol-(*S*)-**1** and enol-(*R*)-**1** were prepared by sublimation at 10–20 °C below the melting points. Based on comparison with the plate-like bulk single crystals obtained by recrystallization from 2-propanol solution at room temperature within several days, the longitudinal direction was assigned to be along the *a* axis and the top surface was assigned to be the (001) face. For X-ray crystallographic analysis and dielectric measurements, several single crystals obtained by slow evaporation of the solution in 2-propanol were put into paraffin oil to wash them and were dried. Remaining crystals were used for differential scanning calorimetry.

2.2.2 Crystal Structure Calculations

Trans-keto-(*S*)-**1**: The skeleton of the *trans*-keto-(*S*)-**1** molecule was constructed from enol-(*S*)-**1** molecule[1] by applying the pedal-motion phenomenon (Scheme 1.1).[5,6] There were two torsional angle degrees of freedom for the constructed *trans*-keto-(*S*)-**1** molecule around the phenylethyl moiety. The angles were determined to achieve the maximum overlap of molecules of *trans*-keto-(*S*)-**1** and enol-(*S*)-**1** molecules; i.e., phenyl rings occupy the same plane and methyl group situates at almost the same place (Figure 2.1c). Such maximum overlap structure of two topochemical isomer molecules has been observed in crystals of photochromic salicylideneamines,[6] in which two isomers occupy the same site, showing a disordered structure. The molecular arrangement (molecular packing and space group) was also taken from the enol-(*S*)-**1** crystal, and thus the presumed crystal structure of *trans*-keto-(*S*)-**1** was constructed.

This crystal structure was optimized by dispersion-corrected density functional theory (DFT-D) calculations (PBE exchange-correlation function with Grimme-06 semi-empirical dispersion correction[7]) using CASTEP.[8] In the calculations, all atom positions and cell parameters were optimized (1,200 eV cut-off level).

Enol-(*S*)-**1**: To compare the *trans*-keto and enol structures in detail, the crystal structure of enol-(*S*)-**1** was also optimized, starting from the observed crystal structure,[1] using the same method as for the *trans*-keto-(*S*)-**1** crystal calculations.

2.2.3 Observation of Photomechanical Motion

Thin, plate-like enol-(*S*)-**1** crystals were prepared as described above and fixed to the tops of needles. UV-LED illuminator (UV-400, 365 nm, 50 mW; Keyence) was used to observe the photomechanical motions. Photomechanical motion videos were recorded using a digital high-speed microscope (VHX-5000; Keyence).

2.2.4 Differential Scanning Calorimetry

Differential scanning calorimetry (DSC) runs of enol-(*S*)-**1** crystals (6.58 mg) were recorded using a DSC8500 (Perkin Elmer) in the temperature range from 10 °C to –10 °C with a rate of 2 °C min^{-1} on cooling and heating under nitrogen at atmospheric pressure in aluminum crucibles with covers.

2.2.5 X-ray Crystallographic Analysis

10 ºC: Single-crystal X-ray diffraction data were collected at 10 °C with R-AXIS RAPID II (Rigaku) using Cu Kα radiation (λ = 1.54186 Å). Correction of absorption effects was performed with ABSCOR.[9] The initial structure was solved by direct methods with SHELXT 2014, and the structure was refined with SHELXL 2016. All hydrogen atom positions were calculated using the riding atom model. UV-LED illuminator (UV-400, 365 nm, 50 mW; Keyence) was employed to collect single-crystal X-ray diffraction data under UV irradiation.

–50 ºC: Single-crystal X-ray diffraction data were collected at –50 °C with R-AXIS RAPID II (Rigaku) using Cu Kα radiation (λ = 1.54186 Å). Correction of absorption effects was performed with NUMABS.[10] The initial structure was solved by direct methods with SHELXS 97, and the structure was refined with SHELXL 97. All hydrogen atom positions were calculated using the riding atom model.

2.2.6 Dielectric Measurements

The dielectric constant ε_r is defined by the equation below:

$$\varepsilon_r = \frac{Cd}{\varepsilon_0 S}, \tag{2.1}$$

where C is the capacitance, in F; S is the area of a crystal surface, in m^2; ε_0 is the electric constant ($\varepsilon_0 \approx 8.854\times10^{-12}$ Fm^{-1}); and d is the thickness of plate crystal, in m. The square plate crystal was fabricated by application of silver-based conductive paste on the (010) and $(0\bar{1}0)$ top surfaces. Capacitance was measured using a capacitance bridge (1kHz, AH 2550A; Andeen-Hagerling, Inc.). The (010) area and the thickness of the crystal were measured using a digital high-speed microscope (VHX-5000; Keyence).

2.3 Results and Discussion

2.3.1 Calculated Crystal Structures

The crystal structure of enol-(*S*)-**1** was already determined, but that of *trans*-keto-(*S*)-**1** was not yet successfully determined.[1] Hence, *in situ* crystallographic analyses were carefully performed under continuous UV irradiation to analyze the crystal structure of *trans*-keto-(*S*)-**1**. Because no disorder was found in the crystals, the crystal structure of *trans*-keto-(*S*)-**1** was calculated by DFT-D calculation (Figure 2.1b). The optimized crystal structure of enol-(*S*)-**1** using DFT-D (Figure 2.1a) belongs to the same space group ($P2_12_12_1$), and has similar geometrical features to the observed structure, in which intramolecular hydrogen bonds formed between the N atom of the C=N Schiff base and the H atom of the 2-OH group of the salicylaldehyde ring; the N···O distance and N···H–O angle are 2.520 Å and 152.82°, respectively. In the crystal structure of enol-(*S*)-**1** obtained from X-ray crystallographic analysis at 10 ºC, an intramolecular hydrogen bond is formed between the N atom of the C=N Schiff base and the H atom of the 2-OH group of the salicyl ring; the N···O distance is 2.591 Å and the N···H–O angle is 160.40°.

Comparing the calculated crystal structure of enol-(*S*)-**1** with that of *trans*-keto-(*S*)-**1**, changes in the unit cell dimensions were observed as shown in Table 2.1. The length of the *a* and *b* axes of the *trans*-keto-(*S*)-**1** unit cell decreased slightly (–3.70% and –3.32%, respectively) and the length of the *c* axis increased (+0.16%). This cell deformation tendency is same as that in the enol-(*S*)-**1** crystal before and under UV irradiation obtained from X-ray crystallographic analyses at 10 ºC (Table 2.2). Moreover, due to the slight shift of molecular position in the *trans*-keto-(*S*)-**1** crystals**,** I observed an N1···C10 distance of 3.262 Å and a C10···N1–H angle of 141.9°, indicating the formation of N–H···π interaction (Figure 2.1c). Therefore, the *a* and *b* axes contracted, and the *c* axis extended.

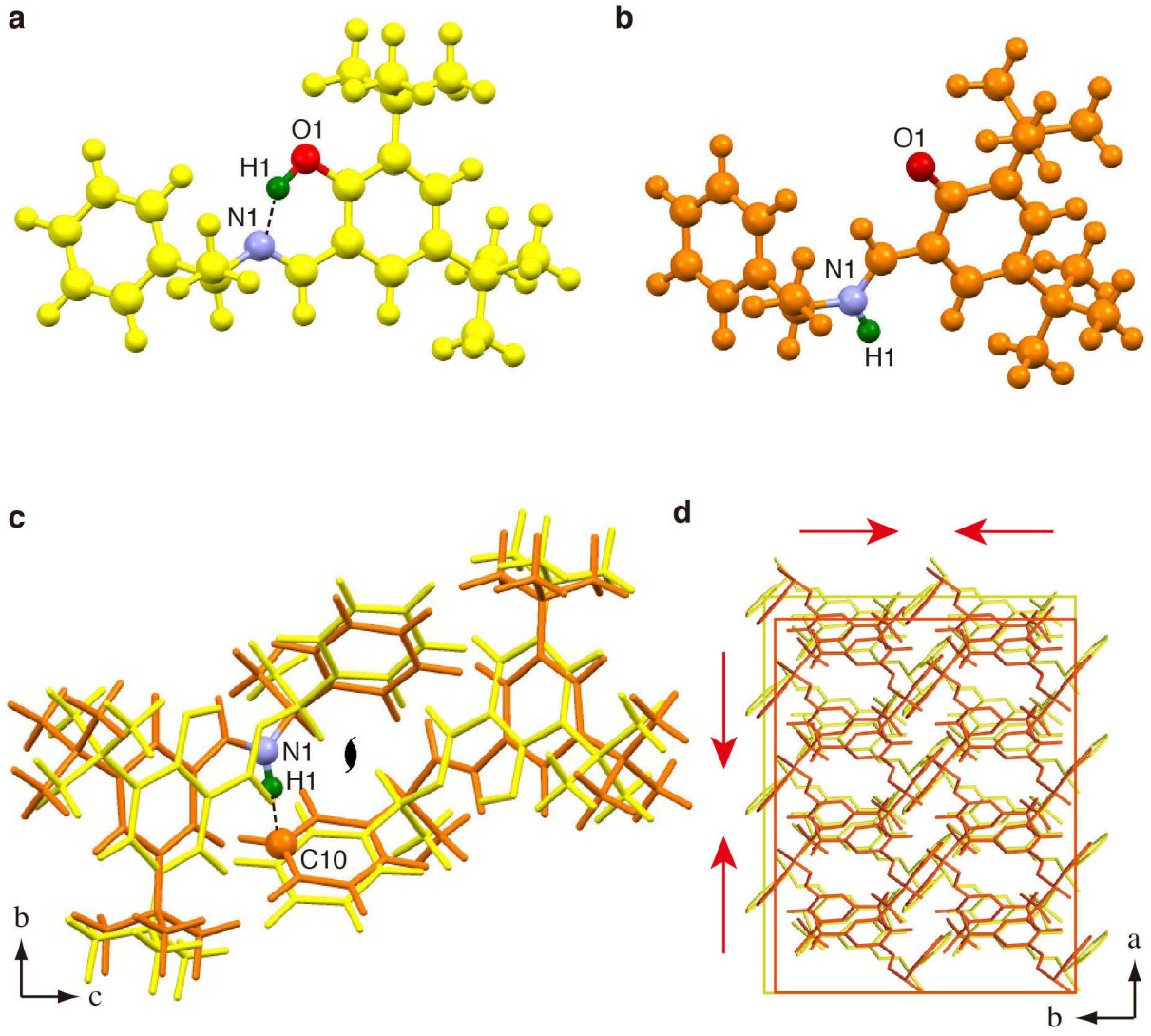

Figure 2.1. Crystal structures determined from DFT-D calculations: ball and stick drawings of (a) enol-(*S*)-**1** (yellow) and (b) *trans*-keto-(*S*)-**1** (orange). Overlaid molecular arrangements on (c) the (100), and (d) (00$\bar{1}$) face. The red arrows in (d) indicate the directions of the shrinkage of the *trans*-keto-(*S*)-**1** crystal along the *a* and *b* axis. Reprinted with permission from "Optical Activity and Optical Anisotropy in Photomechanical Crystals of Chiral Salicylidenephenylethylamines" by Takanabe, A; Tanaka, M.; Johmoto, K.; Uekusa, H.; Mori, T.; Koshima, H.; Asahi, T. *Journal of the American Chemical Society* **2016**, *138*, 15066–15077.[2] Copyright 2016 American Chemical Society.

Table 2.1. Unit cell sizes of enol-(*S*)-**1** and *trans*-keto-(*S*)-**1** crystals obtained from DFT-D calculation. Reprinted with permission from "Optical Activity and Optical Anisotropy in Photomechanical Crystals of Chiral Salicylidenephenylethylamines" by Takanabe, A; Tanaka, M.; Johmoto, K.; Uekusa, H.; Mori, T.; Koshima, H.; Asahi, T. *Journal of the American Chemical Society* **2016**, *138*, 15066–15077.[2] Copyright 2016 American Chemical Society.

	enol-(*S*)-**1**	*trans*-keto-(*S*)-**1**	relative change (%)
a (Å)	6.0802	5.8555	–3.70
b (Å)	9.6333	9.3134	–3.32
c (Å)	35.45346	35.5093	+0.16
volume (Å^3)	2076.5939	1936.4860	–6.75

Table 2.2. Unit cell sizes of enol-(*S*)-**1** crystal before and under UV irradiation obtained from X-ray crystallographic analyses at 10 ºC.

	before UV	under UV	relative change (%)
a (Å)	6.3058(4)	6.2948(3)	–0.17
b (Å)	9.8851(6)	9.8790(5)	–0.06
c (Å)	35.071(2)	35.1336(19)	+0.18
volume (Å^3)	2186.1(2)	2184.83(19)	–0.06

2.3.2 Bending Motion

Although a photomechanical bending of the plate-like crystals of enol-(*S*)-**1** was previously reported, a wide and thin plate-like microcrystal (354 μm long × 87 μm wide × 10 μm thick), prepared by slow sublimation was submitted for the observation of photomechanical motion. Figure 2.2a shows the frontal $(00\bar{1})$ face with the longitudinal direction along the *a* axis, of which the lower portion was fixed to the needle with an adhesive and the upper portion was free. The relationship between the crystal faces and the wide surfaces of both enantiomeric enol-**1** crystals was determined using single-crystal X-ray structure analysis (Figure 2.3). When the $(00\bar{1})$ face was irradiated from the front at 365 nm with a UV-LED illuminator (50 mW cm^{-2}), the crystal bent towards the light source with slight right-handed twisting (Figure 2.2b). Subsequent illumination with a pseudo-white LED lamp (broad bands at 465 and 560 nm) returned the bend and twist to the initial flat shape after 30 s. Irradiation of the (001) surface from the rear induced forward bending with a slight left-handed twist (Figure 2.2c). The repeatability of bending motion was already reported; alternating irradiation of the (001) face with UV and visible light caused a gradual decrease of the tip displacement angle (–15%) after 100 cycles.[1]

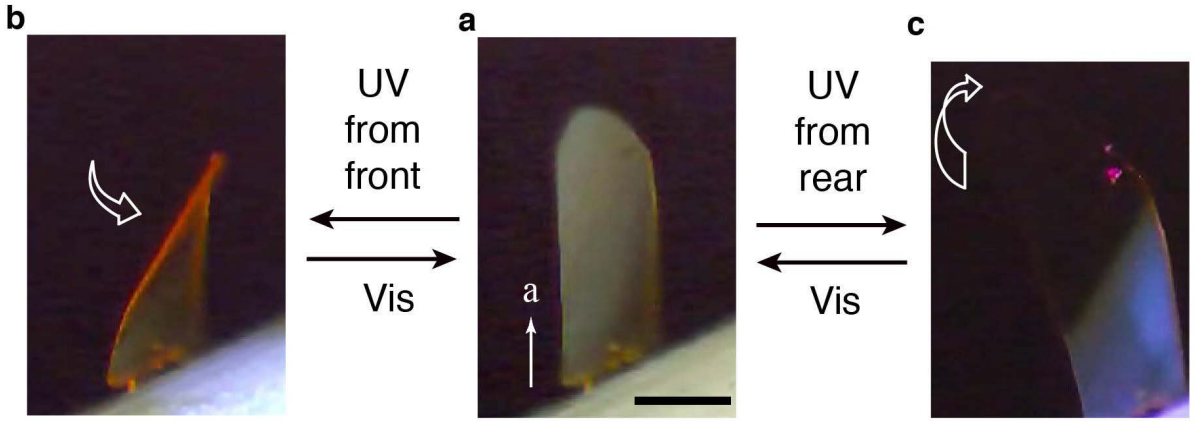

Figure 2.2. Bending with twisting motion of a wide and thin plate-like microcrystal of enol-(*S*)-**1** (a) before UV light irradiation and after irradiation from (b) the front and (c) the rear. The scale bar is 100 μm. Reprinted with permission from "Optical Activity and Optical Anisotropy in Photomechanical Crystals of Chiral Salicylidenephenylethylamines" by Takanabe, A; Tanaka, M.; Johmoto, K.; Uekusa, H.; Mori, T.; Koshima, H.; Asahi, T. *Journal of the American Chemical Society* **2016**, *138*, 15066–15077.[2] Copyright 2016 American Chemical Society.

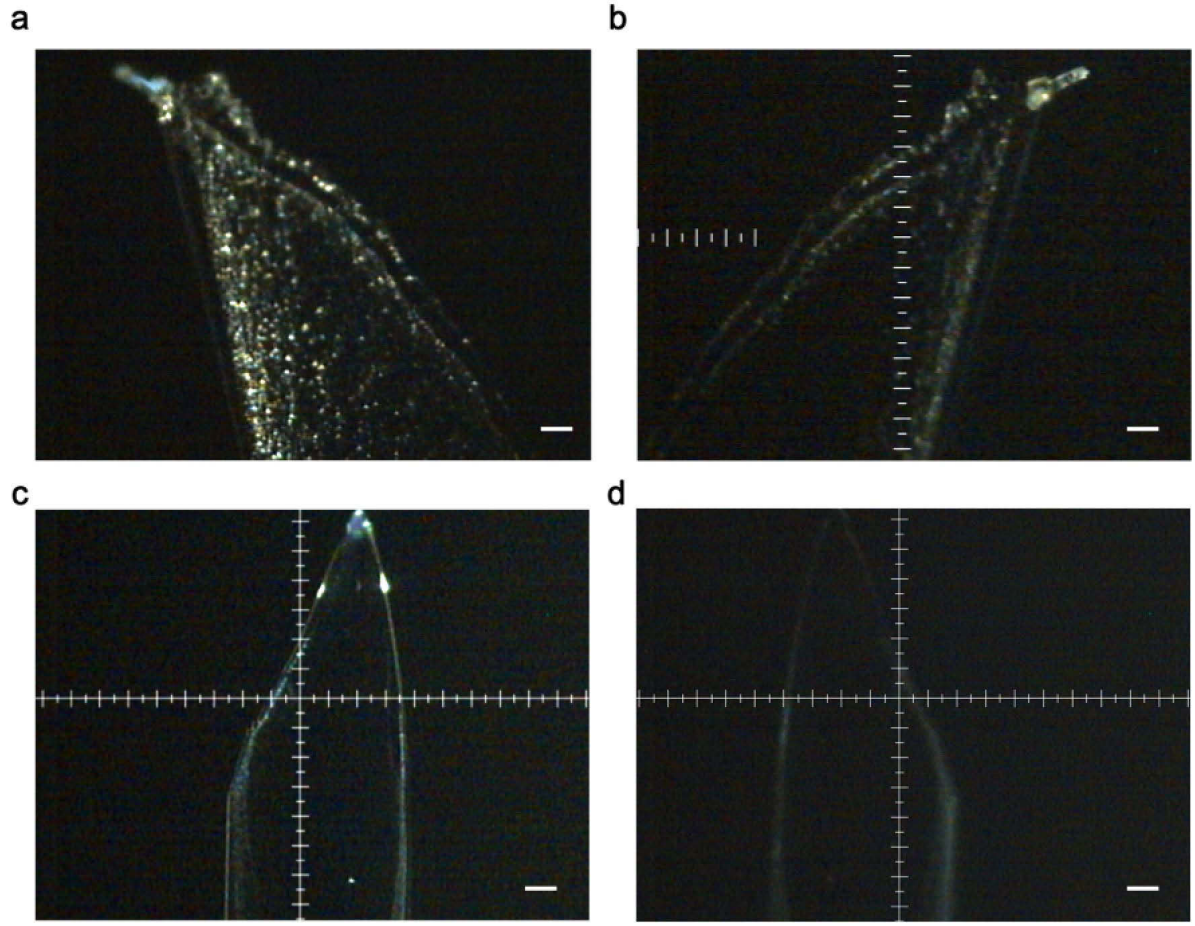

Figure 2.3. Crystal shapes of (a, b) enol-(*S*)-**1** and (c, d) enol-(*R*)-**1** crystal; the top surface (a, c) $(00\bar{1})$ face and (b, d) (001) face. All the faces were determined by using the single crystal X-ray structure analysis. The scale bars are 100 mm. Reprinted with permission from "Optical Activity and Optical Anisotropy in Photomechanical Crystals of Chiral Salicylidenephenylethylamines" by Takanabe, A; Tanaka, M.; Johmoto, K.; Uekusa, H.; Mori, T.; Koshima, H.; Asahi, T. *Journal of the American Chemical Society* **2016**, *138*, 15066–15077.[2] Copyright 2016 American Chemical Society.

2.3.3 Mechanism of Bending and Twisting Motion

I briefly explored a possible mechanism of the bending and twisting motion. An overlay of the molecular arrangements of the enol-(*S*)-**1** (yellow) and the *trans*-keto-(*S*)-**1** (orange) is shown in Figure 2.1d. On the $(00\bar{1})$ face, the molecules of enol-(*S*)-**1** are arranged in a twofold helical manner along the *a* axis to form a columnar structure. Upon UV irradiation of the $(00\bar{1})$ face, both the length and width along the *a* and *b* axes shrink near the front crystal surface due to photoisomerization to the *trans*-keto-(*S*)-**1** molecules. The contraction is considered to occur in the diagonal direction. In contrast, the length and width do not change at the back surface of the crystal, due to a lack of penetration of the irradiated light and no occurrence of photoisomerization. Hence the thin and wide plate-like crystal bends towards the light source with a twisting motion in a right-handed helix (Figure 2.4a). Conversely, UV irradiation of the (001) face causes bending with twisting in a left-handed helix (Figure 2.4b).

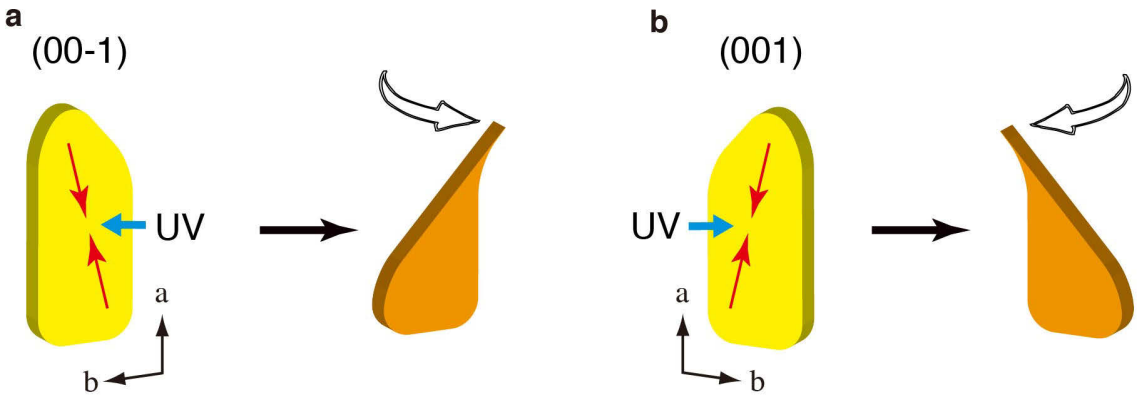

Figure 2.4. Relationship between the direction of twisting and the face of enol-(*S*)-**1** crystal irradiated with UV light: (a) twist in right-handed helix, (b) twist in left-handed helix. The red arrows indicate the directions of the shrinkage of the enol-(*S*)-**1** crystal along the diagonal of the *a* and *b* axes. Reprinted with permission from "Optical Activity and Optical Anisotropy in Photomechanical Crystals of Chiral Salicylidenephenylethylamines" by Takanabe, A; Tanaka, M.; Johmoto, K.; Uekusa, H.; Mori, T.; Koshima, H.; Asahi, T. *Journal of the American Chemical Society* **2016**, *138*, 15066–15077.[2] Copyright 2016 American Chemical Society.

2.3.4 Reversible Single-Crystal-to-Single-Crystal Phase Transition

DSC of enol-(*S*)-**1** was performed over the temperature range from 10 to −10°C at a rate of 2°C min^{-1} with cooling initially and then heating (Figure 2.5). Cooling the crystalline sample of enol-(*S*)-**1** had an exothermic peak at 2.2°C. The phase transition started at 2.7°C and ended at 0.1°C. Heating the crystalline sample of enol-(*S*)-**1** had an endothermic peak at 3.9°C. The reverse phase transition began at 3.6°C and ended at 4.8°C. The sharp shapes of these two peaks and the thermal hysteresis of 1.7°C reveal a first-order phase transition. The enthalpy at the exothermic and endothermic peaks was –0.69 and 0.67 kJ mol^{-1}, respectively.

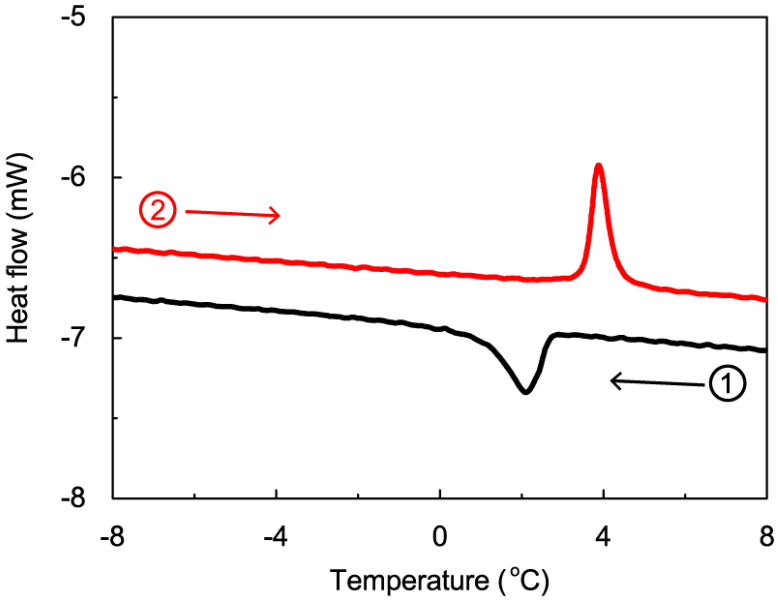

Figure 2.5. DSC curves of enol-(*S*)-**1** crystal on initial cooling and then heating. Reprinted from "Reversible Single-Crystal-to-Single-Crystal Phase Transition of Chiral Salicylidenephenylethylamine" by Takanabe, A; Katsufuji, T.; Johmoto, K.; Uekusa, H.; Shiro, M.; Koshima, H.; Asahi, T. *Crystals* **2017**, *7*, 7,[3] which is an open access article distributed under the terms and conditions of the Creative Commons Attribution (CC-BY) license (http://creativecommons.org/licenses/by/4.0/). Copyright 2016 by the authors; licensee MDPI, Basel, Switzerland.

Figure 2.6 shows the variable-temperature unit cell determination of enol-(*S*)-**1** using a single crystal over the temperature range from −50 to +50°C at 10°C intervals with initial heating and then cooling. The length of the *a* axis changed discontinuously between 0 and 10°C on heating and cooling; the differences were 0.06 and 0.07 Å, respectively (Figure 2.6a). Angle β also changed reversibly from 90° to 92° between 0 and 10°C on heating and cooling (Figure 2.6d). The length of the *c* axis and the volume did not change significantly between 0 and 10°C (Figures 2.6c and e). By contrast, the length of the *b* axis changed continuously on both heating and cooling (Figures 2.6b). The single crystal maintained its transparency without cracking after the heating and cooling cycles, revealing that the phase transition proceeded reversibly via a single crystalline state.

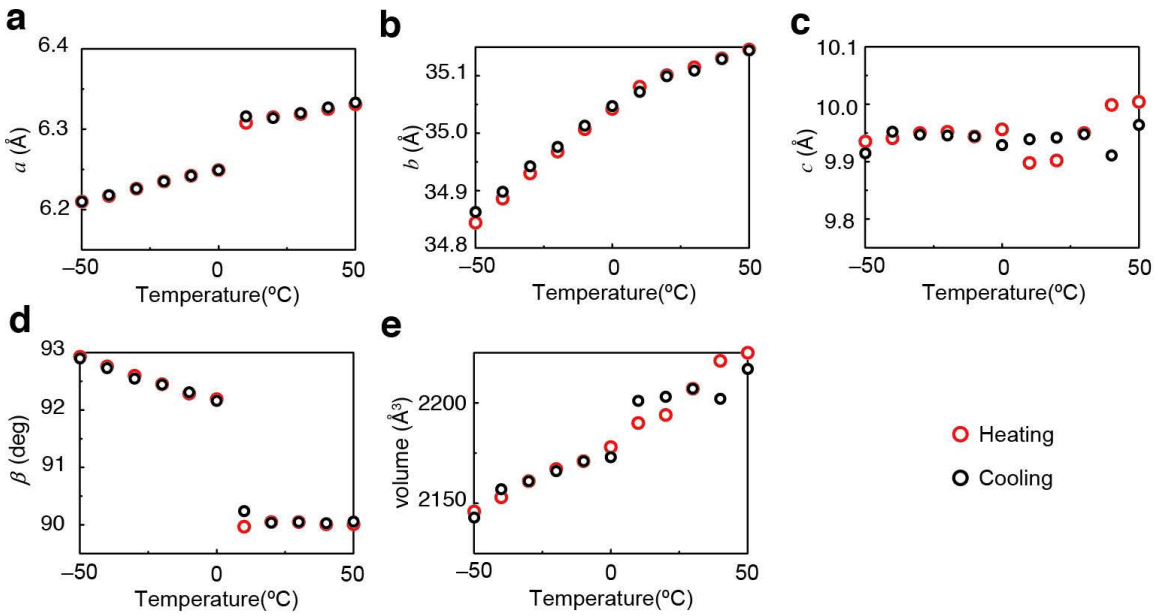

Figure 2.6. Temperature dependence of the lattice constants of enol-(*S*)-**1** single crystal on initial heating and then cooling; lengths of the (a) *a*, (b) *b*, and (c) *c* axes, (d) angle β, and (e) volume. Reprinted from "Reversible Single-Crystal-to-Single-Crystal Phase Transition of Chiral Salicylidenephenylethylamine" by Takanabe, A; Katsufuji, T.; Johmoto, K.; Uekusa, H.; Shiro, M.; Koshima, H.; Asahi, T. *Crystals* **2017**, *7*, 7,[3] which is an open access article distributed under the terms and conditions of the Creative Commons Attribution (CC-BY) license (http://creativecommons.org/licenses/by/4.0/). Copyright 2016 by the authors; licensee MDPI, Basel, Switzerland.

X-ray crystallographic analysis of enol-(*S*)-**1** was performed at 10°C and –50°C (Table 2.3). Note that the crystal axes of enol-(*S*)-**1** at 10°C in this section corresponds to those at –50 ºC so that the molecular conformation and molecular packing differences are easily observed. The enol-(*S*)-**1** crystal at 10°C belongs to in the orthorhombic space group $P2_12_12_1$, which is similar to the finding in a previous report.[1] The enol-(*S*)-**1** crystal at –50°C belongs to the monoclinic space group $P2_1$. After the phase transition by cooling, the lengths of the *a* and *b* axes decreased by –0.09927Å (–1.57%) and –0.2352Å (–0.67%), respectively, while that of the *c* axis increased by +0.04083Å (+0.41%). Overall, the volume decreased by –42.51Å^3 (–1.94%).

Table 2.3. Crystal data for enol-(*S*)-**1** crystals. Note that the crystal axes of enol-(*S*)-**1** at 10°C in this section corresponds to those at –50 ºC so that the molecular conformation and molecular packing differences are easily observed. Reprinted with a slight modification from "Reversible Single-Crystal-to-Single-Crystal Phase Transition of Chiral Salicylidenephenylethylamine" by Takanabe, A; Katsufuji, T.; Johmoto, K.; Uekusa, H.; Shiro, M.; Koshima, H.; Asahi, T. *Crystals* **2017**, *7*, 7,[3] which is an open access article distributed under the terms and conditions of the Creative Commons Attribution (CC-BY) license (http://creativecommons.org/licenses/by/4.0/). Copyright 2016 by the authors; licensee MDPI, Basel, Switzerland.

temperature (°C)	10	–50
crystal system	orthorhombic	monoclinic
space group	$P2_12_12_1$	$P2_1$
a (Å)	6.3058(4)	6.20653(11)
b (Å)	35.071(2)	34.8358(7)
c (Å)	9.8851(6)	9.92593(18)
β (deg)	90	92.7570(10)
volume (Å^3)	2186.1(2)	2143.59(7)
Z	4	4
ρ_{calc} (g cm^{-3})	1.025	1.046
R_1 [I > 2 σ (I)]	0.0681	0.0475
GOF	1.052	1.030

Figure 2.7 shows the Oak Ridge Thermal Ellipsoid Plot (ORTEP) drawings and molecular conformations of the enol-(*S*)-**1** crystals at 10 and –50 ºC. There is one crystallographically independent molecule (A) in the enol-(*S*)-**1** crystal at 10 ºC (Figure 2.7a); the 5-*tert*-butyl group (brown color) is disordered in the 0.217 occupancy. The enol-(*S*)-**1** crystal at –50 ºC consists of two crystallographically independent molecules (B and C) in the asymmetric unit (Figures 2.7b and c). The 5-*tert*-butyl groups (brown color) of both molecules are disordered in the 0.229 (B) and 0.245 (C) occupancies, respectively.

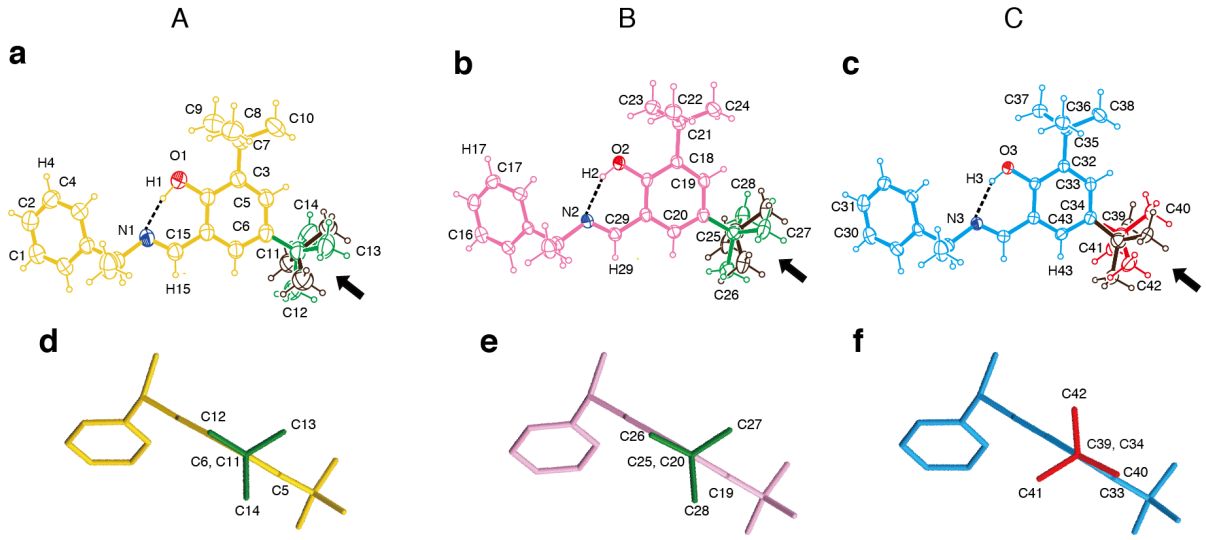

Figure 2.7. ORTEP drawings (a–c) at the 25% probability level, and the molecular conformations (d–f) of enol-(*S*)-**1** crystals at 10 and –50 ºC: (a, d) A molecule at 10 ºC, (b, e) B, and (c, f) C molecules at –50 ºC. The 5-*tert*-butyl groups (blown color) are disordered in the 0.217 (A), 0.229 (B), and 0.245 (C) occupancies, respectively. The viewpoints of molecular conformations of the 5-*tert*-butyl groups are displayed in the ORTEP drawings as black solid arrow. The disordered 5-*tert*-butyl groups in minor occupancies and all hydrogen atoms in d–f are omitted for clarity. Reprinted with a slight modification from "Reversible Single-Crystal-to-Single-Crystal Phase Transition of Chiral Salicylidenephenylethylamine" by Takanabe, A; Katsufuji, T.; Johmoto, K.; Uekusa, H.; Shiro, M.; Koshima, H.; Asahi, T. *Crystals* **2017**, *7*, 7,[3] which is an open access article distributed under the terms and conditions of the Creative Commons Attribution (CC-BY) license (http://creativecommons.org/licenses/by/4.0/). Copyright 2016 by the authors; licensee MDPI, Basel, Switzerland.

In molecule A at 10 ºC, an intramolecular hydrogen bond is formed between the N atom of the C=N Schiff base and the H atom of the 2-OH group of the salicyl ring (black dotted line in Figure 2.7a); the N···O distance is 2.591 Å and the N···H–O angle is 160.40°. In molecules B and C at –50 ºC, similar intramolecular hydrogen bonds (black dotted lines in Figures 2.7b and c) are formed with N···O distances of 2.596 and 2.591 Å and N···H–O angles of 148.67° and 148.94°, respectively.

The dihedral angle between the phenyl and salicyl plane in molecule A at 10 ºC is 41.06º. The corresponding dihedral angles increase slightly to 46.82° and 43.97° in the B and C molecules at –50 ºC, respectively. The analogous salicylideneaniline crystals can cause a photochromic reaction when the dihedral angle between the phenyl and salicyl planes exceeds 30°.[11] Therefore, the enol-(*S*)-**1** crystal at –50 ºC should also have a photochromic nature to the *trans*-keto-form with UV irradiation.

The most significant change in the molecular conformation with the phase transition is that the 5-*tert*-butyl group (red color) of molecule C (Figure 2.7f) in the enol-(*S*)-**1** crystal at –50 ºC rotates by around 60° from the original position (green) of molecule A (Figure 2.7d) in the enol-(*S*)-**1** crystal at 10 ºC, whereas the 5-*tert*-butyl group (green) of molecule B (Figure 2.7e) does not rotate. In comparison, the conformations of the 3-*tert*-butyl groups in molecules B and C do not change drastically from that in molecule A after the phase transition. The torsion angles are shown in Table 2.4.

Table 2.4. Intramolecular hydrogen bonds and molecular conformations for enol-(*S*)-**1** crystals. Reprinted with a slight modification from "Reversible Single-Crystal-to-Single-Crystal Phase Transition of Chiral Salicylidenephenylethylamine" by Takanabe, A; Katsufuji, T.; Johmoto, K.; Uekusa, H.; Shiro, M.; Koshima, H.; Asahi, T. *Crystals* **2017**, *7*, 7,[3] which is an open access article distributed under the terms and conditions of the Creative Commons Attribution (CC-BY) license (http://creativecommons.org/licenses/by/4.0/). Copyright 2016 by the authors; licensee MDPI, Basel, Switzerland.

temperature (ºC)	10	–50	
	molecule A	molecule B	molecule C
intramolecular hydrogen bond			
N···O distance (Å)	2.591	2.596	2.591
N···H–O angle (deg)	160.40	148.67	148.94
dihedral angle between phenyl and salicyl plane (deg)	41.06	46.82	43.97
torsion angle (deg)			
5-*t*-Bu group	61.50 (C5–C6–C11–C13)	63.29 (C19–C20–C25–C27)	126.86 (C33–C34–C39–C42)
	–59.21 (C5–C6–C11–C14)	–55.24 (C19–C20–C25–C28)	6.27 (C33–C34–C39–C40)
	178.68 (C5–C6–C11–C12)	–175.97 (C19–C20–C25–C26)	–115.53 (C33–C34–C39–C41)
3-*t*-Bu group	123.57 (C5–C3–C7–C9)	121.41 (C19–C18–C21–C23)	125.70 (C33–C32–C35–C37)
	3.95 (C5–C3–C7–C10)	1.53 (C19–C18–C21–C24)	6.05 (C33–C32–C35–C38)
	–115.50 (C5–C3–C7–C8)	–117.63 (C19–C18–C21–C22)	–112.10 (C33–C32–C35–C36)

In the enol-(*S*)-**1** crystal at 10 ºC, four A molecules (yellow) exist in a unit cell (Figure 2.8a), and a pair of A molecules is arranged in a 2-fold helical manner along all axes (Figures 2.8a–c) to form a herringbone structure along the *a* axis (Figure 2.8c). In the enol-(*S*)-**1** crystal at –50 ºC, two B molecules (light pink) and two C molecules (light blue) coexist in a unit cell, and two pairs of B and C molecules are arranged in a 2-fold helical manner along the *b* axis (Figure 2.8d). The B and C molecules are arranged alternately along the *a* axis to form a pseudo-herringbone structure (Figure 2.8f).

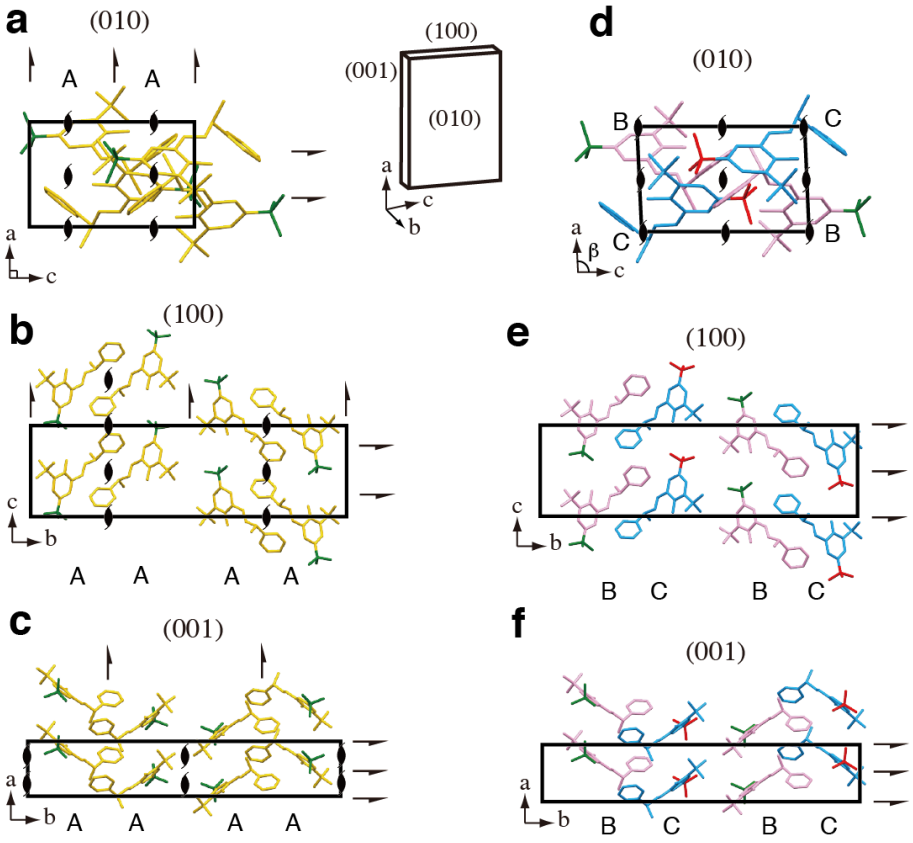

Figure 2.8. Crystal shape and molecular packings of the enol-(*S*)-**1** crystals at (a–c) 10 ºC and (d–f) –50ºC: (a, d) (010), (b, e) (100), and (c, f) (001) faces. The disordered 5-*tert*-butyl groups in minor occupancies and all hydrogen atoms are omitted for clarity. Reprinted with a slight modification from "Reversible Single-Crystal-to-Single-Crystal Phase Transition of Chiral Salicylidenephenylethylamine" by Takanabe, A; Katsufuji, T.; Johmoto, K.; Uekusa, H.; Shiro, M.; Koshima, H.; Asahi, T. *Crystals* **2017**, *7*, 7,[3] which is an open access article distributed under the terms and conditions of the Creative Commons Attribution (CC-BY) license (http://creativecommons.org/licenses/by/4.0/). Copyright 2016 by the authors; licensee MDPI, Basel, Switzerland.

I discuss a possible mechanism for the reversible SCSC phase transition, based on the changes in the molecular conformation and packing arrangement on the (001) face of the enol-(*S*)-**1** crystals at 10 and –50ºC (Figure 2.9). The 5-*tert*-butyl groups of the A molecules of the right column rotate by approximately 60° (red circular arrow, Figure 2.9a) at the phase transition temperature $T_c \approx 3$°C under cooling; consequently, the A molecules of the right column change into C molecules (Figure 2.9b). However, the A molecules of the left column do not rotate at T_c under cooling; consequently, the A molecules of the left column change into B molecules (Figure 5b). Hence, two crystallographically independent molecules (B and C) are generated by these asymmetrical conformation changes in a pair of A molecules.

As described above, the dihedral angle 41.6° between the phenyl and salicyl planes in molecule A increases slightly to 46.82° and 43.97° in molecules B and C, respectively. Accordingly, the salicyl rings of the A molecules rotate slightly so that they are almost perpendicular to the (001) face (light blue circular arrow, Figure 2.9a). The dihedral angle between the salicyl plane and the (001) face increases from 80.94° (A) to 85.90° (B) and 81.39° (C). These conformation changes from A to B and C cause the loss of helical axes along the *a* and *c* axes, which induces the reordering of the packing arrangement from the orthorhombic space group $P2_12_12_1$ to the monoclinic space group $P2_1$.

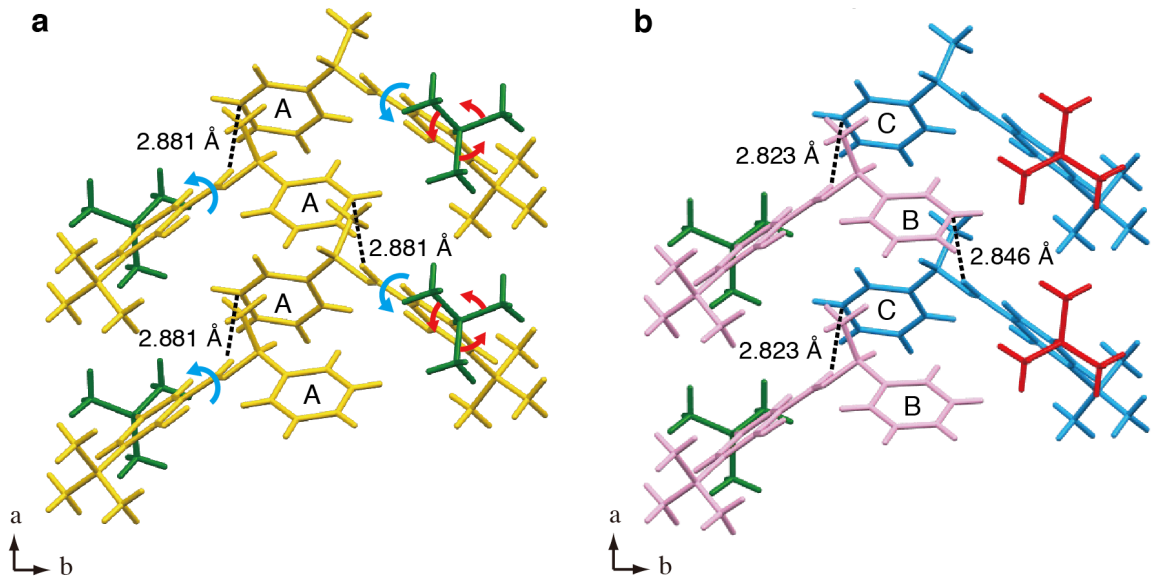

Figure 2.9. Molecular arrangements with the intermolecular interactions on the (001) face of the enol-(*S*)-**1** crystals at (a) 10 ºC and (b) –50 ºC. The left A molecules are converted into the B molecules after the phase transition. The right A molecules are converted into the C molecules. The disordered 5-*tert*-butyl groups in minor occupancies are omitted for clarity. Reprinted with a slight modification from "Reversible Single-Crystal-to-Single-Crystal Phase Transition of Chiral Salicylidenephenylethylamine" by Takanabe, A; Katsufuji, T.; Johmoto, K.; Uekusa, H.; Shiro, M.; Koshima, H.; Asahi, T. *Crystals* **2017**, *7*, 7,[3] which is an open access article distributed under the terms and conditions of the Creative Commons Attribution (CC-BY) license (http://creativecommons.org/licenses/by/4.0/). Copyright 2016 by the authors; licensee MDPI, Basel, Switzerland.

The rotation of the salicyl rings toward the perpendicular to the (001) face leads to closer packing in the direction along the *a* axis. As a result, the length of the *a* axis shrinks discontinuously from 6.3058 to 6.2065 Å at T_c. Before the phase transition, a weak intermolecular C–H···π interaction forms between the Schiff base and the phenyl plane of the A molecules at 10 ºC; the distance is 2.881 Å (black dotted line, Figures 2.9a and 2.10a). After the phase transition by cooling, the distances of the C–H···π interactions between the B and C molecules shorten to 2.823 and 2.846 Å, respectively (Figures 2.9b and 2.10b). However, the changes in molecular conformation and the reordering of the packing arrangement are very small, which leads to the reversible SCSC phase transition with no destruction of the crystal lattice.

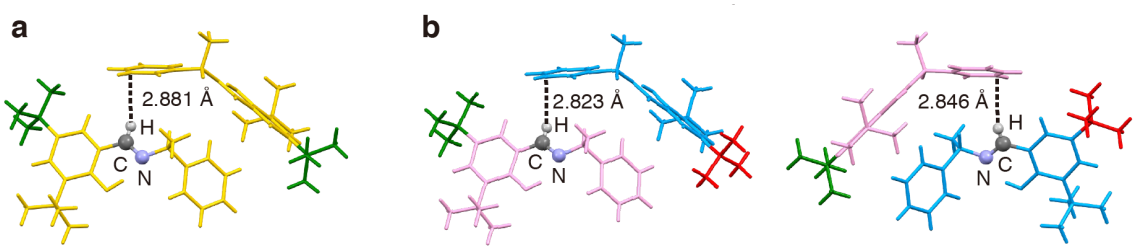

Figure 2.10. C–H···π interaction in the enol-(*S*)-**1** crystals at (a) 10 ºC and (b) –50 ºC. Reprinted with a slight modification from "Reversible Single-Crystal-to-Single-Crystal Phase Transition of Chiral Salicylidenephenylethylamine" by Takanabe, A; Katsufuji, T.; Johmoto, K.; Uekusa, H.; Shiro, M.; Koshima, H.; Asahi, T. *Crystals* **2017**, *7*, 7,[3] which is an open access article distributed under the terms and conditions of the Creative Commons Attribution (CC-BY) license (http://creativecommons.org/licenses/by/4.0/). Copyright 2016 by the authors; licensee MDPI, Basel, Switzerland.

The SCSC phase transition should lead to an anomalous change in the dielectric constant. Millimeter-size square plate crystals of enol-(*S*)-**1** were obtained by slow evaporation of the 2-propanol solution at room temperature. The top surfaces were identified as the (010) and (0$\bar{1}$0) faces by X-ray crystallography analysis. Hence, the dielectric constant of the depth direction along the *b* axis was measured. A square plate crystal (5.4×4.8×0.7 mm long×wide×thick) was fabricated by coating the (010) and (0$\bar{1}$0) top surfaces with a silver-based conductive paste, and enameled copper wires were attached to both top surfaces (Figures 2.11a and b). The temperature dependence of the real part of the dielectric constant ε_r was measured along the *b* axis at 1 kHz (see the Experimental Section). The *T*–ε_r curve revealed two step-like dielectric anomalies at around 3.4 and 3.9°C upon cooling and then heating, respectively (Figure 2.11c), in agreement with the DSC result (Figure 2.5). This result also indicates that the transition is a first-order structural phase transition.

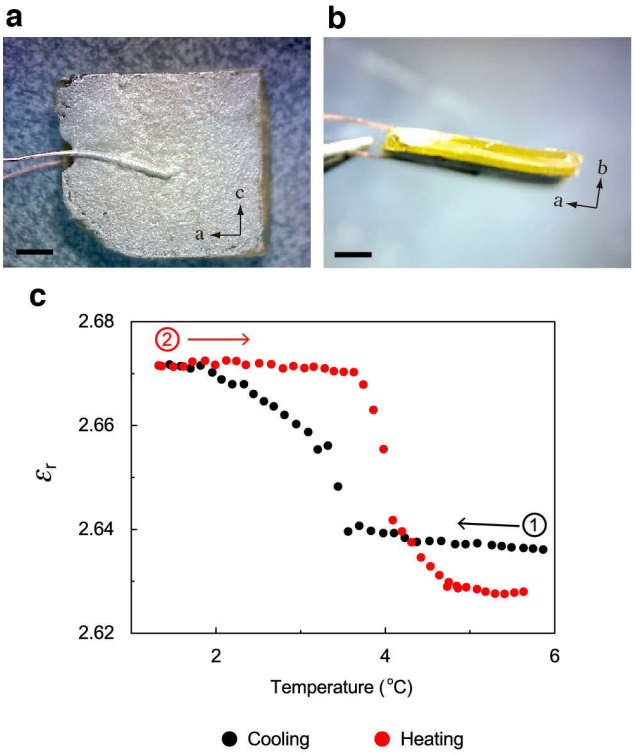

Figure 2.11. Square plate crystal of enol-(*S*)-**1** with application of silver paste and enameled copper wires: (a) the (010) top face and (b) the (001) side face. The scale bar is 1 mm. (c) Temperature dependence of dielectric constant for the enol-(*S*)-**1** crystal along the *b* axis. The cooling scan was switched into the heating scan at 1.4 °C. Reprinted from "Reversible Single-Crystal-to-Single-Crystal Phase Transition of Chiral Salicylidenephenylethylamine" by Takanabe, A; Katsufuji, T.; Johmoto, K.; Uekusa, H.; Shiro, M.; Koshima, H.; Asahi, T. *Crystals* **2017**, *7*, 7,[3] which is an open access article distributed under the terms and conditions of the Creative Commons Attribution (CC-BY) license (http://creativecommons.org/licenses/by/4.0/). Copyright 2016 by the authors; licensee MDPI, Basel, Switzerland.

The dielectric constant ε_r increased from 2.636 to 2.671 (+1.33%) on cooling from 5.7°C to 1.3°C (Figure 2.11c). From the temperature dependence of the lattice constants in Figure 2.6, the surface area of the (010) face should decrease (–0.83%) and the thickness along the *b* axis should also decrease (–0.09%) in the phase transition by cooling. The calculated change in the dielectric constant caused by the slight decreases in surface area and depth is +0.74% from eq 2.1, indicating a slight increase. Hence, the estimated real change in the dielectric constant corrected with the crystal volume shrinkage is +0.59% (= 1.33% – 0.74%) from eq 2.1. This small change in the dielectric constant at the phase transition is derived from the small changes in the molecular conformation and packing arrangement between the crystals above and below T_c. The maximum ε_r value (2.67) of the enol-(*S*)-**1** crystal along the *b* axis at 1.5°C is similar to that (2.7) of benzyl at –189°C,[12] but is lower than those reported for ferroelectric organic crystals.[13] As shown in the packing diagrams (Figures 2.8 and 2.9), the intermolecular interactions in both the enol-(*S*)-**1** crystals at 10 and –50 ºC are the van der Waals force and CH–π interactions alone. Such weak intermolecular interactions might have induced the small dielectric constant ε_r. In fact, a large ε_r value (11) at room temperature has been reported for the croconic acid crystal, in which strong hydrogen-bonded sheets are formed.[14]

2.4 Conclusions

The plate-like enol-(*S*)-**1** crystal caused bending motion with twisting upon UV irradiation, due to shrinkage along the length and width based on the optimized crystal structure of the photoisomerized *trans*-keto-isomer by calculation.

The chiral crystal of enol-(*S*)-**1** undergoes a reversible SCSC phase transition at $T_c \approx 3$°C from the room-temperature form in orthorhombic space group $P2_12_12_1$ to the low-temperature form in monoclinic space group $P2_1$. The crystal below T_c should also have a photochromic nature to the *trans*-keto-form with UV irradiation. Photochromic reaction in the crystal below T_c may induce the photomechanical motion. Therefore, the enol-(*S*)-**1** crystal may be an interesting material which shows photomechanical motions both in room-temperature and low-temperature phase.

2.5 References

(1) Koshima, H.; Matsuo, R.; Matsudomi, M.; Uemura, Y.; Shiro, M. *Cryst. Growth Des.* **2013**, *13*, 4330–4337.

(2) Takanabe, A; Tanaka, M.; Johmoto, K.; Uekusa, H.; Mori, T.; Koshima, H.; Asahi, T. *J. Am. Chem. Soc.* **2016**, *138*, 15066–15077.

(3) Takanabe, A; Katsufuji, T.; Johmoto, K.; Uekusa, H.; Shiro, M.; Koshima, H.; Asahi, T. *Crystals* **2017**, *7*, 7 (10 pp).

(4) Smith, H. E.; Cook, S. L.; Warren, M. E., Jr. *J. Org. Chem.* **1964**, *29*, 2265–2272.

(5) (a) Harada, J.; Ogawa, K.; Tomoda, S. *Acta Crystallogr., Sect. B: Struct. Sci.* **1997**, *B53*, 662–672. (b) Harada, J.; Ogawa, K. *Chem. Soc. Rev.* **2009**, *38*, 2244–2252.

(6) (a) Harada, J.; Uekusa, H.; Ohashi, Y. *J. Am. Chem. Soc.* **1999**, *121*, 5809–5810. (b) Johmoto, K.; Sekine, A.; Uekusa, H.; Ohashi, Y. *Bull. Chem. Soc. Jpn.* **2009**, *82*, 50–57.

(7) Marom, N.; Tkatchenko, A.; Rossi, M.; Gobre, V. V.; Hod, O.; Scheffler, M.; Kronik, L. *J. Chem. Theory Comput.* **2011**, *7*, 3944–3961.

(8) Clark, S. J.; Segall, M. D.; Pickard, C. J.; Hasnip, P. J.; Probert, M. J.; Refson, K.; Payne, M. C. *Z. Kristallogr.* **2005**, *220*, 567–570.

(9) *ABSCOR*; Rigaku Corporation: Tokyo, Japan, 1995.

(10) *NUMABS*; Rigaku Corporation: Tokyo, Japan, 1999.

(11) Johmoto, K.; Ishida, T.; Sekine, A.; Uekusa, H.; Ohashi, Y. *Acta Crystallogr., Sect. B: Struct. Sci.* **2012**, *68*, 297–304.

(12) Almeida, A.; Dos Santos, M. L.; Chaves, M. R.; Amaral, M. H.; Tolédano, J. C.; Périgaud, A.; Savary, H. *Ferroelectrics* **1988**, *79*, 253–256.

(13) Horiuchi, S.; Tokura, Y. *Nat. Mater.* **2008**, *7*, 357–366.

(14) Horiuchi, S.; Tokunaga, Y.; Giovannetti, G.; Picozzi, S.; Itoh, H.; Shimano, R.; Kumai1, R.; Tokura, Y. *Nature* **2010**, *463*, 789–792.

Chapter 3

Measurements of Chiroptical and Optical Anisotropic Properties of Chiral Salicylidenephenylethylamine Crystals using Generalized High-Accuracy Universal Polarimeter

3.1 Introduction

As described in Chapter 1, the simultaneous measurements of the chiroptical and optical anisotropic properties are necessary for evaluating the optical responses of chiral photomechanical crystals. In this Chapter, I describe the LB, LD, CB, and CD spectra of the photomechanical crystals of both enantiomeric enol-(*S*)-**1** and enol-(*R*)-**1** (Scheme 1.1) before and under continuous UV light irradiation simultaneously measured using G-HAUP. I also discuss the correlation between the four optical properties and the crystal structure. This Chapter is reproduced with permission from "Optical Activity and Optical Anisotropy in Photomechanical Crystals of Chiral Salicylidenephenylethylamines" by Takanabe, A; Tanaka, M.; Johmoto, K.; Uekusa, H.; Mori, T.; Koshima, H.; Asahi, T. *Journal of the American Chemical Society* **2016**, *138*, 15066–15077.[1] Copyright 2016 American Chemical Society. Consent from all authors has been secured.

3.2 Principle of High-Accuracy Universal Polarimeter Method

Details of the principle of the original[2–4] and the extended HAUP methods have been described elsewhere.[5–7] In this Section, I briefly explain the basic formula of the HAUP method by following the previous report[7] with slight modifications. The principle of the HAUP method is to measure the transmitted light intensities passing through a polarizer, sample, and then analyzer as a quadratic function of azimuth angles of the polarizer from an arbitrary origin and the analyzer from the crossed Nicols position. The G-HAUP employs a simple optical system that contains only two optical elements: a polarizer and an analyzer (Figure 3.1). The polarization direction of the transmitted light through the polarizer is orthogonal to that passing through the analyzer (i.e., the crossed Nicols position).

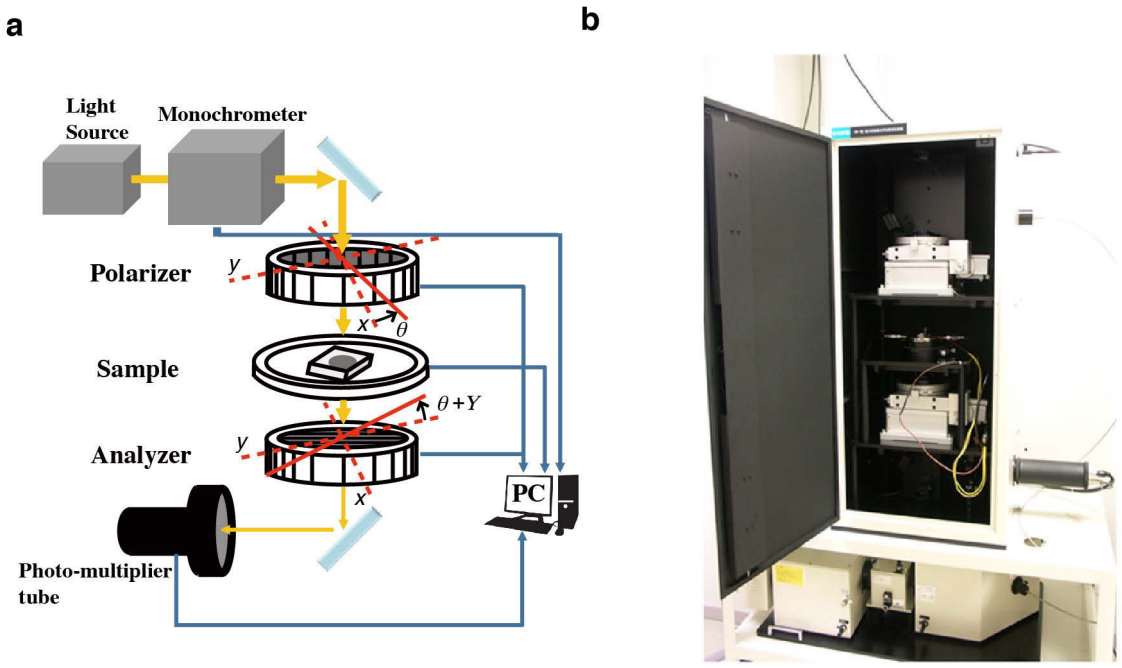

Figure 3.1. (a) Schematic drawing and (b) photograph of the G-HAUP apparatus. Here, θ represent the azimuthal angle of polarizer from an arbitrary origin and Y represent the deflecting angle of analyzer from the crossed Nicols position. Reprinted with permission from "Optical Activity and Optical Anisotropy in Photomechanical Crystals of Chiral Salicylidenephenylethylamines" by Takanabe, A; Tanaka, M.; Johmoto, K.; Uekusa, H.; Mori, T.; Koshima, H.; Asahi, T. *Journal of the American Chemical Society* **2016**, *138*, 15066–15077.[1] Copyright 2016 American Chemical Society.

Due to this simple optical configuration, systematic errors, except those relating to the polarizer and analyzer, are excluded. In the HAUP method, systematic errors originating from parasitic ellipticities of the polarizer and the analyzer (p and q, respectively) and a small error angle (δY, attributed to the displacement of the crossed Nicols configuration) are evaluated and eliminated.[3] Here, I define θ as an azimuth angle of polarizer from an arbitrary origin; Y as the azimuth angle of analyzer from the crossed Nicols position; θ_0 as an extinction position angle of polarizer from the arbitrary origin obtained by

$$\left(\frac{\partial(I/I_0)}{\partial\theta}\right)_{Y'=0} = 0;$$

θ' as the azimuth angle of polarizer from θ_0; and Y' as the azimuth angle of analyzer from δY. That is, $\theta = \theta_0 + \theta'$ and $Y = \delta Y + Y'$. The θ' and Y' values are independently and precisely obtained in the practical HAUP experiment. The clockwise direction from the viewpoint of an observer is defined as the positive direction for all angles.

The ratio, Γ, of the intensity of transmitted light and intensity of incident light, I and I_0, respectively, are represented as follows:

$$\Gamma(\theta', Y') = I/I_0 = A''(\theta') + B''(\theta')Y' + C''Y'^2, \tag{3.1}$$

$$A''(\theta') = H''_{11} + H''_{12}\theta' + H''_{13}\theta'^2, \tag{3.2}$$

$$B''(\theta') = H''_{21} + H''_{22}\theta', \tag{3.3}$$

$$C'' = H''_{31}, \tag{3.4}$$

where,

$H''_{11} \rightarrow$ independent of θ' and Y',

$H''_{12} = 0$,

$$H''_{13} = e^E + e^{-E} - 2\cos\Delta, \tag{3.5}$$

$$H''_{21} = -b'_1 p + b'_2 q + a_1 \delta Y + 2c_1 k' - 2c_2(\sin\Delta)k, \tag{3.6}$$

$$H''_{22} = 2(e^E - \cos\Delta), \tag{3.7}$$

$$H''_{23} = e^E, \tag{3.8}$$

where,

$$a_1 = \frac{2\sin^2\Delta}{e^E+e^{-E}-2\cos\Delta},$$
$$b'_1 = -\frac{2\left(e^{-E}-\cos\Delta\right)\sin\Delta}{e^E+e^{-E}-2\cos\Delta},$$
$$b'_2 = -\frac{2\left(\mathrm{e}^E-\cos\Delta\right)\sin\Delta}{e^E+e^{-E}-2\cos\Delta},$$
$$c_1 = \frac{K}{K^2+1} = \frac{E/\Delta}{(E/\Delta)^2+1},$$
$$c_2 = \frac{1}{K^2+1} = \frac{1}{(E/\Delta)^2+1}.$$

The extinction position angle, θ_0, can be expressed under the same approximation as follows:

$$\theta_0 = -a_2(p+q) - b_2\delta Y + c_1 k + c_2 k' + N, \tag{3.9}$$

where,

$$a_2 = \frac{\sin\Delta}{e^E+e^{-E}-2\cos\Delta},$$
$$b_2 = \frac{e^E-\cos\Delta}{e^E+e^{-E}-2\cos\Delta}.$$

Here, N is the difference of θ_0 from its absolute value; Δ and E represent the phase difference and the total linear dichroism of the sample, respectively; k and k' represent the ellipticity derived from CB and CD of the sample, respectively. Using these quantities, LB, LD, CB, and CD are defined according to the previous report[7]:

$$\mathrm{LB} = n_s - n_f \equiv \frac{\Delta\lambda}{2\pi d}, \tag{3.10}$$

$$\mathrm{LD} = m_s - m_f \equiv \frac{E\lambda}{2\pi d}, \tag{3.11}$$

$$\mathrm{CB} = n_L - n_R \equiv \frac{\Delta k\lambda}{\pi d} = 2k\ \mathrm{LB}, \tag{3.12}$$

$$\mathrm{CD} = m_L - m_R \equiv -\frac{\Delta k'\lambda}{\pi d} = 2k'\ \mathrm{LB}, \tag{3.13}$$

where n is the refractive index; m is the absorption coefficient; subscripts s and f are axes of the slow and fast light rays, respectively; subscripts R and L are the right and left circular polarization, respectively; λ is the wavelength of incident light; d is the thickness of the sample.

In the HAUP method, the LB, LD, CB and CD values are determined according to the previous report[7] with slight modifications:

(i) The transmitted light intensities, I, were measured as quadratic functions of θ' and Y'. By least-squares fittings using eqs 3.1–3.4, the $I_0 \cdot H''_{ij}$ $(i, j = 1, 2, 3)$ values at each θ' position and θ_0 are determined. From the θ' dependences of H''_{13}, H''_{22} and H''_{31}, i.e., eqs 3.5, 3.7 and 3.8, the Δ, E and I_0 values were calculated. Note that only the recorded phase difference, Δ_r $(0 \le \Delta_r \le \pi)$, can be obtained from this procedure. The real Δ value was obtained using the relationship

$$\Delta = 2l\pi \pm \Delta_r,$$

where l is usually determined using a Ehringhaus compensator. As an example, raw experimental results from the analysis of enol-(*S*)-**1** without UV irradiation at 20ºC are shown in Figure 3.2. The thickness of the sample was 6.5 mm which was measured by laser microscopy. From eqs 3.10 and 3.11, LB and LD were obtained, as shown in Figure 3.11a.

(ii) To obtain CB and CD from experimental data, the evaluation of systematic errors is initially needed. The p value can be determined by a preceding experiment with an achiral crystal $LiNbO_3$ or MgF_2, because the value of p is independent of the sample setting. Until now, this procedure has been adopted in various crystals.[5,7,8–10] For this study, the p value at 20ºC was determined to be 1.0×10^{-4} by the wavelength dependence measurements at 20ºC of achiral MgF_2 (100) plate crystal.

The q and δY values were successfully determined by the approximations below. From eq 3.12, optical rotatory power (ORP)[11] is defined as follows:

$$\mathrm{ORP} = \frac{\pi}{\lambda}\mathrm{CB} = \frac{\pi}{\lambda}2k\ \mathrm{LB} = \frac{\Delta k}{d}. \tag{3.14}$$

Additionaly, the ORP dispersion (ORD) spectra is related to the absorption spectrum of the optical active sample by the Drude expression[12] as follows:

$$\mathrm{ORP} = \sum_j \frac{A(\lambda_j)}{\lambda^2 - \lambda_j^2}, \tag{3.15}$$

where λ_j is the wavelength of transition from the ground state to the excited state j, and $A(\lambda_j)$ is a constant depending on the absorption strength of this transition. Therefore, I assumed that k is dependent on λ from eqs 3.14 and 3.15 as follows:

$$k = \frac{d}{\Delta}\sum_j \frac{A(\lambda_j)}{\lambda^2 - \lambda_j^2}. \tag{3.16}$$

The optimum values of q, δY and N are obtained from least-squares fittings using eqs 3.6 and 3.9 and the p value by assuming that k is dependent of λ and $k' = 0$ in the wavelength regions, where the sample has no absorption.[7] In the case of the both enantiomeric enol-**1** crystals without and with UV irradiation, I made the following approximations: (α) k is dependent of λ at the wavelength without UV irradiation as follows:

$$k = \frac{A'_{330}}{\Delta(\lambda^2 - 330^2)}, \tag{3.17}$$

where $A'_{330}=A_{330}\times d$, and $k' = 0$ above 400 nm. (β) With UV irradiation, k is represented as follows:

$$k = \frac{A'_{330}}{\Delta(\lambda^2 - 330^2)} + \frac{A'_{460}}{\Delta(\lambda^2 - 460^2)}, \tag{3.18}$$

where $A'_{460}=A_{460}\times d$, and $k' = 0$ above 550 nm.

The systematic error parameters q and δY of enol-(*S*)-**1** without UV irradiation determined by least-squares fittings are as follows:

$$q = -2.61\times10^{-4}$$

$\delta Y = 3.83\times10^{-4}$.

The values of q and δY obtained by least-squares fittings for any other experimental data in this study varied between 10^{-4}–10^{-3} and 10^{-5}–10^{-3}, respectively. In comparison with previous studies,[10,13,14] these values are acceptable.

The k and k' values are calculated by introducing the obtained Δ and E, and systematic errors to eqs 3.6 and 3.9, as shown in Figure 3.3. Finally CB and CD are determined from eqs 3.12 and 3.13, as shown in Figure 3.11c.

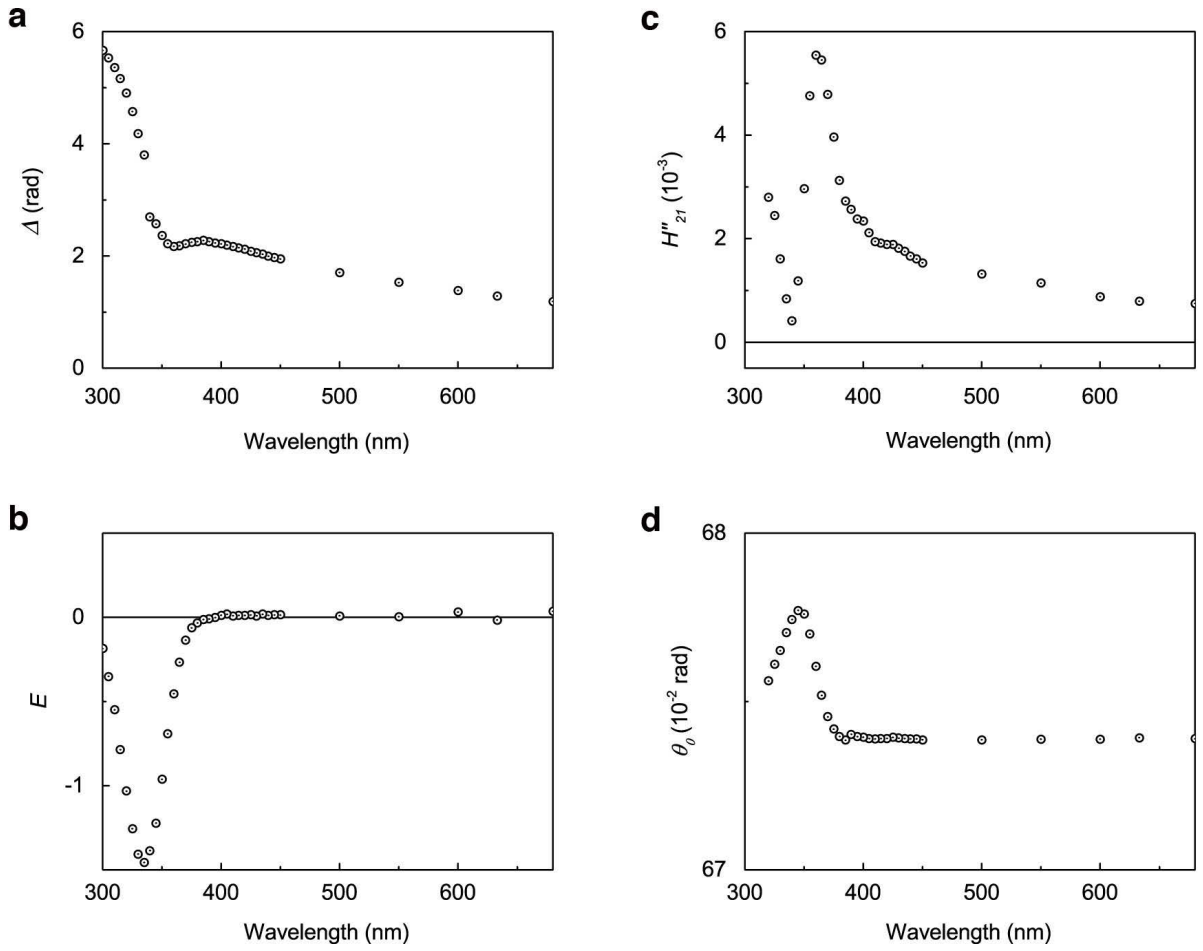

Figure 3.2. Raw experimental results from the analysis of enol-(*S*)-**1** on the (001) face at 20ºC: (a) Δ, (b) E, (c) H''_{21} and (d) θ_0. Reprinted with permission from "Optical Activity and Optical Anisotropy in Photomechanical Crystals of Chiral Salicylidenephenylethylamines" by Takanabe, A; Tanaka, M.; Johmoto, K.; Uekusa, H.; Mori, T.; Koshima, H.; Asahi, T. *Journal of the American Chemical Society* **2016**, *138*, 15066–15077.[1] Copyright 2016 American Chemical Society.

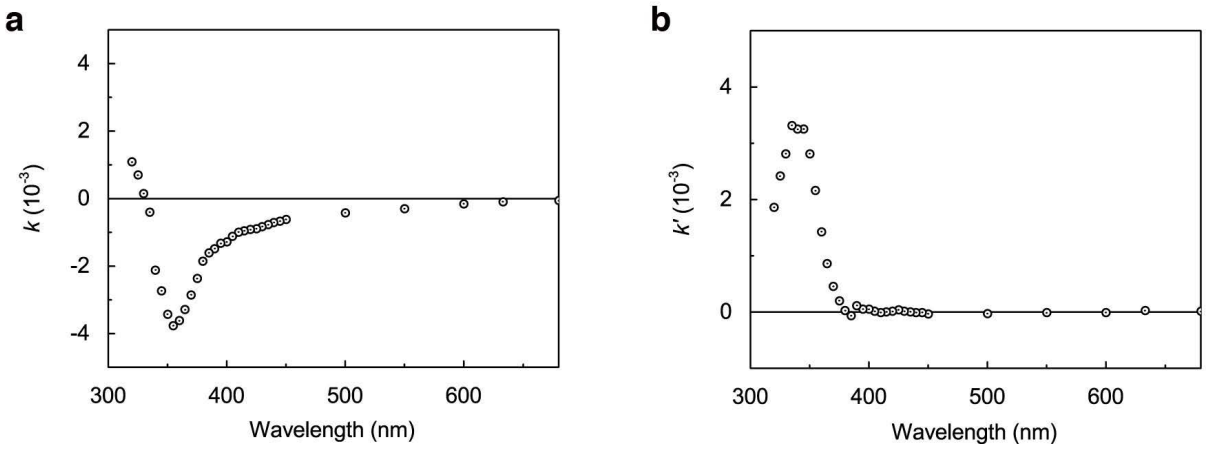

Figure 3.3. (a) *k* and (b) *k'* spectra calculated from Figure 3.2. Reprinted with permission from "Optical Activity and Optical Anisotropy in Photomechanical Crystals of Chiral Salicylidenephenylethylamines" by Takanabe, A; Tanaka, M.; Johmoto, K.; Uekusa, H.; Mori, T.; Koshima, H.; Asahi, T. *Journal of the American Chemical Society* **2016**, *138*, 15066–15077.[1] Copyright 2016 American Chemical Society.

3.3 Experimental Section

3.3.1 Sample Preparation

The enol-(*S*)-**1** and enol-(*R*)-**1** (100) plate-like crystals were prepared according to Subsection 2.2.1.[15] Thin, plate-like single crystals of enol-(*S*)-**1** and enol-(*R*)-**1** were prepared by sublimation at 10–20 °C below the melting points. The thicknesses of all samples for the HAUP measurement were measured by laser microscopy (VK-X200; Keyence). Using silicone grease, the samples were fixed on a thin Cu plate with a pinhole of diameter 0.5 mm.

3.3.2 Measurements of Linearly Polarized Ultraviolet-visible Absorption Spectra of Thin Single Crystals

Enol-(*S*)-**1** crystals prepared by sublimation were fixed on a Cu plate with a pinhole of diameter approximately 0.5 mm. This sample was set on the sample stage of HAUP (Figure 3.1). The HAUP apparatus is described in the previous section. The spectra of transmitted light intensity at four angles of linearly polarized light in the range 0° to 90° (from parallel to perpendicular to the *a* axis) were measured using the HAUP apparatus without analyzer. Then, the spectra of transmitted light intensity were measured under UV light irradiation (10 mW cm^{-2}). After removing enol-(*S*)-**1** crystal, the spectra of transmitted light intensity were measured with and without UV irradiation, as a blank. All measurements were performed at 298 K. Finally, linearly polarized UV-Vis absorption spectra were calculated according to the Beer-Lambert-Bouguer law (Figure 3.6).

3.3.3 Simultaneous Measurements of Linear Birefringence, Linear Dichroism, Circular Birefringence and Circular Dichroism using Generalized High-Accuracy Universal Polarimeter

Enol-(*S*)-**1** and enol-(*R*)-**1** crystals prepared as described above were fixed with silicon grease to a Cu plate with a pinhole of diameter approximately 0.5 mm. This sample was set on the sample stage of HAUP. The HAUP apparatus (Figure 3.1), theory and analysis are

described in the previous section. HAUP measurements were performed before and under continuous UV irradiation. In the latter case, UV-LED light (365 nm) was continuously irradiated at low power (5 mW cm^{-2}) from a direction almost vertical to the light path of the HAUP to prevent incidence to the photo-multiplier tube (Figure 3.5).

3.3.4 Electronic Transition Calculations

All calculations were carried out with the Gaussian 09 package.[16] The B3LYP functional[17,18] was adopted because it is well-known that hybrid functionals describe the ground and excited state. The 6-311G basis set[19] was applied in conjunction with the B3LYP functional, since it represents a good balance between quality of the results and computational cost. The input molecular geometries of enol-(*S*)-**1** and *trans*-keto-(*S*)-**1** were generated from the calculated crystal structures (Tables 3.2 and 3.3). The obtained HOMO and LUMO orbitals of enol-(*S*)-**1** and *trans*-keto-(*S*)-**1** are shown in Figure 3.14.

3.3.5 Observation of Photomechanical Motion upon Linearly Polarized Light

Thin, plate-like enol-(*S*)-**1** crystals were prepared as described above and fixed to the tops of needles. UV-LED illuminator (UV-400, 365 nm, 50 mW; Keyence) was used to observe the photomechanical motions. To produce a linearly polarized light, Glan-Tompson prism polarizer was applied between the sample and the UV LED light illuminator. Because of the presence of the Glan-Thompson prism polarizer, the intensity of the UV light was decreased (30 mW cm^{-2}). Photomechanical motion videos were recorded using a digital high-speed microscope (VHX-5000; Keyence).

3.3.6 Solution Circular Dichroism and Optical Rotatory Dispersion Spectrophotometry

Solutions of enol-(*S*)-**1** and enol-(*R*)-**1** in hexane were prepared at the same concentration (500 μM). CD spectra were measured on a circular dichroism spectrometer (J-820; JASCO) with ORD measurement unit (ORD-M) using a standard cell. The scan speed was 200 nm

min^{-1}. The cumulated number was 2. The CD, ORD, and absorbance units were converted into molar CD, specific optical rotation, and molar absorption coefficient, respectively.

3.3.7 Calculation of Circular Dichroism Spectra of Various Forms of (*S*)-1

Details of the CD calculation have been described elsewhere[20] and are described according to the previous reports[20] with slight modifications: Briefly, all CD calculations were performed on Linux PCs using the Turbomole 6.6 program suite.[21] Geometries were fully optimized at the dispersion-corrected density functional theory (3rd generation; DFT-D3 with BJ dumping), with an AO basis set of valence triple-ξ quality at the TPSS-D3/def2-TZVP level.[22] The resolution of identity (RI) approximation was employed and the corresponding auxiliary basis sets were taken from the Turbomole basis set library. The numerical quadrature grid m5 was employed and the convergence criterion for the optimization regarding the change of total energy between two subsequent optimization cycles was set to 10^{-7} E_h. All excited-state calculations were performed with the above DFT-D3 optimized ground-state geometries, thus corresponding to the vertical transition approximation. The CD spectra were calculated by the time-dependent, second-order approximate coupled-cluster singles and doubles model (RI-CC2 method), employing the same def2-TZVP basis set.[23] A relatively robust length-gauge oscillator strength was used throughout this study. The CD spectra were simulated by overlapping Gaussian functions for each transition, where the width of the band at 1/e height was fixed at 0.4 eV, and the overall excitation energy was shifted by 0.3 eV. These values are purely empirical and have no rigorous ground, but are able to successfully reproduce and match the experimental CD spectra, thus facilitating interpretation of the spectra.

3.4 Results and Discussion

3.4.1 Linearly Polarized Ultraviolet-visible Spectra

Thin and wide plate-like enol-(*S*)-**1** and enol-(*R*)-**1** crystals with smooth surfaces are required for HAUP measurements, due to the transmission optical system of the apparatus (Figure 3.1). Most thin specimens are prepared by polishing single crystals. However, it was extremely difficult to decrease the thickness of the single enol-(*S*)-**1** crystals grown by recrystallization to less than a few tens of μm by polishing with lapping films. Furthermore, the polish scratches remained even when using a lapping film coated with a soft Fe_2O_3 polishing agent with very fine particles (0.3 μm). The specimen preparation problem was overcome by applying the sublimation method. The enol-(*S*)-**1** powders were put in a 30 mL glass beaker and a few glass plates were placed against its inside wall. Then the beaker was covered and heated at 80°C for several weeks. After much trial and error, I used this gentle sublimation method to obtain very thin and wide plate-like single enol-(*S*)-**1** crystals, whose thickness was less than 10 μm, and length and width were approximately 3 and 1 mm, respectively (Figure 3.4a). The (001) top surface was sufficiently smooth and suitable for HAUP measurement. Similarly, I obtained thin, plate-like crystals of enol-(*R*)-**1** by this sublimation method. Using silicone grease, the thin crystal was fixed on a thin Cu plate with a 0.5 mm-diameter pinhole for the light beam to pass through (Figure 3.4b).

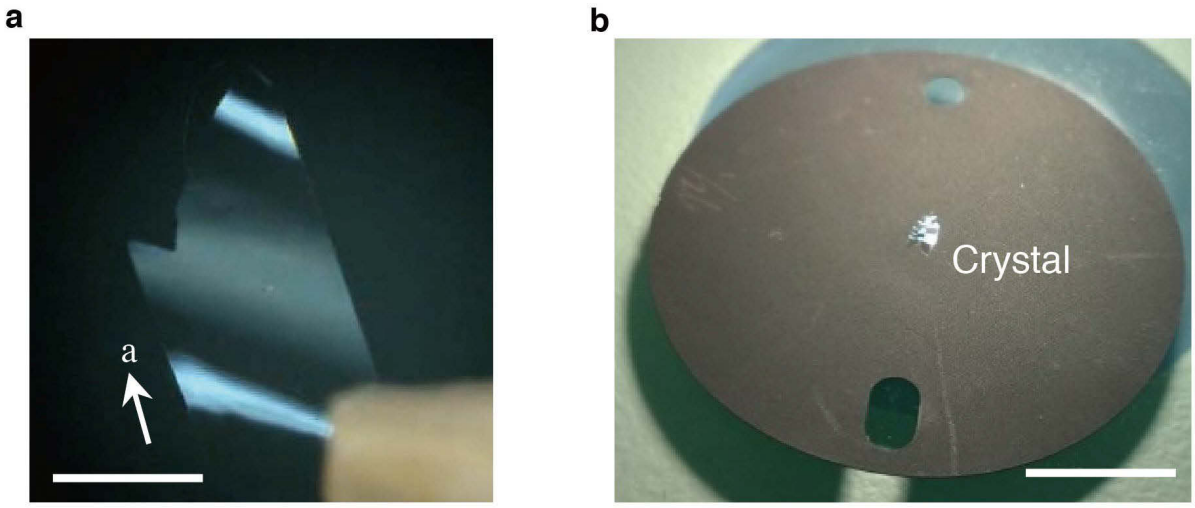

Figure 3.4. (a) Photograph of a thin plate-like crystal of enol-(*S*)-**1** obtained by sublimation. The scale bar is 500 μm. (b) The crystal fixed on a Cu sample plate with a pinhole of 0.5 mm in diameter. The scale bar is 10 mm. Reprinted with permission from "Optical Activity and Optical Anisotropy in Photomechanical Crystals of Chiral Salicylidenephenylethylamines" by Takanabe, A; Tanaka, M.; Johmoto, K.; Uekusa, H.; Mori, T.; Koshima, H.; Asahi, T. *Journal of the American Chemical Society* **2016**, *138*, 15066–15077.[1] Copyright 2016 American Chemical Society.

Linearly polarized ultraviolet-visible (UV-Vis) absorption spectra of enol-(*S*)-**1** crystal, before and under continuous UV irradiation, were measured using the HAUP with the analyzer removed. The polarized light was incident perpendicularly on the (001) top surface of the thin (10 μm) crystal and transmitted parallel to the *c* axis. UV-LED light (365 nm) was continuously irradiated at low power (10 mW cm^{-2}) from a direction almost vertical to the HAUP light path, to prevent incidence to the photo-multiplier tube (Figure 3.5). Bending of the crystal by the UV irradiation was prevented by fixing the crystals to the Cu plate (thickness: 0.12 mm) with silicone grease.

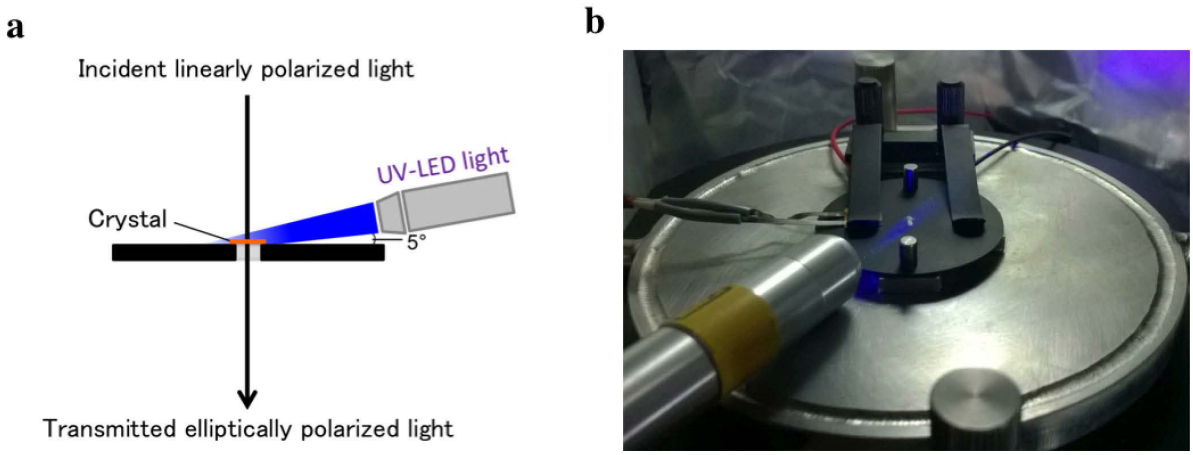

Figure 3.5. (a) Schematic representation and (b) photograph of UV light irradiation for the HAUP measurement. Reprinted with permission from "Optical Activity and Optical Anisotropy in Photomechanical Crystals of Chiral Salicylidenephenylethylamines" by Takanabe, A; Tanaka, M.; Johmoto, K.; Uekusa, H.; Mori, T.; Koshima, H.; Asahi, T. *Journal of the American Chemical Society* **2016**, *138*, 15066–15077.[1] Copyright 2016 American Chemical Society.

Before UV irradiation, a strong absorption peak at 330 nm was observed, which was derived from the π–π* transition of the intramolecular hydrogen-bonded salicylidenimino moiety (Figure 3.6a).[24,25] The peak heights decreased as the polarization direction was changed from parallel (0°) to perpendicular (90°) to the *a* axis, showing the anisotropic character of the crystal. Under UV irradiation, a new absorption peak at 460 nm appeared due to the formation of *trans*-keto-(*S*)-**1** by photochemical hydrogen transfer reaction (Figure 3.6b), consistent with the previous study.[26,27] This absorption peak affects the crystal color from pale yellow to reddish-orange. Both absorption bands at 330 and 460 nm yielded maxima (peak heights) at the parallel (0°) polarization direction of the linearly polarized light to the *a* axis. Both peak heights decreased as the polarization direction changed from parallel (0°) to perpendicular (90°) to the *a* axis.

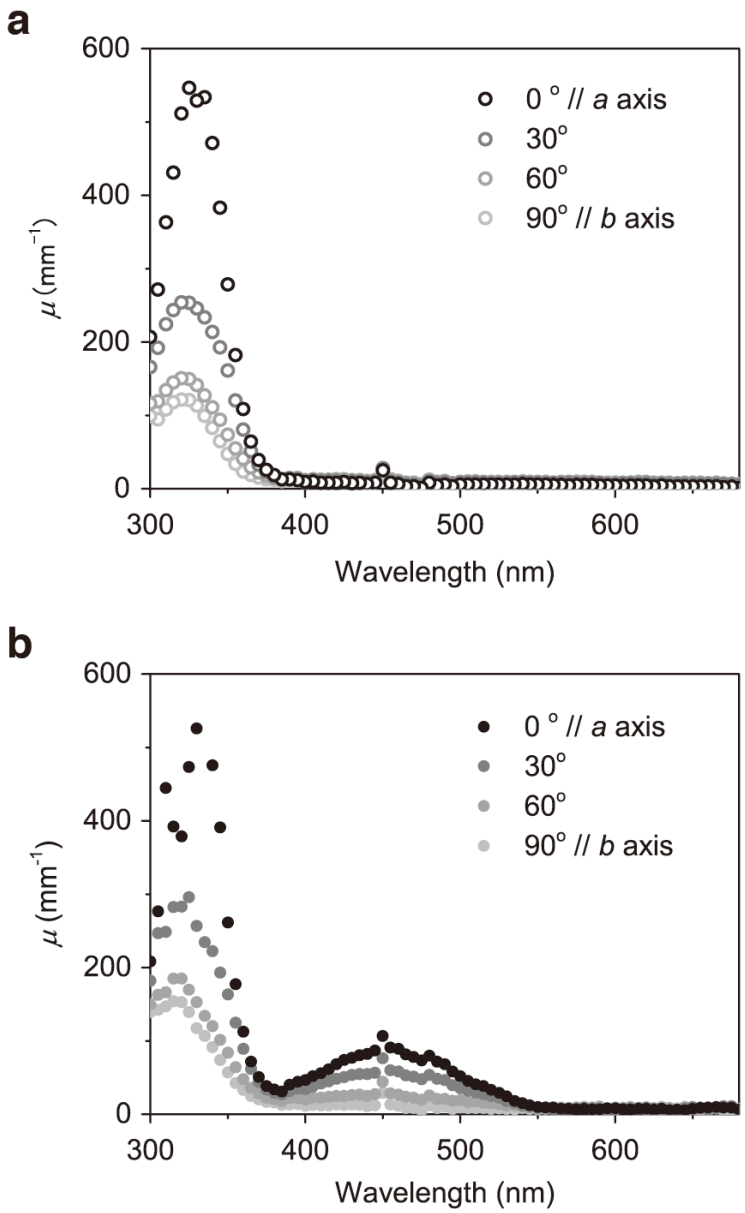

Figure 3.6. Linearly polarized UV-Vis absorption spectra of enol-(*S*)-**1** crystal on the (001) face (a) before and (b) under continuous UV light irradiation at 365 nm. The value of μ expresses absorption coefficient. The polarization directions of incident linearly polarized light were changed from parallel to perpendicular to the *a* axis. Reprinted with permission from "Optical Activity and Optical Anisotropy in Photomechanical Crystals of Chiral Salicylidenephenylethylamines" by Takanabe, A; Tanaka, M.; Johmoto, K.; Uekusa, H.; Mori, T.; Koshima, H.; Asahi, T. *Journal of the American Chemical Society* **2016**, *138*, 15066–15077.[1] Copyright 2016 American Chemical Society.

3.4.2 High-Accuracy Universal Polarimeter Measurements

I adopted the HAUP method[7] to simultaneously measure all optical anisotropic (LB, LD) and chiroptical (CB, CD) spectra of both the enol-(*S*)-**1** and enol-(*R*)-**1** crystals, before and under continuous UV irradiation. Measurements were performed in the wavelength region between 300 and 680 nm at 20 ºC. The thicknesses of the thin, plate-like crystals of enol-(*S*)-**1** and enol-(*R*)-**1** were 6.5 and 7.6 μm, respectively.

Figure 3.7 shows the LB, LD, CB, and CD spectra of the enol-(*S*)-**1** and enol-(*R*)-**1** crystals on the (001) face before UV irradiation. Optical properties of enol-(*R*)-**1** crystal in the wavelength range of 340 to 365 nm could not be measured as understood from Figure 3.7, because the value of recorded phase differences in this wavelength region belong to the inaccurate region for the HAUP measurement ($0.9\pi < \Delta_r \leq \pi$, or $\cos \Delta_r$ almost equals to –1). The LB and LD spectra between the S and R enantiomeric crystals are coincident (Figure 3.7a and b), because optical anisotropic properties are not related to the chirality of the crystals. The LD peak at 330 nm was observed to be negative, which corresponds to the π–π* transition of the intramolecularly hydrogen-bonded salicylidenimino moiety. At around the LD peak, the LB spectra exhibited anomalous dispersion of negative peaks at 360 nm. Consequently, the Kramers–Kronig relationship between the LB and LD spectra is satisfied,[28] as shown in Figure 3.11a.

The CD spectra of enol-(*S*)-**1** and enol-(*R*)-**1** crystals revealed, respectively, a strong negative and positive Cotton effect at 330 nm, which mirror each other (Figure 3.7d). The CB spectrum of enol-(*S*)-**1** crystals also exhibited anomalous dispersion of negative peaks at 360 nm with changes in sign at the CD peaks (Figure 3.7c). Although the data plots of enol-(*R*)-**1** in the wavelength range of 340 to 365 nm could not be measured, the CB spectrum of enol-(*R*)-**1** is considered to exhibit anomalous dispersions of positive peak at around 360 nm because the CB spectra of enol-(*S*)-**1** and enol-(*R*)-**1** crystals should mirror each other. The

baseline is slightly shifted to the positive in the CB spectra, which I consider to be caused by the inaccuracy of systematic error evaluations. The Kramers–Kronig relationship between the CB and CD spectra is also satisfied (Figure 3.11c). It is reasonable that the magnitudes of the CB and CD are approximately 10^{-4}, smaller by two orders than the 10^{-2} of the LB and LD. These consistent results indicate that the CB and CD spectra were successfully obtained by the HAUP method.

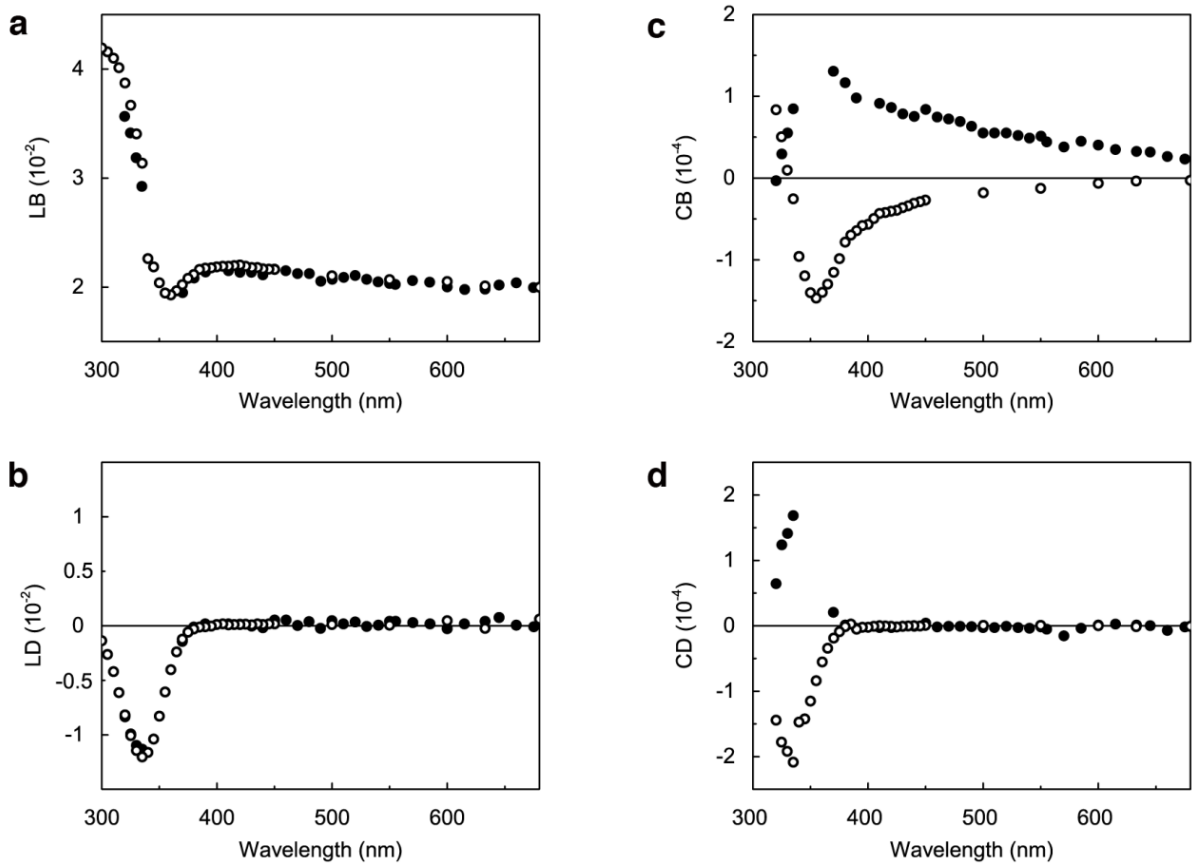

Figure 3.7. Anisotropic optical and chiroptical spectra of enol-(*S*)-**1** (black open circles) and enol-(*R*)-**1** (black solid circles) crystals on the (001) face at 293 K: (a) LB, (b) LD, (c) CB, and (d) CD. Reprinted with permission from "Optical Activity and Optical Anisotropy in Photomechanical Crystals of Chiral Salicylidenephenylethylamines" by Takanabe, A; Tanaka, M.; Johmoto, K.; Uekusa, H.; Mori, T.; Koshima, H.; Asahi, T. *Journal of the American Chemical Society* **2016**, *138*, 15066–15077.[1] Copyright 2016 American Chemical Society.

I then attempted to measure the LB, LD, CB, and CD spectra of both enantiomeric enol-**1** crystals under UV irradiation. UV-LED light (365 nm) was continuously irradiated from a direction almost vertical to the HAUP light path at low power (5 mW cm^{-2}) to minimize incidence of the UV light to the photo-multiplier tube (Figure 3.5). Crystal bending by UV irradiation was prevented by fixing the crystals to the Cu plate with silicone grease. Even under such weak UV irradiation, the thicknesses of the enol-(*S*)-**1** and enol-(*R*)-**1** crystals decreased from 6.2 to 5.4 μm (–0.8 μm, –12.9%), and from 7.1 to 6.3 μm (–0.8 μm, –11.3%), respectively, after three days required for the HAUP measurement. To explain this decrease in thickness, I measured the surface temperature of the crystal specimens using infrared (IR) thermometers and found that the surface temperature was elevated by approximately 0.5° C under UV irradiation.

The surface temperature at the spots 5–7 inside the pinhole immediately elevated by 0.6–0.9 degree upon UV irradiation with the UV-LED light at 365 nm, and returned to the initial temperature after stopping irradiation (Figure 3.8). The reason that the temperature at the place (spots 1–4, 8, and 9) except the pinhole was higher than that inside the pinhole (spots 5–7) is likely due to the better heat absorption by the black Cu sample plate.

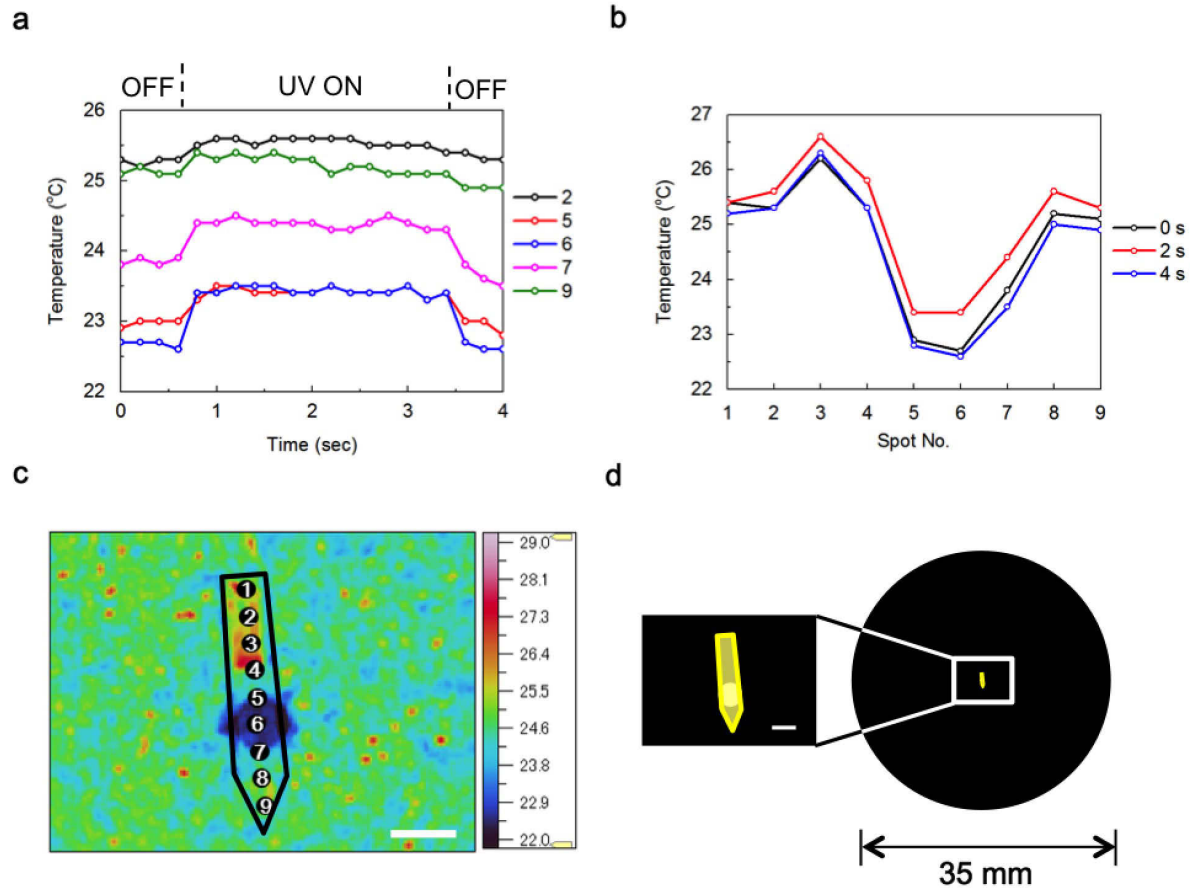

Figure 3.8. (a) Time dependence and (b) spot dependence of surface temperature change of the enol-(*S*)-**1** crystal upon UV (365 nm) irradiation measured by IR thermometer (Apiste FSV-2000). (c) IR thermographic image. The crystal form is lined in black color. The spot numbers are manually defined. (d) The right drawing represents the thin platelike crystal fixed on a Cu sample plate with a pinhole of 0.5 mm in diameter. The left drawing represents the enlarged view of the white rectangle box area. The white scale bar is 0.5 mm. Reprinted with permission from "Optical Activity and Optical Anisotropy in Photomechanical Crystals of Chiral Salicylidenephenylethylamines" by Takanabe, A; Tanaka, M.; Johmoto, K.; Uekusa, H.; Mori, T.; Koshima, H.; Asahi, T. *Journal of the American Chemical Society* **2016**, *138*, 15066–15077.[1] Copyright 2016 American Chemical Society.

The temperature profile (Figure 3.9) shows that the surface temperature of the crystal sample did not change by the incident light (330 nm) of the HAUP. In contrast, the surface temperature elevated by around 0.5 degree by the irradiation with the UV-LED light at 365 nm. Periodical temperature drop of 18 min interval was due to the ON/OFF of room air-conditioner. It is most probably thought that the slight heating of crystals caused the decrease of thickness due to the quite long time for about 3 days required for the HAUP measurement.

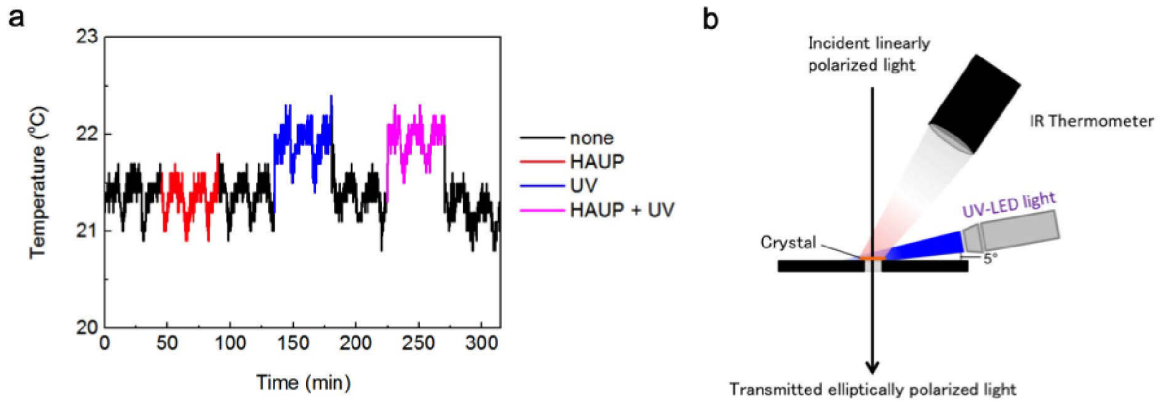

Figure 3.9. (a) In situ surface temperature profile of the enol-(*S*)-**1** crystal measured by IR thermometer (JAPAN SENSOR TMHX-CSE0500-0040H0.7) and (b) schematic representation of *in situ* surface temperature measurement. In the graph (a), the thin platelike crystal fixed on the Cu plate was mounted on the sample stage of the HAUP apparatus. The measurement area of the IR thermometer was 0.7 mm in diameter. Black line: none means no incident light of the HAUP (blank). Red line: HAUP means that the sample was irradiated by the incident light (330 nm) during the HAUP measurement. Blue line: UV means that the sample was irradiated with UV-LED light at 365 nm for proceeding the photoisomerization to the *trans*-keto-(*S*)-**1**. Pink line: HAUP + UV means that the sample was irradiated by both the incident light of HAUP (330 nm) and UV-LED light (365 nm). The each measurement time interval was 45 min. Reprinted with permission from "Optical Activity and Optical Anisotropy in Photomechanical Crystals of Chiral Salicylidenephenylethylamines" by Takanabe, A; Tanaka, M.; Johmoto, K.; Uekusa, H.; Mori, T.; Koshima, H.; Asahi, T. *Journal of the American Chemical Society* **2016**, *138*, 15066–15077.[1] Copyright 2016 American Chemical Society.

These results above suggest that the crystal thickness might decrease by gradual sublimation from the top surface of the specimens heated during the long measurement period, despite temperature control with a thermostat. Therefore, when I obtain LB, LD, CB, and CD from raw experimental data via HAUP measurement, I should take into account the decrease in thickness of the specimen by UV irradiation. The specimen thickness at each wavelength was corrected by dividing the total change in thickness by the number of HAUP measurements.

Figure 3.10 shows the LB, LD, CB, and CD spectra under continuous UV irradiation at 365 nm, which represents the spectra at the photostationary state of the reactant enol-**1** and the product *trans*-keto-**1**. New LD peaks corresponding to *trans*-keto-(*S*)-**1** and *trans*-keto-(*R*)-**1** appeared at around 460 nm, and the magnitudes of the LD peaks at 330 nm decreased slightly. The LD spectra of the S and R *trans*-keto isomers were coincident with each other (Figure 3.10b). At around the weak LD peak, the LB spectra exhibited a slight anomalous dispersion of positive and negative peaks at around 410 and 360 nm (Figure 3.10a). The changes of LB and LD spectra before and under UV irradiation are shown in Figures 3.12a and b, respectively. These results confirm that the Kramers–Kronig relationship between the LB and LD spectra is satisfied (Figure 3.11b).

New small negative and positive CD peaks appeared at 460 nm due to the formation of *trans*-keto-(*S*)-**1** and *trans*-keto-(*R*)-**1** crystals, respectively, and the magnitudes of CD peaks at 330 nm decreased slightly (Figure 3.10d). The CB spectra also exhibited anomalous dispersions of negative [enol-(*S*)-**1**] and positive [enol-(*R*)-**1**] peaks at 500 and 360 nm with a change in sign at the new CD peak (Figure 3.10c). The baseline is shifted slightly to the positive in the CB spectra, which I consider to be caused by the inaccuracy of systematic error evaluations. The Kramers–Kronig relationship between the CB and CD spectra is roughly satisfied (Figure 3.11d). As shown in Figure 3.12 combined with Figures 3.7 and

3.10, the CD and CB spectra under weak UV light irradiation are also successfully measured by the HAUP method.

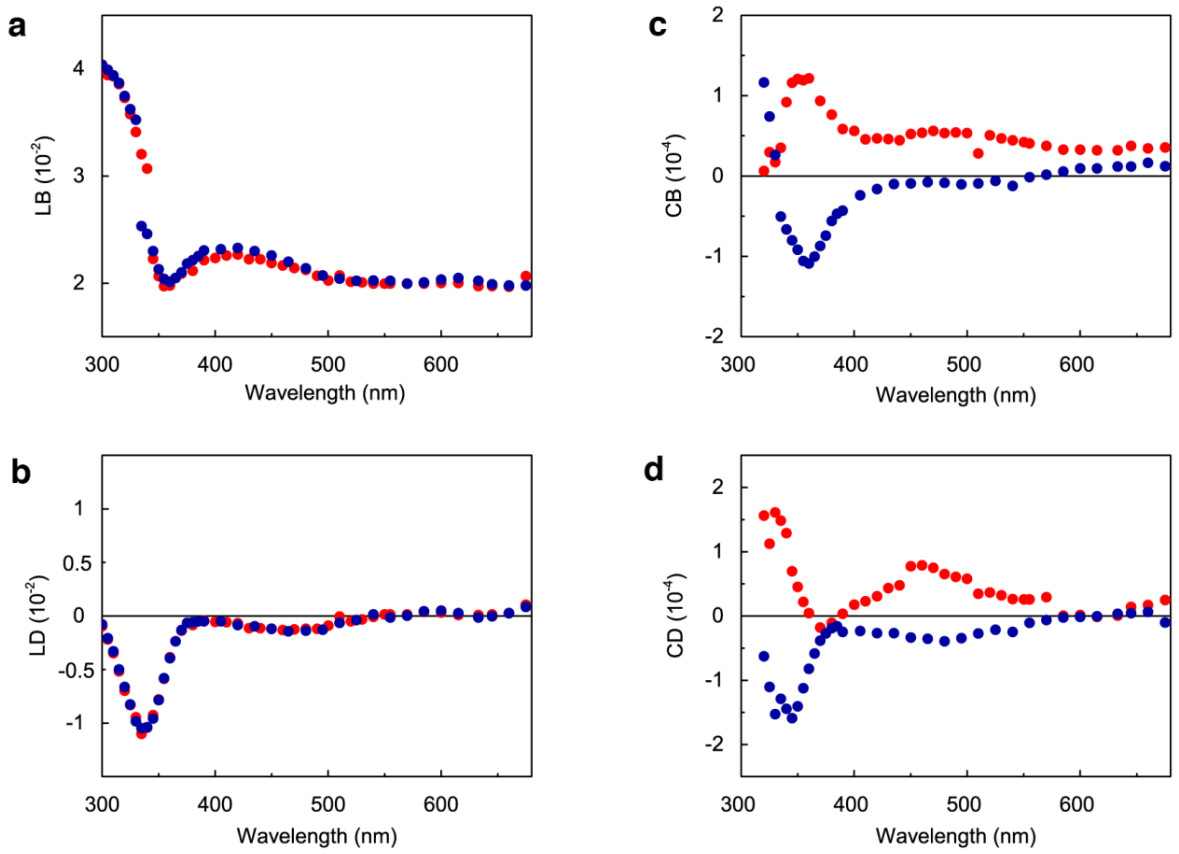

Figure 3.10. Anisotropic optical and chiroptical spectra of enol-(*S*)-**1** (dark blue solid circles) and enol-(*R*)-**1** (red solid circles) crystals on the (001) face under continuous UV light irradiation at 365 nm: (a) LB, (b) LD, (c) CB, and (d) CD. Reprinted with permission from "Optical Activity and Optical Anisotropy in Photomechanical Crystals of Chiral Salicylidenephenylethylamines" by Takanabe, A; Tanaka, M.; Johmoto, K.; Uekusa, H.; Mori, T.; Koshima, H.; Asahi, T. *Journal of the American Chemical Society* **2016**, *138*, 15066–15077.[1] Copyright 2016 American Chemical Society.

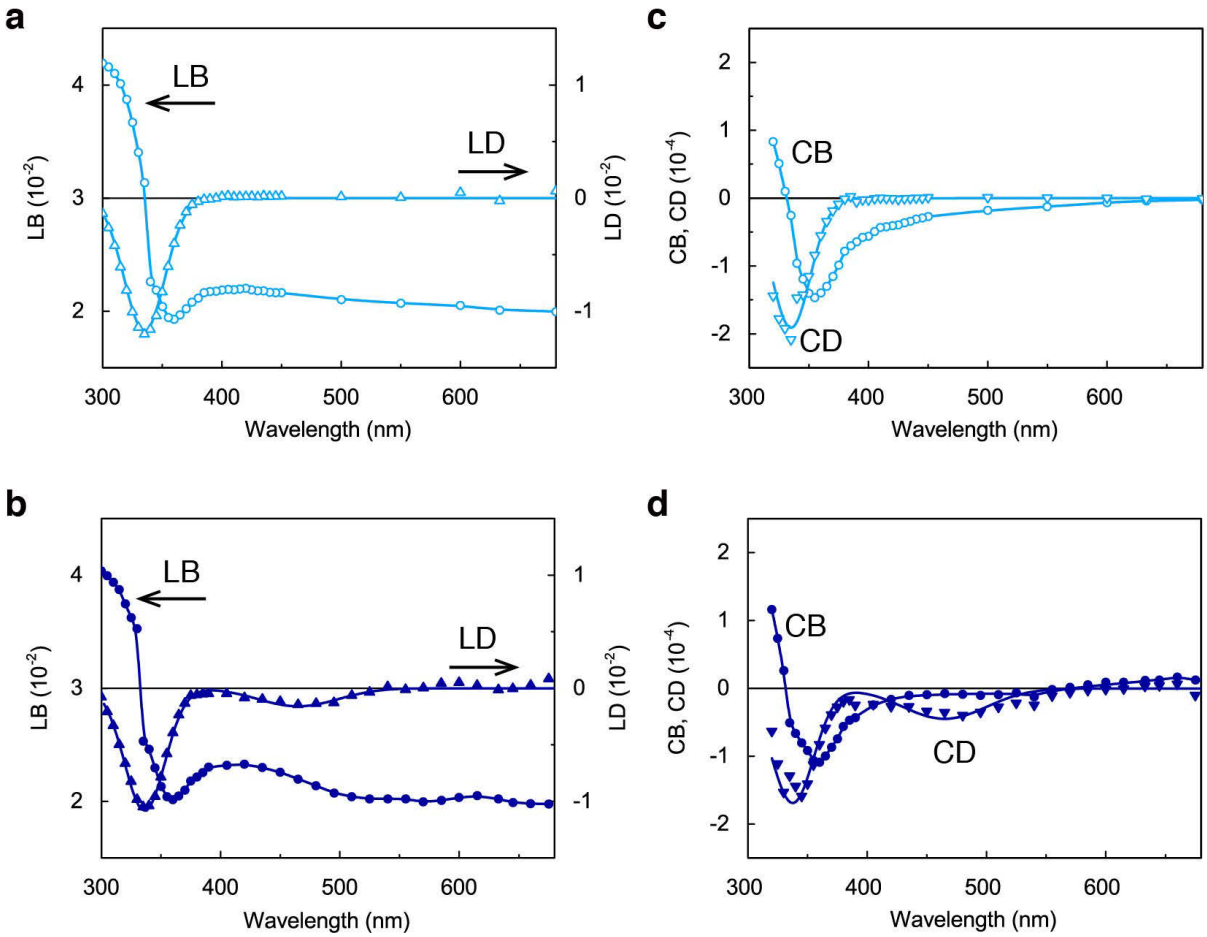

Figure 3.11. Optical anisotropic and chiroptical spectra of enol-(*S*)-**1** crystal on the (001) face: LB (left vertical axis, light blue circles) and LD (right vertical axis, light blue triangles) (a) without and (b) with UV irradiation: CB (dark blue circles) and CD (dark blue triangles) (c) without and (d) with UV irradiation. The curve lines of LB and CB are served as an eye guide, and those of LD and CD are fitted by Gaussian functions. All the graphs indicate that the Kramers–Kronig relationship hold between (a, b) the LD and LB as well as (c, d) the CD and CB before and under continuous UV irradiation. Reprinted with permission from "Optical Activity and Optical Anisotropy in Photomechanical Crystals of Chiral Salicylidenephenylethylamines" by Takanabe, A; Tanaka, M.; Johmoto, K.; Uekusa, H.; Mori, T.; Koshima, H.; Asahi, T. *Journal of the American Chemical Society* **2016**, *138*, 15066–15077.[1] Copyright 2016 American Chemical Society.

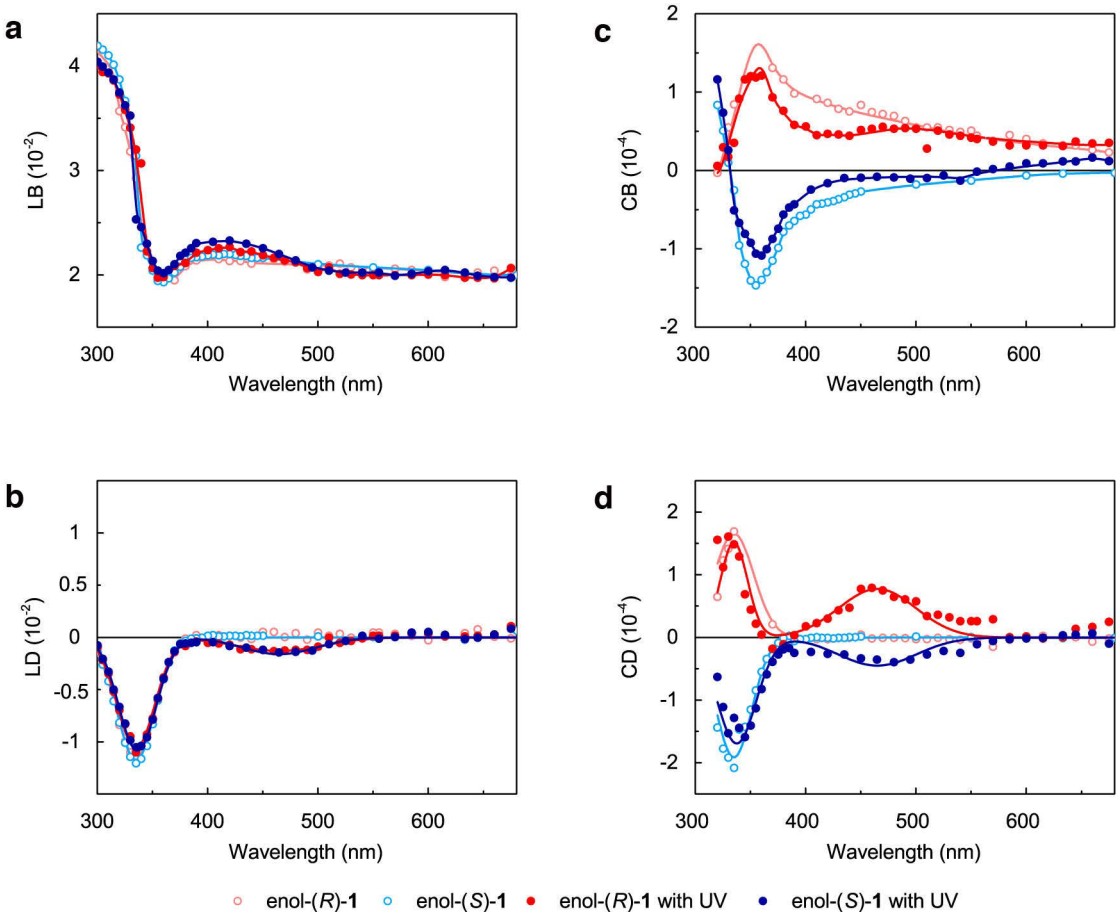

Figure 3.12. Optical anisotropic and chiroptical spectra of enol-(*S*)-**1** and enol-(*R*)-**1** crystals on the (001) face: (a) LB, (b) LD, (c) CB, and (d) CD. These properties were measured with the G-HAUP without and under continuous UV light irradiation at 365 nm. The curve lines are served as an eye guide (a, c) and are fitted by Gaussian functions (b, d). Reprinted with permission from "Optical Activity and Optical Anisotropy in Photomechanical Crystals of Chiral Salicylidenephenylethylamines" by Takanabe, A; Tanaka, M.; Johmoto, K.; Uekusa, H.; Mori, T.; Koshima, H.; Asahi, T. *Journal of the American Chemical Society* **2016**, *138*, 15066–15077.[1] Copyright 2016 American Chemical Society.

3.4.3 Relationship between Optical Properties and Crystal Structure

The linearly polarized UV-Vis absorption spectra of the enol-(*S*)-**1** crystal without and with UV irradiation yielded a maximum peak height in the (0°) polarization direction parallel to the *a* axis, and decreased as the polarization direction changed to yield the minimum absorption perpendicular (90°) to the *a* axis (Figure 3.6). This means that the direction of the electronic transition dipole moment as a single crystal are almost parallel to the *a* axis on the (001) face of the enol-(*S*)-**1** without and with UV irradiation (Figure 3.13). I calculated the orbitals of a single molecule of enol-(*S*)-**1** and *trans*-keto-(*S*)-**1** in a single crystal. I confirmed that the highest occupied molecular orbital (HOMO) and lowest unoccupied molecular orbital (LUMO) are related to the strongest absorption in enol-(*S*)-**1** and *trans*-keto-(*S*)-**1** at around 330 nm and 460 nm, respectively, and are of π type (Figure 3.14). Hence, strong absorptions induced by linearly polarized light in the polarization direction parallel to the *a* axis on the (001) face of the enol-(*S*)-**1** crystal without and with UV irradiation are mainly affected by the directions of the π–π* transition dipole moments of the enol-(*S*)-**1** and *trans*-keto-(*S*)-**1** crystals.

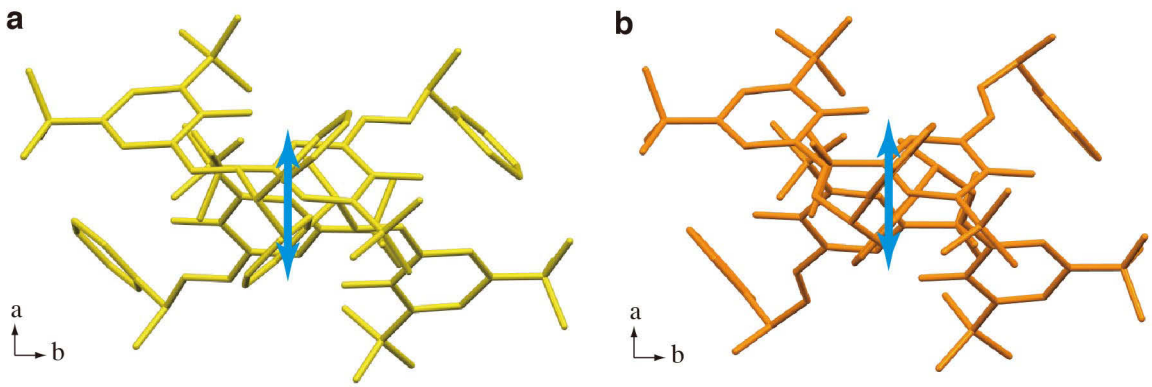

Figure 3.13. Molecular arrangements of (a) enol-(*S*)-**1** and (b) *trans*-keto-(*S*)-**1** crystals on the (001) plane. The both crystal structures are obtained from the DFT-D calculation. All hydrogen atoms are omitted for clarity. The direction of the electronic transition dipole moment as a single crystal might be almost parallel to the *a* axis.

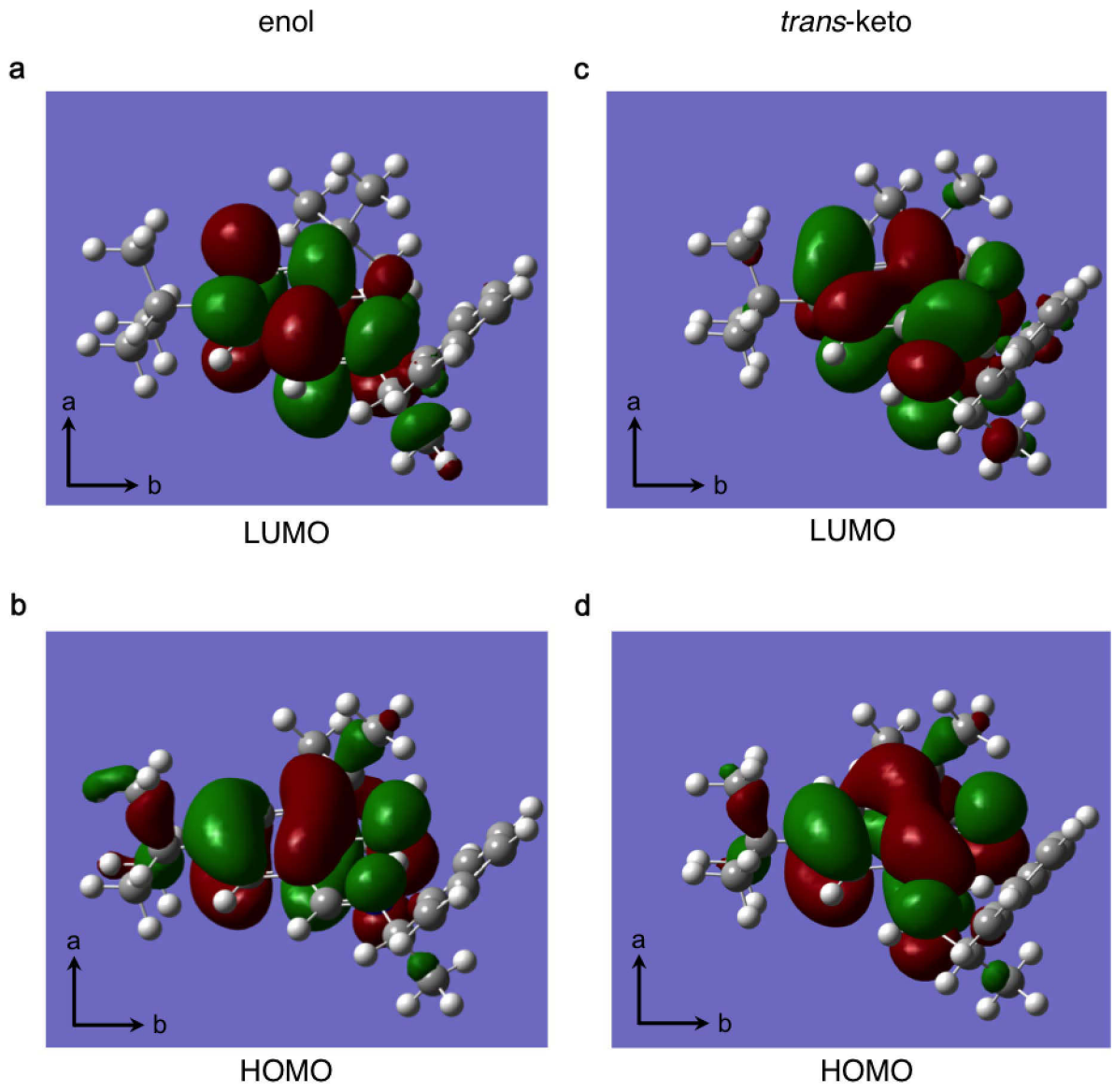

Figure 3.14. Visualization of (b, d) HOMO and (a, c) LUMO orbitals involved in the electronic transitions of calculated (a, b) enol-(*S*)-**1** and (c, d) *trans*-keto-(*S*)-**1**. All molecules are projected on the (001) face. Reprinted with permission from "Optical Activity and Optical Anisotropy in Photomechanical Crystals of Chiral Salicylidenephenylethylamines" by Takanabe, A; Tanaka, M.; Johmoto, K.; Uekusa, H.; Mori, T.; Koshima, H.; Asahi, T. *Journal of the American Chemical Society* **2016**, *138*, 15066–15077.[1] Copyright 2016 American Chemical Society.

I examined the correlation between the photomechanical motion of enol-(*S*)-**1** crystal and the polarization direction of irradiated UV light. Figure 3.15a shows the frontal (010) face with the longitudinal direction along the *a* axis, whose lower portion was fixed to the needle with an adhesive and the upper portion was free. Upon irradiation from left with linearly polarized UV light at 365 nm almost parallel to the *a* axis, the plate-like crystal (4,516 μm long × 380 μm wide × 97 μm thick) bent (Figure 3.15b). According to the relationship between the direction of twisting and the face of enol-(*S*)-**1** crystal irradiated with UV light (Figure 2.4), the irradiated face was determined to be the $(00\bar{1})$ face. On the other hand, polarized UV light almost perpendicular to the *a* axis did not induce any bending motion (Figure 3.15c). I shortly explored the possible mechanism of this bending with twisting motion of thin platelike enol-(*S*)-**1** crystal depending on the polarization direction of linearly polarized light. Upon linearly polarized UV irradiation of the $(00\bar{1})$ face almost parallel to the *a* axis, both the length and width along the *a* and *b* axes shrink to the diagonal direction near the irradiated surface due to the photoisomerization to the *trans*-keto-(*S*)-**1** molecules. In contrast, both the length and the width do not change at the back surface due to lack of penetration of the irradiated light and no occurrence of photoisomerization. Hence the wide platelike crystal bends towards the light source with twisting motion in right-handed helix (Figure 3.15b). Upon linearly polarized UV irradiation of the $(00\bar{1})$ face almost perpendicular to the *a* axis, both the length and width along the *a* and *b* axes change a very little near the irradiated surface due to the low photoisomerization to the *trans*-keto-(*S*)-**1** molecules. Similarly, both the length and the width do not change at the back surface due to lack penetration of the irradiated light. Hence the wide platelike crystal scarecely bends towards the light source (Figure 3.15c).

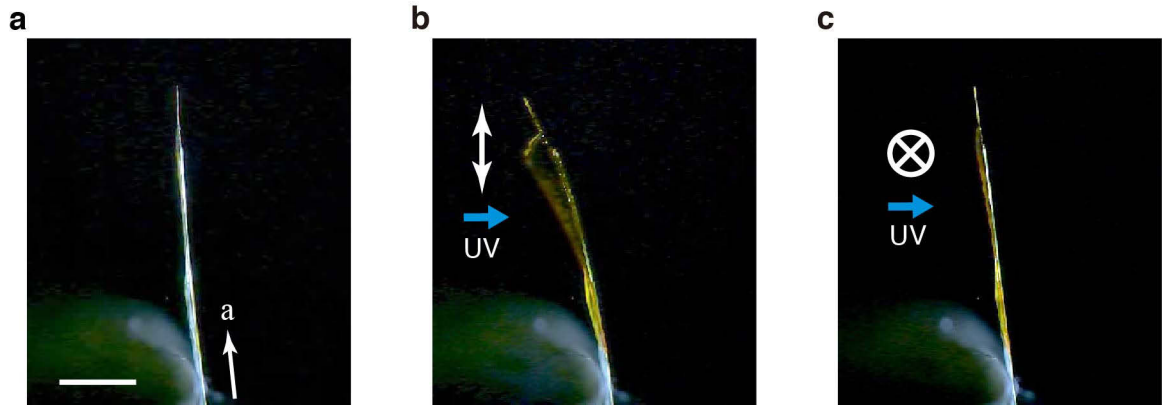

Figure 3.15. Bending behavior of a platelike enol-(*S*)-**1** crystal (4516 μm long × 380 μm wide × 97 μm thick) (a) before and upon irradiation from left to the $(00\bar{1})$ face with (b) linearly polarized UV light parallel and (c) perpendicular polarization direction to the *a* axis. The scale bar is 1 mm. Reprinted with permission from "Optical Activity and Optical Anisotropy in Photomechanical Crystals of Chiral Salicylidenephenylethylamines" by Takanabe, A; Tanaka, M.; Johmoto, K.; Uekusa, H.; Mori, T.; Koshima, H.; Asahi, T. *Journal of the American Chemical Society* **2016**, *138*, 15066–15077.[1] Copyright 2016 American Chemical Society.

LD spectra were independently calculated from the linearly polarized UV-Vis absorption spectra (Figure 3.6) by:

$$\mathrm{LD} = \frac{\lambda}{4\pi d}[-\ln \Gamma_{\perp} - (-\ln \Gamma_{\parallel})],$$

where λ, d, and Γ are wavelength, sample thickness parallel to the direction of the incident light, and the ratio of intensity of transmitted light to intensity of incident light, respectively. The subscripts $\parallel$ and $\perp$ are the polarization directions of incident linearly polarized light parallel and perpendicular to the orientation axis, respectively.[29] For the enol-(*S*)-**1** crystal, $\parallel$ and $\perp$ corresponded to the *a* and *b* axes on the (001) plane, respectively. Figure 3.16 shows the calculated LD spectra of enol-(*S*)-**1** crystal before and under continuous UV irradiation at 365 nm. The signs of both LD peaks at 330 nm and 460 nm were negative, which were coincident with those obtained by the HAUP measurements (Figures 3.7b and 3.10b).

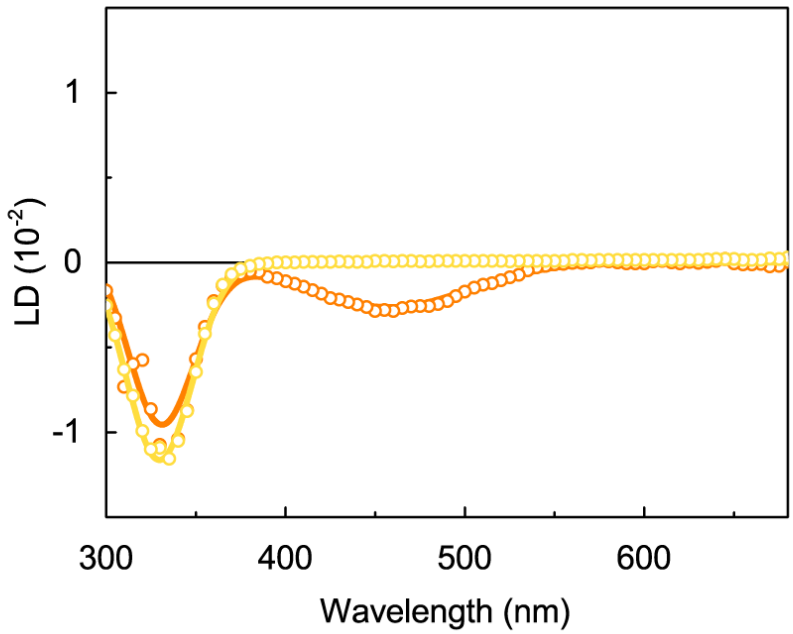

Figure 3.16. LD spectra of the enol-(*S*)-**1** crystal before (black open triangles) and under continuous UV light irradiation (black solid triangles) calculated from the linearly polarized absorption spectra in Figure 3.6. Reprinted with permission from "Optical Activity and Optical Anisotropy in Photomechanical Crystals of Chiral Salicylidenephenylethylamines" by Takanabe, A; Tanaka, M.; Johmoto, K.; Uekusa, H.; Mori, T.; Koshima, H.; Asahi, T. *Journal of the American Chemical Society* **2016**, *138*, 15066–15077.[1] Copyright 2016 American Chemical Society.

The conversion of photoisomerization of enol-(*S*)-**1** to *trans*-keto-(*S*)-**1** was calculated to be 18±3.2% by comparison with the LD values fitted by Gaussian functions (Figure 3.16) at 330 nm, before and under continuous UV irradiation. On the other hand, the conversions of enol-(*S*)-**1** and enol-(*R*)-**1** crystals from the LD spectra by the HAUP measurement (Figures 3.7b and 3.10b) were calculated to be 10±1.1% and 8.4±3.4%, respectively. The smaller conversions are probably caused by the lower power (5 mW cm^{-2}) of the irradiated UV light in the HAUP measurement compared to that (10 mW cm^{-2}) in the measurement of the linearly polarized UV-Vis absorption spectra (Figure 3.16). Normally, the photoisomerization should reach the photostationary state under continuous UV irradiation. Assuming that the photoisomerization reaction proceeded completely to produce the *trans*-keto-(*S*)-**1** at 100% yield, the magnitudes of the LD peaks at 460 nm are estimated to be -1.55×10^{-2} and -1.47×10^{-2} from the conversions (18% and 10%) of enol-(*S*)-**1** by the linearly polarized light absorption measurement (Figure 3.16) and the HAUP measurement (Figures 3.17b), respectively, which are very similar.

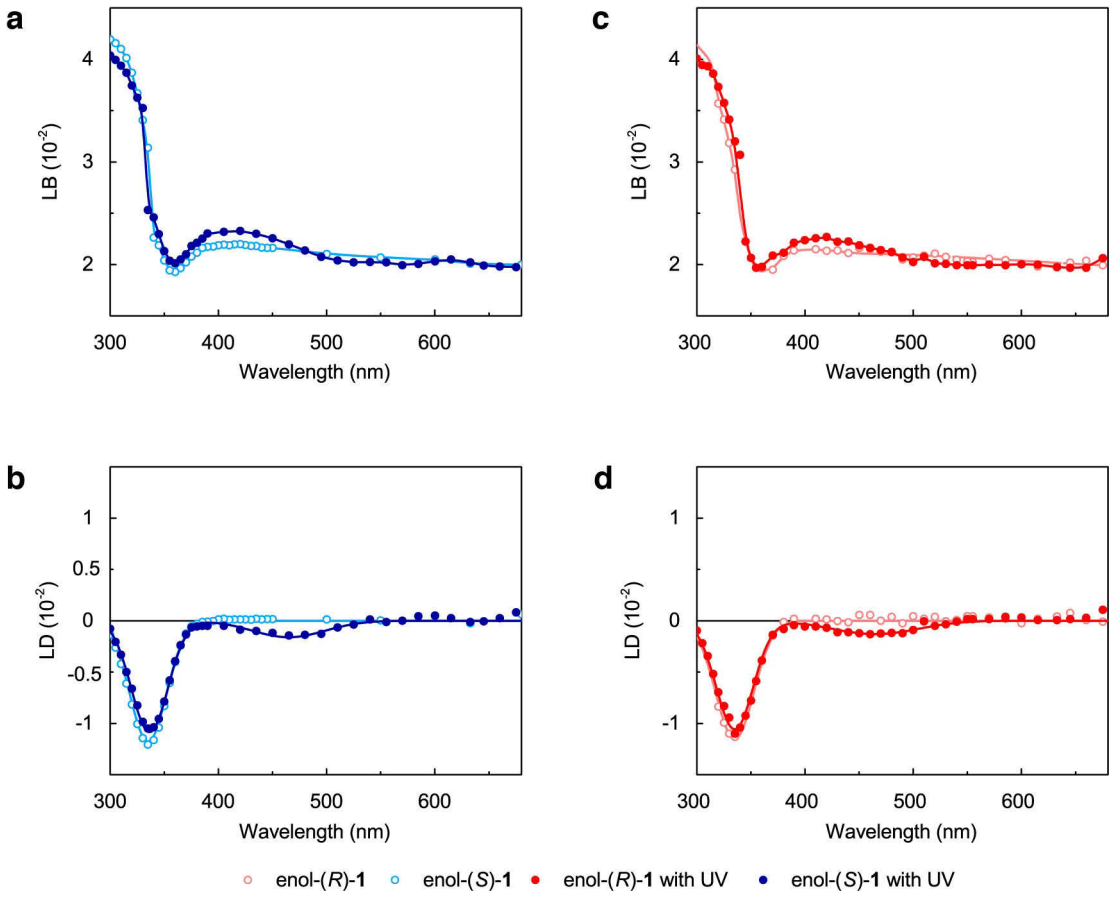

Figure 3.17. Optical anisotropic properties of (a, b) enol-(*S*)-**1** and (c, d) enol-(*R*)-**1** crystals on the (001) face: (a, c) LB and (b, d) LD without and with UV irradiation. The curve lines are served as an eye guide (a, c) and are fitted by Gaussian functions (b, d). Reprinted with permission from "Optical Activity and Optical Anisotropy in Photomechanical Crystals of Chiral Salicylidenephenylethylamines" by Takanabe, A; Tanaka, M.; Johmoto, K.; Uekusa, H.; Mori, T.; Koshima, H.; Asahi, T. *Journal of the American Chemical Society* **2016**, *138*, 15066–15077.[1] Copyright 2016 American Chemical Society.

The LB of both enantiomeric enol-**1** crystals along the *c* axis showed a relatively lower value (0.02) above 600 nm than the previously reported organic crystals (Table 3.1). As shown in the packing diagrams (Figure 3.18a and b) the total intermolecular interaction in the enol-(*S*)-**1** crystal along all directions is the Van der Waals force alone. This very weak molecular interaction may have induced such a small LB. In fact, a much larger value (0.4) for the LB of the chiral cocrystal composed of tryptamine and 4-chlorobenzoic acid have been reported (Table 3.1).[14] This cocrystal exhibits strong intermolecular interactions, such as the ionic bridging, hydrogen bonding, and the π–π interaction of the aromatic moieties. Under UV irradiation, the weak N–H···π intermolecular interaction is formed in the *trans*-keto-(*S*)-**1** (Figure 2.1c). However, the total intermolecular interactions along the *c* axis appear to be weak because molecular packing in the *trans*-keto-(*S*)-**1** crystal (Figure 3.18c and d) is similar to that of enol-(*S*)-**1** (Figures 3.18a and b). Hence, the differences in LB magnitudes above 600 nm of the enol-**1** crystals were small before and under continuous UV irradiation (Figures 3.18a and c).

Table 3.1. Linear birefringences and optical rotatory powers of organic crystals. Reprinted with permission from "Optical Activity and Optical Anisotropy in Photomechanical Crystals of Chiral Salicylidenephenylethylamines" by Takanabe, A; Tanaka, M.; Johmoto, K.; Uekusa, H.; Mori, T.; Koshima, H.; Asahi, T. *Journal of the American Chemical Society* **2016**, *138*, 15066–15077.[1] Copyright 2016 American Chemical Society.

crystal	λ (nm)	LB (10^{-2})	ρ (deg mm^{-1})	Ref.
(*S*)-salicylidenephenylethylamine	632.8	2.0	ρ_3 –5.2	this work
M-cocrystal: tryptamine/4-chlorobenzoic acid	632.8	18.5	ρ_1 +138	14
		21.1	ρ_2 –56	
		39.7	ρ_3 –355	
oxo amide	496.5	14.4	ρ_1 –79	30
		11.1	ρ_2 –32	
		3.4	ρ_3 –68	
L-glutamic acid	632.8	12.1	ρ_1 –31	31
		11.0	ρ_2 –98	
		0.9	ρ_3 +5.4	
L-aspartic acid	632.8	10.1	ρ_1 +223	32
		2.5	ρ_2 –19	
		12.7	ρ_3 –31	
Rochelle salt $NaKC_4H_4O_6 \cdot 4H_2O$	632.8	0.12	ρ_1 –1.0	33
lysozyme	488	0.24	ρ_1 –2.1	34
		0.24	ρ_3 +2.5	
azobenzene derivative intercalated into $K_4Nb_6O_{17}$	450	0.25	+0.1	7
laminated collagen membrane	300	0.88	–20	10

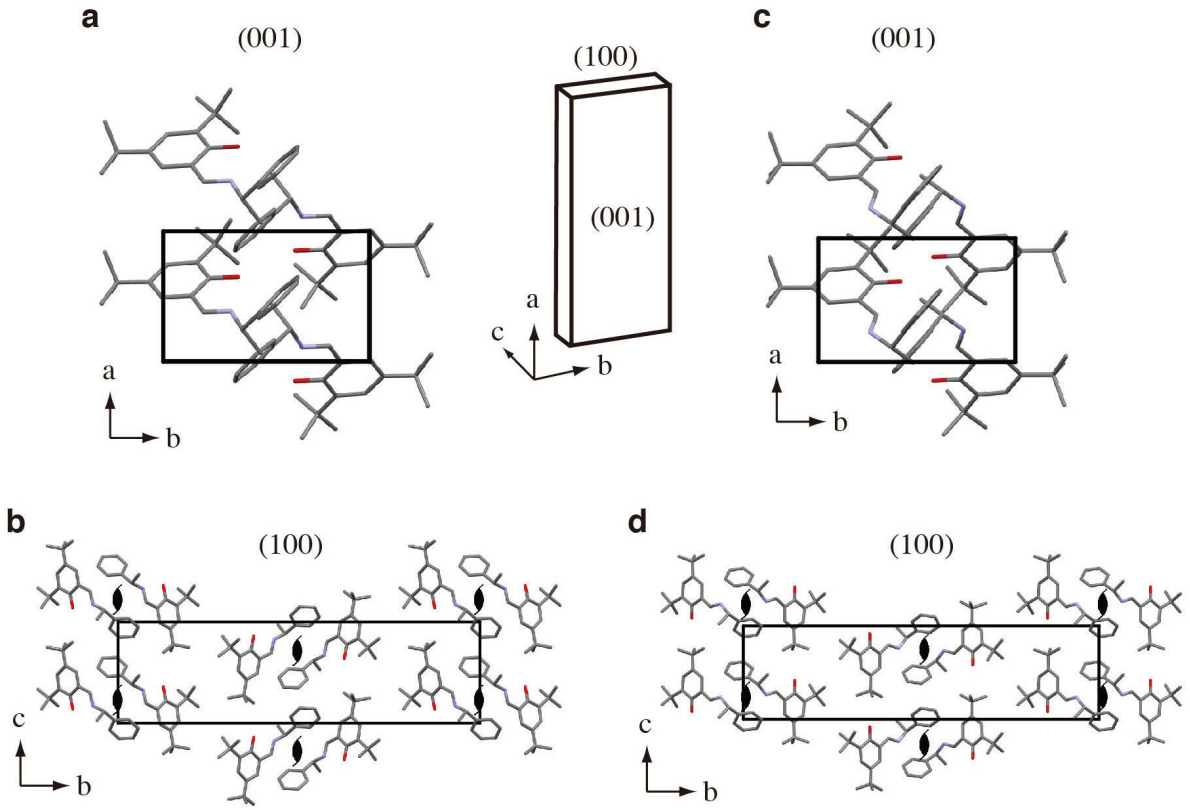

Figure 3.18. Molecular arrangements of (a,b) enol-(*S*)-**1** and (c,d) *trans*-keto-(*S*)-**1** crystals on (a,c) (001) and (b,d) (100) planes. The both crystal structures are obtained from the DFT-D calculation. All hydrogen atoms are omitted for clarity. Reprinted with permission from "Optical Activity and Optical Anisotropy in Photomechanical Crystals of Chiral Salicylidenephenylethylamines" by Takanabe, A; Tanaka, M.; Johmoto, K.; Uekusa, H.; Mori, T.; Koshima, H.; Asahi, T. *Journal of the American Chemical Society* **2016**, *138*, 15066–15077.[1] Copyright 2016 American Chemical Society.

Upon UV irradiation of the enol-(*S*)-**1** crystal, strain and stress are generated by changes in unit cell sizes due to photoisomerization to *trans*-keto-(*S*)-**1** near the crystal surface. The strain and stress values have been reported to be –0.31 % and 0.68 MPa, respectively.[26] Despite the total prevention of bending motion by fixing the crystal to a thin Cu plate with silicon grease for the HAUP measurement, internal stress should arise even under weak UV irradiation (5 mW cm^{-2}), and thereby the observed LB (Figure 3.10a) might include the birefringence caused by stress. However, it is suggested that the stress birefringence along the *c* axis might be very small due to the high similarity between LB values above 600 nm before and under UV irradiation (Figure 3.12a).

As an expression of optical activity in solution, specific optical rotation (α) has been commonly used instead of CB in chemistry and biochemistry.[14] Hence, the ORP (ρ) is calculated from eq 3.14 to compare the obtained CB value with the data in the previous report. ORP spectra of enol-(*S*)-**1** and enol-(*R*)-**1** crystals are shown in Figure 3.19a. The signs of ORP dispersion along the *c* axis are opposite to those in the hexane solution, which represents the signs averaged from every direction (Figures 3.20). In hexane, optical rotation spectra of enol-(*S*)-**1** and enol-(*R*)-**1** exhibited anomalous dispersions of positive and negative peaks at 351 nm with change in signs at the positive and negative CD peaks at 331 nm, respectively. A strong absorption peak at 328 nm was observed. This suggests that the contribution from the ORP dispersion along the *c* axis might be small, or the ORP dispersions along the *a* and/or *b* axes might be largely positive in sign.

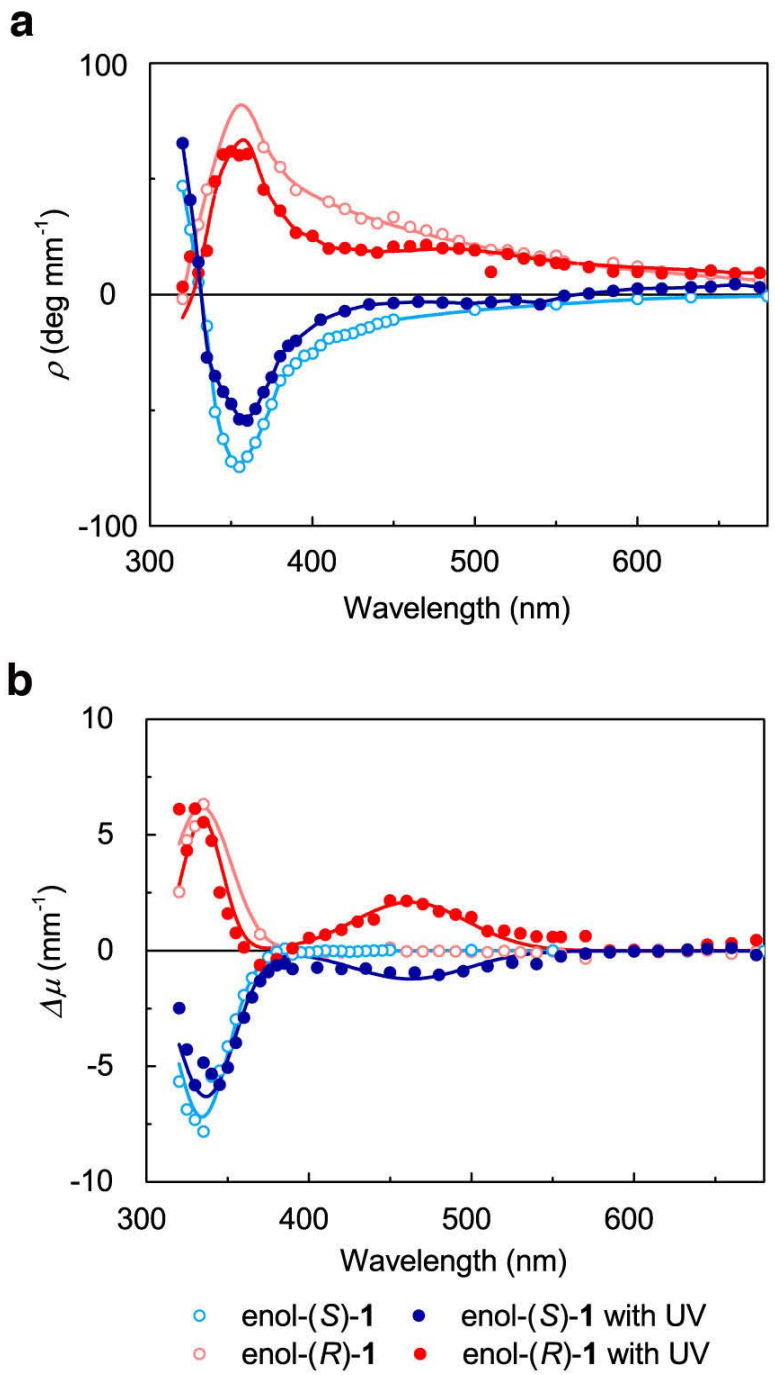

Figure 3.19. (a) ORP and (b) CD spectra of enol-(*S*)-**1** and enol-(*R*)-**1** crystals on the (001) face before and under continuous UV irradiation. Reprinted with permission from "Optical Activity and Optical Anisotropy in Photomechanical Crystals of Chiral Salicylidenephenylethylamines" by Takanabe, A; Tanaka, M.; Johmoto, K.; Uekusa, H.; Mori, T.; Koshima, H.; Asahi, T. *Journal of the American Chemical Society* **2016**, *138*, 15066–15077.[1] Copyright 2016 American Chemical Society.

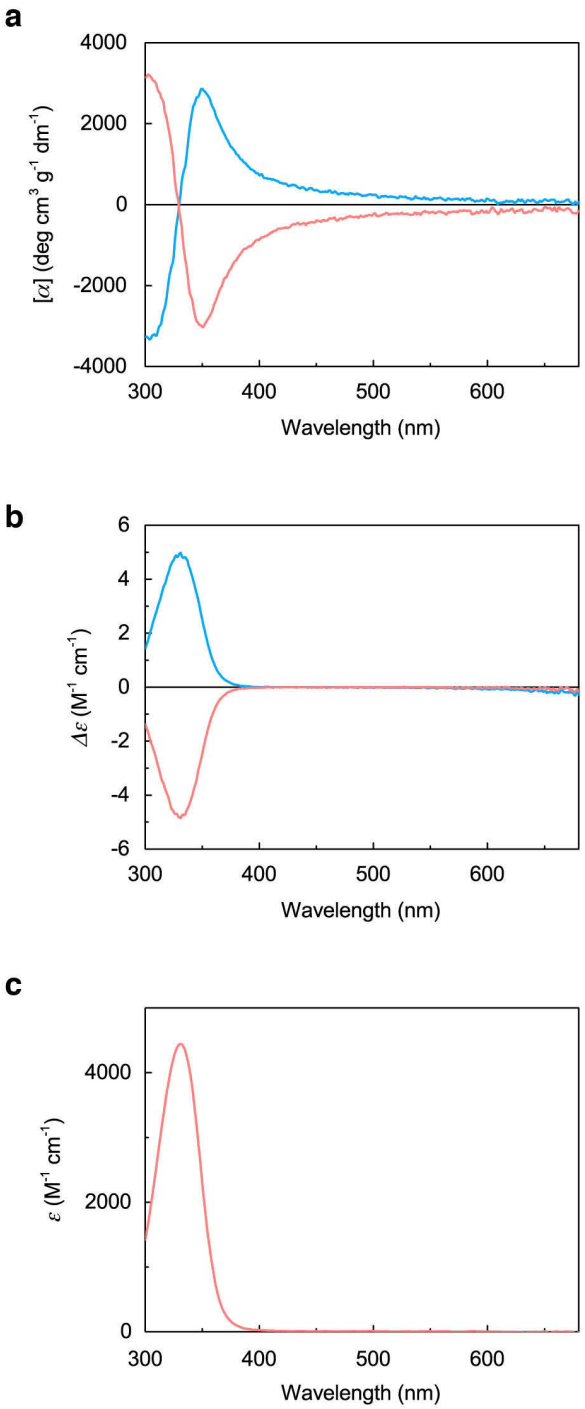

Figure 3.20. (a) Optical rotation, (b) CD, and (c) UV-Vis absorption spectra of enol-(*S*)-**1** (blue) and enol-(*R*)-**1** (pink) in hexane. Concentration is 0.016 g (100 mL)$^{-1}$. Reprinted with permission from "Optical Activity and Optical Anisotropy in Photomechanical Crystals of Chiral Salicylidenephenylethylamines" by Takanabe, A; Tanaka, M.; Johmoto, K.; Uekusa, H.; Mori, T.; Koshima, H.; Asahi, T. *Journal of the American Chemical Society* **2016**, *138*, 15066–15077.[1] Copyright 2016 American Chemical Society.

The ρ value of enol-(*S*)-**1** crystals along the *c* axis at 632.8 nm before UV irradiation was calculated to be –5.2 deg mm^{-1} after compensating the baseline by (S–R)/2, because the baseline of ORP spectra (Figure 3.19a) of enol-(*S*)-**1** and enol-(*R*)-**1** is shifted slightly to the positive. The ρ value seems smaller than in previous reports of organic crystals, as shown in Table 3.1. From eq 3.14, the magnitude of ORP is directly proportional to the magnitude of LB and *k*. Therefore, a small ORP should be induced by small LB and *k* values.

Molar CD, $\Delta\varepsilon$ (absorbance difference between right and left circularly polarized light at 1 M and 1 cm path length) has been commonly used as a unit of CD in solution. Herein I use $\Delta\mu$ (absorbance per 1 mm thickness) as an expression of CD in a crystal. CD is calculated as:

$$\mathrm{CD} = \frac{\lambda}{4\pi d}[-\ln \Gamma_l - (-\ln \Gamma_r)],$$

where the subscripts *r* and *l* are the incident right and left circular polarized light, respectively. Then, the $\Delta\mu$ can be calculated as:

$$\Delta\mu = \frac{1}{d}[-\ln \Gamma_l - (-\ln \Gamma_r)] = \frac{4\pi}{\lambda}\mathrm{CD},$$

The $\Delta\mu$ spectra of enol-(*S*)-**1** and enol-(*R*)-**1** crystals are shown in Figure 3.19b. The signs of both CD ($\Delta\mu$) peaks at 330 nm are opposite to those in the hexane solution, as shown in Figure 3.20b.

The conversions of enol-(*S*)-**1** and enol-(*R*)-**1** to *trans*-keto-(*S*)-**1** and *trans*-keto-(*R*)-**1** were calculated to be 15±3.9% and 13±10%, respectively, by comparison with the CD spectra (Figure 3.12d) at 330 nm by the HAUP measurement, i.e., almost comparable. On the other hand, as mentioned above, the conversions of enol-(*S*)-**1** and enol-(*R*)-**1** calculated from the LD spectra (Figures 3.16b and d) by the HAUP measurement were 10% and 8.4%, respectively, showing different conversion values from the CD spectra. After the 3 days required for HAUP measurement, the sample thickness decreased due to gradual sublimation under UV light irradiation. The deterioration of the surface condition of the sample may have

affected the accuracy of the HAUP measurement, especially in CD and CB due to the very small order of 10^{-4} (Figures 3.7c and d; 3.10c and d). Therefore, it might be desirable to adopt 10% and 8.4% as the conversions calculated from the LD spectra.

The CD and UV-Vis spectra of isolated molecule **1** were simulated by the combined quantum chemical calculations. The geometries of enol-(*S*)-**1**, *cis*-keto-(*S*)-**1** and *trans*-keto-(*S*)-**1** were optimized using the dispersion-corrected DFT method at the DFT-D3(BJ)-TPSS/def2-TZVP level.[22] The geometry thus obtained for the enol form was found to be generally consistent with that obtained by the X-ray crystallographic structure (Table 3.2).[26] The rotational strengths were then calculated by the time-dependent approximate coupled cluster method (RI-CC2/def2-TZVP).[23] The CD and UV-Vis spectra were simulated by overlapping Gaussian functions for each transition, where the width of the band at 1/e height is fixed at 0.4 eV and the excitation energies were red-shifted by 0.3 eV (Figure 3.21).[20]

The calculated CD and UV-Vis spectra for the enol-(*S*)-**1** reproduced the solution experiment results well (Figure 3.20). The calculated CD spectrum for *trans*-keto-(*S*)-**1** exhibits the positive Cotton effect at 460 nm, same sign for enol-(*S*)-**1** at 330 nm. Conversely, *cis*-keto-(*S*)-**1** exhibits the negative Cotton effect at 440 nm. As the signs of Cotton effects of enol-(*S*)-**1** with UV irradiation at 330 nm and 460 nm obtained by the HAUP measurement are same, the Cotton effect of *cis*-keto-(*S*)-**1** might not contribute to the results obtained using HAUP with UV irradiation. This may be because the *cis*-keto form was not generated upon photoirradiation. This explanation is consistent with the previous report on photoisomerization of salicylideneaniline.[35]

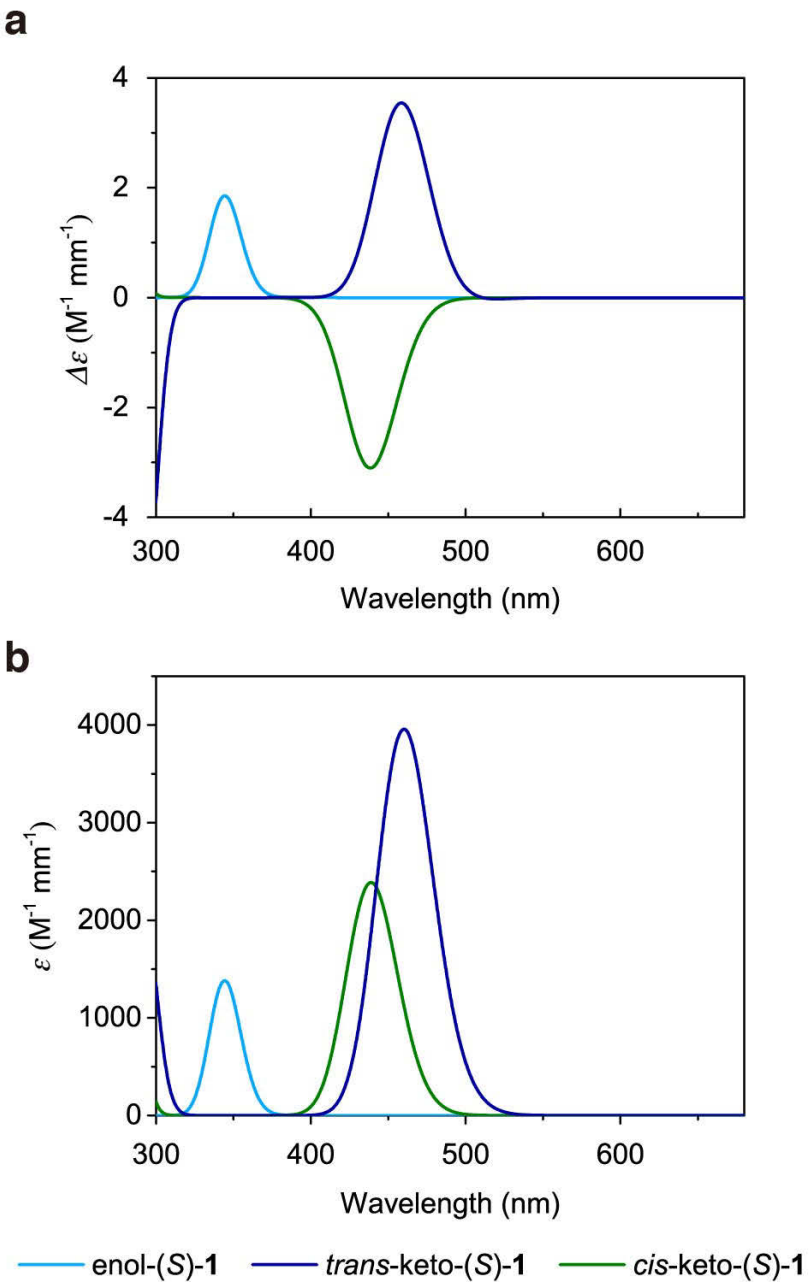

Figure 3.21. Calculated (a) CD and (b) UV-Vis absorption spectra of (*S*)-**1** molecule. Reprinted with permission from "Optical Activity and Optical Anisotropy in Photomechanical Crystals of Chiral Salicylidenephenylethylamines" by Takanabe, A; Tanaka, M.; Johmoto, K.; Uekusa, H.; Mori, T.; Koshima, H.; Asahi, T. *Journal of the American Chemical Society* **2016**, *138*, 15066–15077.[1] Copyright 2016 American Chemical Society.

Finally, I discuss the dissymmetry parameter, g ($|\Delta\mu|/\mu$), in the crystalline state. The g value of enol-(*S*)-**1** crystal along the c axis was calculated to be 0.013 from the $|\Delta\mu|$ (6.9 mm^{-1}) of the negative CD peak at 330 nm (Figure 3.19b) and the μ (551 mm^{-1}) of the linearly polarized absorption peak parallel to the a axis at 330 nm (Figure 3.6a). On the other hand, the g value of enol-(*S*)-**1** in hexane solution was calculated to be 0.0010 from Figures 3.20a and b, and the g value from the calculated CD and absorption (Figure 3.21) was 0.0016, revealing that the g value of enol-(*S*)-**1** crystal obtained by the HAUP measurement without UV irradiation is around 10 times larger than g values in the solution and by the calculation. To our knowledge, this is the first report of a comparison of the g value of a single crystal along the crystal axis, not the optic axis, with that in solution and by calculation. For reference, the g value of L-alanine of the thin deposited film, not a single crystal, has been reported to be 0.0091 at 184 nm,[36] which is around 45 times larger than the g value in solution (0.0002).[37,38] In conclusion, the intermolecular and intramolecular interactions in crystalline state might enhance the dissymmetry parameter, g.

Table 3.2. Cartesian atomic positions for enol-(*S*)-**1** generated from the calculated crystal structure. Reprinted with permission from "Optical Activity and Optical Anisotropy in Photomechanical Crystals of Chiral Salicylidenephenylethylamines" by Takanabe, A; Tanaka, M.; Johmoto, K.; Uekusa, H.; Mori, T.; Koshima, H.; Asahi, T. *Journal of the American Chemical Society* **2016**, *138*, 15066–15077.[1] Copyright 2016 American Chemical Society.

atom	x (Å)	y (Å)	z (Å)
C	3.003	6.139	13.488
C	2.184	6.963	12.67
C	1.445	6.386	11.607
C	1.559	5.008	11.439
H	0.987	4.542	10.639
C	2.362	4.166	12.233
C	3.084	4.759	13.252
H	3.722	4.172	13.91
C	3.77	6.704	14.569
H	4.41	6.021	15.151
C	3.77	9.348	16.873
C	4.043	9.274	18.24
H	4.78	8.557	18.598
C	3.385	10.104	19.147
H	3.616	10.028	20.21
C	2.439	11.02	18.688
H	1.929	11.685	19.386
C	2.145	11.089	17.326
H	1.404	11.801	16.965

atom	x (Å)	y (Å)	z (Å)
C	2.805	10.254	16.427
H	2.566	10.296	15.366
C	4.57	8.509	15.9
H	5.046	7.68	16.458
C	5.671	9.355	15.248
H	5.215	10.148	14.639
H	6.304	8.737	14.598
H	6.293	9.818	16.022
C	0.581	7.244	10.681
C	1.471	8.275	9.961
H	0.851	8.9	9.301
H	2.227	7.767	9.346
H	1.982	8.927	10.677
C	–0.517	7.963	11.485
H	–1.176	7.232	11.973
H	–1.133	8.571	10.805
H	–0.095	8.621	12.252
C	–0.117	6.403	9.607
H	–0.798	5.66	10.048
H	0.606	5.882	8.961
H	–0.717	7.068	8.971
C	2.383	2.667	11.967
C	0.976	2.093	12.205
H	0.964	1.01	12.018

atom	x (Å)	y (Å)	z (Å)
H	0.238	2.57	11.543
H	0.663	2.265	13.246
C	2.807	2.404	10.514
H	2.126	2.89	9.802
H	2.799	1.324	10.308
H	3.82	2.79	10.332
C	3.365	1.94	12.888
H	4.392	2.305	12.744
H	3.347	0.865	12.67
H	3.094	2.083	13.942
N	3.723	7.973	14.846
O	2.133	8.288	12.917
H	2.762	8.45	13.741

Table 3.3. Cartesian atomic positions for *trans*-keto-(*S*)-**1** generated from the calculated crystal structure. Reprinted with permission from "Optical Activity and Optical Anisotropy in Photomechanical Crystals of Chiral Salicylidenephenylethylamines" by Takanabe, A; Tanaka, M.; Johmoto, K.; Uekusa, H.; Mori, T.; Koshima, H.; Asahi, T. *Journal of the American Chemical Society* **2016**, *138*, 15066–15077.[1] Copyright 2016 American Chemical Society.

atom	x (Å)	y (Å)	z (Å)
C	2.939	6.56	13.612
C	2.103	7.271	12.62
C	1.378	6.437	11.663
C	1.513	5.077	11.764
H	0.972	4.453	11.055
C	2.327	4.386	12.722
C	3.034	5.138	13.62
H	3.67	4.653	14.364
C	3.63	7.398	14.475
H	3.48	8.462	14.288
C	4.258	8.832	17.265
C	4.425	8.636	18.639
H	5.193	7.948	18.998
C	3.629	9.32	19.562
H	3.795	9.169	20.629
C	2.651	10.211	19.117
H	2.038	10.759	19.833
C	2.475	10.411	17.746
H	1.723	11.119	17.394

atom	x (Å)	y (Å)	z (Å)
C	3.272	9.726	16.832
H	3.129	9.908	15.77
C	5.165	8.124	16.269
H	5.917	7.562	16.841
C	5.878	9.115	15.35
H	5.16	9.687	14.749
H	6.564	8.604	14.661
H	6.444	9.83	15.957
C	0.568	7.093	10.552
C	1.545	7.864	9.646
H	0.995	8.312	8.81
H	2.299	7.18	9.232
H	2.053	8.661	10.203
C	–0.501	8.045	11.117
H	–1.202	7.498	11.76
H	–1.08	8.474	10.285
H	–0.05	8.86	11.691
C	–0.158	6.065	9.684
H	–0.87	5.469	10.273
H	0.538	5.383	9.175
H	–0.73	6.59	8.906
C	2.333	2.867	12.677
C	0.899	2.344	12.866
H	0.897	1.248	12.798

atom	x (Å)	y (Å)	z (Å)
H	0.216	2.74	12.103
H	0.519	2.637	13.855
C	2.869	2.379	11.321
H	2.266	2.767	10.489
H	2.84	1.281	11.289
H	3.905	2.713	11.17
C	3.196	2.258	13.779
H	4.246	2.559	13.676
H	3.137	1.165	13.688
H	2.837	2.559	14.776
N	4.449	7.097	15.486
O	2.039	8.534	12.613
H	4.686	6.119	15.687

3.5 Conclusions

Optical anisotropic and chiroptical spectra of the chiral photomechanical enol-(*S*)-**1** and enol-(*R*)-**1** crystals on the (001) face were simultaneously measured using the G-HAUP before and under continuous UV light irradiation. The HAUP measurement was achieved by the careful preparation of thin (< 10 mm) plate-like crystals by gentle sublimation, and by the prevention of crystal bending under UV irradiation by fixing the crystal to the sample plate with silicon grease. The CD spectra of the S and R crystals revealed a negative and positive Cotton effect, respectively at 330 nm, and new peaks appeared at 460 nm under UV light irradiation due to the photoisomerization to the S and R *trans*-keto isomers. The magnitudes of CB and CD were around 10^{-4}, i.e., smaller by two orders than those of LB and LD (around 10^{-2}). The Kramers–Kronig relationship held between the LB and the LD, as well as the CB and the CD, before and under continuous UV irradiation. The CB and CD spectra obtained by the HAUP measurement were the opposite of those measured in the hexane solution, and those simulated by quantum chemical calculation. The dissymmetry parameter (g) value of the crystal along the c axis was around 10 times larger than those in the solution and by calculation. This demonstrates that the dissymmetry parameter could be enhanced by intramolecular and intermolecular interactions in the crystals. In this study, the long measurement time caused a slight deterioration of crystal samples. Improvement of the G-HAUP apparatus is required to shorten the measurement time.

3.6 References

(1) Takanabe, A; Tanaka, M.; Johmoto, K.; Uekusa, H.; Mori, T.; Koshima, H.; Asahi, T. *J. Am. Chem. Soc.* **2016**, *138*, 15066–15077.

(2) Kobayashi, J.; Uesu, Y. *J. Appl. Cryst.* **1983**, *16*, 204–211.

(3) Kobayashi, J.; Kumomi, H.; Saito, K. *J. Appl. Crystallogr.* **1986**, *19*, 377–381.

(4) Kobayashi, J.; Asahi, T.; Takahashi, S.; Glazer, A. M. *J. Appl. Crystallogr.* **1988**, *21*, 479–484.

(5) Kobayashi, J.; Asahi, T.; Sakurai, M.; Takahashi, M.; Okubo, K.; Enomoto, Y. *Phys. Rev. B* **1996**, *53*, 11784–11790.

(6) Asahi, T.; Osaka, T.; Kobayashi, J. *Proc. SPIE* **2001**, *4467*, 20–30.

(7) Tanaka, M.; Nakamura, N.; Koshima, H.; Asahi, T. *J. Phys. D: Appl. Phys.* **2012**, *45*, 175303 (8pp).

(8) Asahi, T.; Osaka, T.; Abrahams, S. C.; Miyazaki, R.; Asai, H.; Nanamatsu, S.; Kobayashi, J. *Proc. SPIE* **2003**, *5218*, 223–232.

(9) Matsuki, R.; Asahi, T.; Kobayashi, J.; Asai, H. *Chirality* **2004**, *16*, 286-293.

(10) Nakagawa, K.; Harper-Lovelady, H.; Tanaka, Y.; Tanaka, M.; Yamato, M.; Asahi, T. *Chem. Commun.* **2014**, *50*, 15086–15089.

(11) Lowry, T. M.; *Optical Rotatory Power*; Dover Publications, New York, 1964.

(12) Barron, L. D.; *Molecular Light Scattering and Optical Activity*; Cambridge University Press, Cambridge, 2009.

(13) Asahi, T.; Nakamura, M.; Kobayashi, J.; Toda, F.; Miyamoto, H. *J. Am. Chem. Soc.* **1997**, *119*, 3665–3669.

(14) Koshima, H.; Nagano, M.; Asahi, T. *J. Am. Chem. Soc.* **2005**, *127*, 2455–2463.

(15) Smith, H. E.; Cook, S. L.; Warren, M. E., Jr. *J. Org. Chem.* **1964**, *29*, 2265–2272.

(16) Frisch M. J.; Trucks G. W.; Schlegel H. B.; Scuseria G. E.; Robb M. A.; Cheeseman J. R.; Scalmani G.; Barone V.; Mennucci B.; Petersson G. A.; Nakatsuji H.; Caricato M.; Li X.; Hratchian H. P.; Izmaylov A. F.; Bloino J.; Zheng G.; Sonnenberg J. L.; Hada M.; Ehara M.; Toyota K.; Fukuda R.; Hasegawa J.; Ishida M.; Nakajima T.; Honda Y.; Kitao O.; Nakai H.; Vreven T.; Montgomery J. A. Jr.; Peralta J. E.; Ogliaro F.; Bearpark M.; Heyd J. J.; Brothers E.; Kudin K. N.; Staroverov V. N.; Keith T.; Kobayashi R.; Normand J.; Raghavachari K.; Rendell A.; Burant J. C.; Iyengar S. S.; Tomasi J.; Cossi M.; Rega N.; Millam N. J.; Klene M.; Knox J. E.; Cross J. B.; Bakken V.; Adamo C.; Jaramillo J.; Gomperts R.; Stratmann R. E.; Yazyev O.; Austin A. J.; Cammi R.; Pomelli C.; Ochterski J. W.; Martin R. L.; Morokuma K.; Zakrzewski V. G.; Voth G. A.; Salvador P.; Dannenberg J. J.; Dapprich S.; Daniels A. D.; Farkas Ö.; Foresman J. B.; Ortiz J. V.; Cioslowski J.; Fox D. J. *Gaussian 09*, revision B.01; Gaussian, Inc.: Wallingford, CT, 2010.

(17) Becke, A. D. *J. Chem. Phys.* **1993**, *98*, 5648–5652.

(18) Lee, C.; Yang, W.; Parr, R. *Phys. Rev. B* **1988**, *37*, 785–789.

(19) Krishnan, R.; Binkley, J. S.; Seeger, R.; Pople, J. A. *J. Chem. Phys.* **1980**, *72*, 650–654.

(20) (a) Wakai, A.; Fukasawa, H.; Yang, C.; Mori, T.; Inoue, Y. *J. Am. Chem. Soc.* **2012**, *134*, 4990–4997. (b) Nakai, Y.; Mori, T.; Sato, K.; Inoue, Y. *J. Phys. Chem. A* **2013**, *117*, 5082–5092. (c) Nakai, Y.; Mori, T.; Inoue, Y. *J. Phys. Chem. A* **2013**, *117*, 83–93. (d) Nakai, Y.; Mori, T.; Inoue, Y. *J. Phys. Chem. A* **2012**, *116*, 7372–7385. (e) Toda, M.; Matsumura,

C.; Tsurukawa, M.; Okuno, T.; Nakano, T.; Inoue, Y.; Mori, T. *J. Phys. Chem. A* **2012**, *116*, 9340–9346. (f) Mori, T.; Inoue, Y.; Grimme, S. *J. Phys. Chem. A* **2007**, *111*, 4222–4234. (g) Mori, T.; Grimme, S.; Inoue, Y. *J. Org. Chem.* **2007**, *72*, 6998–7010.

(21) Turbomole V6.6 2014, a development of University of Karlsruhe and Forschungszentrum Karlsruhe GmbH, 1989–2007, Turbomole GmbH, since 2007; available from http://www.turbomole.com.

(22) (a) Grimme, S.; Antony, J.; Ehrlich, S.; Krieg, H. *J. Chem. Phys.* **2010**, *132*, 154104/1–18. (b) Grimme, S.; Ehrlich, S.; Goerigk, L. *J. Comput. Chem.* **2011**, *32*, 1456–1465. (c) Tao, J.; Perdew, J. P.; Staroverov, V. N.; Scuseria, G. E. *Phys. Rev. Lett.* **2003**, *91*, 146401/1–4.

(23) (a) Christiansen, R.; Koch, H.; Jørgensen, P. *Chem. Phys. Lett.* **1995**, *243*, 409–418. (b) Hättig, C.; Weigend, F. *J. Chem. Phys.* **2000**, *113*, 5154–5161. (c) Hättig, C.; Kohn, A. *J. Chem. Phys.* **2002**, *117*, 6939–6951.

(24) Heinert, D.; Martell, A. E. *J. Am. Chem. Soc.***1963**, *85*, 183–188.

(25) (a) Smith, H. E.; Records, R. Tetrahedron **1966**, *22*, 813–824. (b) Smith, H. E.; Neergaard, J. R.; Burrows, E. P.; Chen, F. *J. Am. Chem. Soc.* **1974**, *96*, 2908–2916.

(26) Koshima, H.; Matsuo, R.; Matsudomi, M.; Uemura, Y.; Shiro, M. *Cryst. Growth Des.* **2013**, *13*, 4330–4337.

(27) Presti, D.; Labat, F.; Pedone, A.; Frisch, M. J.; Hratchian, H.P.; Ciofini, I.; Menziani, M. C.; Adamo, C. *J. Chem. Theory Comput.* **2014**, *10*, 5577–5585.

(28) Toll, J. S. *Phys. Rev.* **1956**, *104*, 1760–1770.

(29) Shopa, Y.; Ftomyn, N. *Acta. Phys. Pol. A* **2010**, *117*, 114–116.

(30) Asahi, T.; Nakamura, M.; Kobayashi, J.; Toda, F.; Miyamoto, H. *J. Am. Chem. Soc.* **1997**, *119*, 3665–3669.

(31) Asahi, T.; Utsumi, H.; Itagaki, Y.; Kagomiya, I.; Kobayashi, Z. *Acta Crystallogr., Sect. A: Found. Crystallogr.* **1996**, *52*, 766–769.

(32) Asahi, T.; Takahashi, M.; Kobayashi, J. *Acta Crystallogr., Sect. A: Found. Crystallogr.* **1997**, *53*, 763–771.

(33) Kobayashi, J.; Uchino, K.; Asahi, T. *Phys. Rev.B* **1991**, *43*, 5706–5712.

(34) Kobayashi, J.; Asahi, T.; Sakurai, M.; Kagomiya, I.; Asai, H.; Asami, H. *Acta Crystallogr., Sect. A: Found. Crystallogr.* **1998**, *54*, 581–590.

(35) Johmoto, K.; Ishida, T.; Sekine, A.; Uekusa H.; Ohashi, Y. *Acta Crystallogr. Sect. B: Struct. Sci.* **2012**, *68*, 297–304.

(36) Tanaka, M.; Yagi-Watanabe, K.; Kaneko, F.; Nakagawa K. *J. Phys. Chem. A* **2010**, *114*, 11928–11932.

(37) Matsuo, K.; Matsushima, Y.; Fukuyama, T.; Senba, S.; Gekko K.; *Chem. Lett.* **2002**, *31*, 826–827.

(38) Goto, T.; Ikehata, A.; Morisawa, Y.; Ozaki, Y. *J. Phys. Chem. A* **2013**, *117*, 2517–2528.

Chapter 4

Development of the Fast-type High-Accuracy Universal Polarimeter using Charge-coupled Device Spectrometer

4.1 Introduction

In Chapter 3, I described the LB, LD, CB, and CD properties in photomechanical crystals of chiral salicylidenephenylethylamines before and under UV irradiation simultaneously measured using G-HAUP. However, the measuring time was very long because a hundred of transmitted light measurements are required even in a single wavelength, and a fine interval of wavelength scans is needed to measure a small change in LB, LD, CB, and CD spectra. Even under weak UV irradiation, the thicknesses of the chiral salicylidenephenylethylamine crystal decreased (approximately –10%) after three days required for the HAUP measurement due to the gradual sublimation from the top surface of the specimens by the photothermal effect under UV irradiation, despite temperature control with a thermostat.[1] When I obtained the LB, LD, CB, and CD spectra from the raw experimental data via the HAUP measurement, I had to take into account the decrease in thickness of the specimen. Hence, improvement of the G-HAUP apparatus is required to shorten the measurement time.

To achieve simultaneous LB, LD, CB, and CD measurements in a short time, I have developed a CCD-HAUP which is a fast-type high-accuracy universal polarimeter. The novel instrument is equipped with a CCD spectrometer that makes possible to detect white transmitted light at once. The measurement of the CCD-HAUP for the whole wavelength region is completed within the measurement time of the G-HAUP for a single wavelength. In this Chapter, I describe the instrumentation and performance of the CCD-HAUP and

applications to α-quartz and chiral photomechanical enol-(*S*)-**1** and enol-(*R*)-**1** crystals. This Chapter is reproduced with a slight modification from "Fast-type High-Accuracy Universal Polarimeter Using Charge-coupled Device Spectrometer" by Takanabe, A.; Koshima, H.; Asahi, T. *AIP Advances* **2017**, in press, DOI: 10.1063/1.4977440,[2] which is an open access article distributed under the terms and conditions of the Creative Commons Attribution (CC-BY) license (http://creativecommons.org/licenses/by/4.0/). Copyright 2017 Author(s). Consent from all authors has been secured.

4.2 Experimental Section

4.2.1 System of Fast-type High-Accuracy Universal Polarimeter using Charge-coupled Device Spectrometer

Figure 4.1 shows the schematic drawing and photograph of the CCD-HAUP system. A 150-W xenon discharge lamp (BSO-X150, Bunkoukeiki) was employed in this system as light source. White light passed through a polarizer, sample, and analyzer. Glan–Thompson prisms made of $CaCO_3$ crystal purchased from Karl Lambrecht were used as polarizer and analyzer. θ' and Y' values were independently and precisely altered using precision rotation stages (RA10A-W, Kohzu Precision). The white light transmitted intensity was detected at once using a CCD spectrometer (Glacier X, B&W Tek). Blaze wavelength was 530 nm. The number of pixels was 2048. The light intensity in the wavelength range of 350–1050 nm could be detected by this CCD spectrometer. This was the most significant change of the optical system from the G-HAUP where the monochromatic transmitted light intensity was detected using a photomultiplier and a lock-in amplifier. Using a CCD spectrometer, transmitted light in the rage of 350–680 nm could be measured at once. This optical system allowed us to quickly measure the LB, LD, CB and CD spectra in the wavelength region from 350 to 680 nm, because the whole measurement of the CCD-HAUP was completed within the measurement time of the G-HAUP for a single wavelength. Principle of the HAUP method was not changed (see Section 3.2).

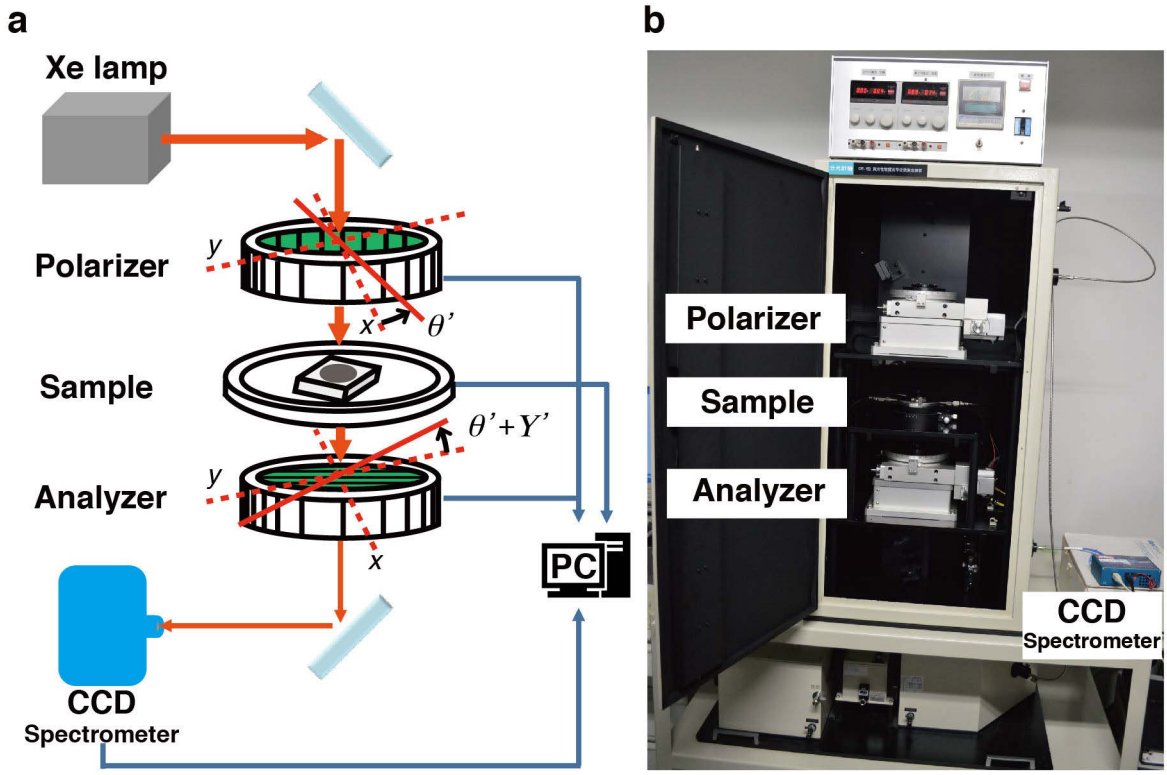

Figure 4.1. (a) Schematic drawing and (b) photograph of the CCD-HAUP apparatus. Sample stage has a temperature control unit. Here, θ' represent the polarizer from θ_0 and Y' represent the deflecting angle of analyzer from δY. Reprinted from "Fast-type High-Accuracy Universal Polarimeter Using Charge-coupled Device Spectrometer" by Takanabe, A.; Koshima, H.; Asahi, T. *AIP Advances* **2017**, in press, DOI: 10.1063/1.4977440,[2] which is an open access article distributed under the terms and conditions of the Creative Commons Attribution (CC-BY) license (http://creativecommons.org/licenses/by/4.0/). Copyright 2017 Author(s).

4.2.2 Materials

MgF_2: I purchased an achiral MgF_2 (100) plate crystal from Crystal Base. This plate crystal was polished to decrease the thickness to 52.6 μm, and put on a thin Cu plate with a pinhole 0.7 mm in diameter.

α-Quartz: I purchased a (100) α-quartz plate crystal ($P3_221$) from Crystal Base. The surface of the (100) plate crystal was polished with diamond slurry (abrasive grain diameter of 3.0 μm) and colloidal silica (32.5 nm) using polishing machines (Precision Lapping Machine, Nano Factor Tokyo, Japan and Metaserv 2000, Illinois, USA, respectively) to decrease their thickness and obtain flat and smooth surfaces. After that, this specimen was mounted on a Cu plate with a pinhole approximately 0.7 mm in diameter. The thickness was 35.7 μm.

Enantiomeric salicylidenephenylethylamines: To compare the LB, LD, CB, CD spectra measured using CCD-HAUP with G-HAUP[3], the sample preparation of enol-(*S*)-**1** and enol-(*R*)-**1** (Scheme 1.1) crystals were same as described in Subsection 3.3.1.

4.3 Performance of Fast-type High-Accuracy Universal Polarimeter using Charge-coupled Device Spectrometer

To evaluate the performance of the CCD-HAUP system, the HAUP measurement in the range of 425–600 nm were performed on an achiral MgF_2 crystal as a standard sample. The raw experimental results (Δ, E, H'_{21}, and θ_0) from the analysis of MgF_2 crystal using with the CCD-HAUP and the G-HAUP are almost consistent each other (Figure 4.2). These four parameters are very important to obtain the LB, LD, CB, and CD, as described in Section 3.2. Hence, the LB, LD, CB, and CD should be measured using with the CCD-HAUP.

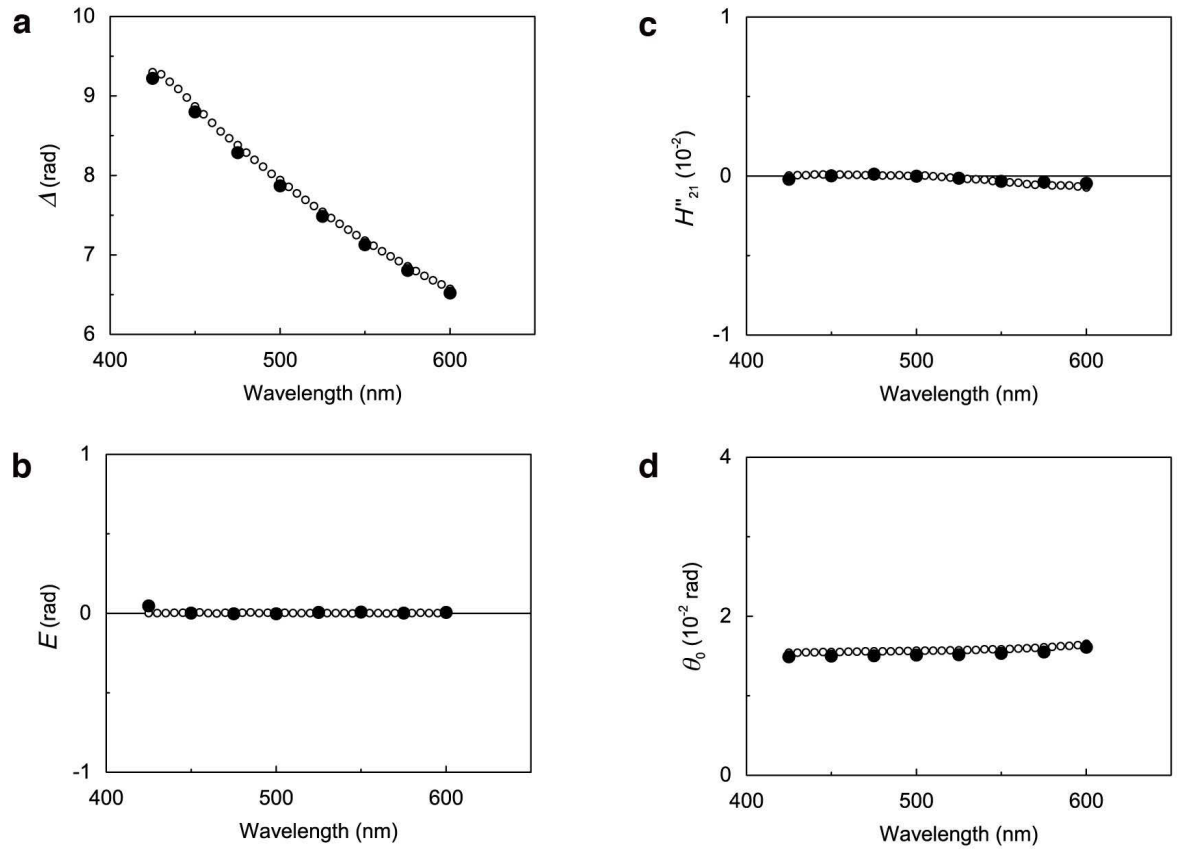

Figure 4.2. Raw experimental results from the analysis of an achiral MgF_2 crystal on the (100) face measured using the G-HAUP (black open circles) and the CCD-HAUP (black solid circles) at 20ºC: (a) Δ, (b) E, (c) H''_{21}, and (d) θ_0. Reprinted from "Fast-type High-Accuracy Universal Polarimeter Using Charge-coupled Device Spectrometer" by Takanabe, A.; Koshima, H.; Asahi, T. *AIP Advances* **2017**, in press, DOI: 10.1063/1.4977440,[2] which is an open access article distributed under the terms and conditions of the Creative Commons Attribution (CC-BY) license (http://creativecommons.org/licenses/by/4.0/). Copyright 2017 Author(s).

The accuracy of Δ, E, H'_{21}, and θ_0 values were estimated to be 0.7×10^{-1}, 0.9×10^{-2}, 0.1×10^{-3}, and 0.5×10^{-3} by averaging the deviations of the experimental values obtained using the CCD-HAUP from the experimental values obtained using the G-HAUP. The precision of Δ, E, H'_{21}, and θ_0 were also estimated to be 0.3×10^{-2}, 0.3×10^{-2}, 0.1×10^{-4}, and 0.7×10^{-5} as the standard errors of three MgF_2 experiments.

Figure 4.3 shows the LB and LD spectra of MgF_2 crystal on (100) face. The LB values (1.18×10^{-2} at 600 nm) obtained using the CCD-HAUP are consistent with those obtained using the G-HAUP, which are also consistent with the published values.[4,5] The measured LD values were zero because a MgF_2 crystal is transparent in visible region. The measuring time of the CCD-HAUP was 1.5 h. On the other hand, that of G-HAUP was 24 h. The results reveal that the LB spectrum of an anisotropic crystal was rapidly measured using the CCD-HAUP system with almost same accuracy as the G-HAUP.

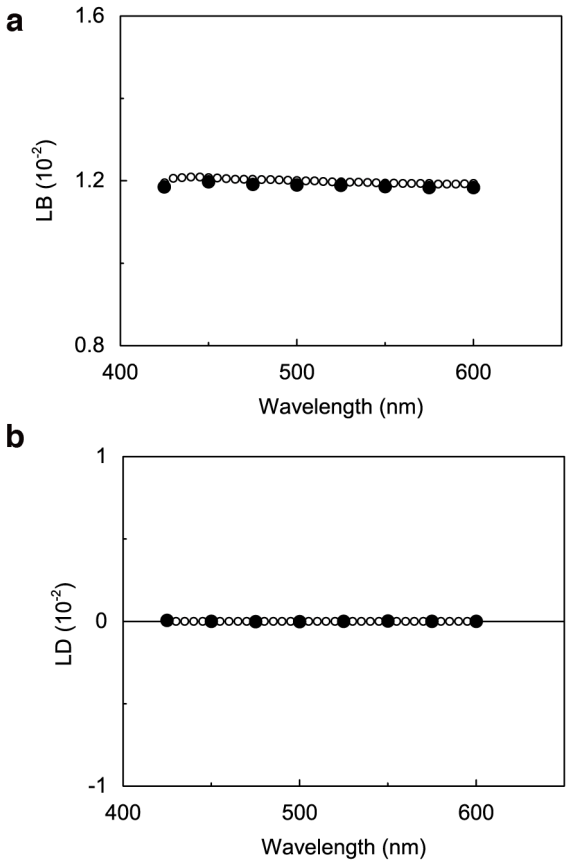

Figure 4.3. (a) LB and (b) LD spectra of an achiral MgF_2 crystal on (100) face measured using the G-HAUP (black open circles) and the CCD-HAUP (black solid circles). Reprinted from "Fast-type High-Accuracy Universal Polarimeter Using Charge-coupled Device Spectrometer" by Takanabe, A.; Koshima, H.; Asahi, T. *AIP Advances* **2017**, in press, DOI: 10.1063/1.4977440,[2] which is an open access article distributed under the terms and conditions of the Creative Commons Attribution (CC-BY) license (http://creativecommons.org/licenses/by/4.0/). Copyright 2017 Author(s).

4.4 Measurements of Chiral Crystals using Fast-type High-Accuracy Universal Polarimeter using Charge-coupled Device Spectrometer

4.4.1 α-Quartz

The CCD-HAUP measurements are applied to obtain both the chiroptical and anisotropic properties of chiral crystals. To confirm that the CB can be measured accurately, α-quartz plate crystal ($P3_221$) was initially measured. Figure 4.4 shows the raw experimental results (Δ, E, H'_{21}, θ_0) from the analysis of α-quartz plate ($P3_221$) using with the CCD-HAUP and the G-HAUP. The q and δY values were successfully determined by the approximations below. By assuming that k is dependent of λ as follows:

$$k = \frac{s}{\lambda} + t, \tag{4.1}$$

where, s and t are constants, and $k' = 0$ in the measured wavelength region. The optimum values of q, δY and N, and the constants s and t are obtained by least-squares fittings using eqs 3.6 and 3.9 and the p value (1.0×10^{-4}).

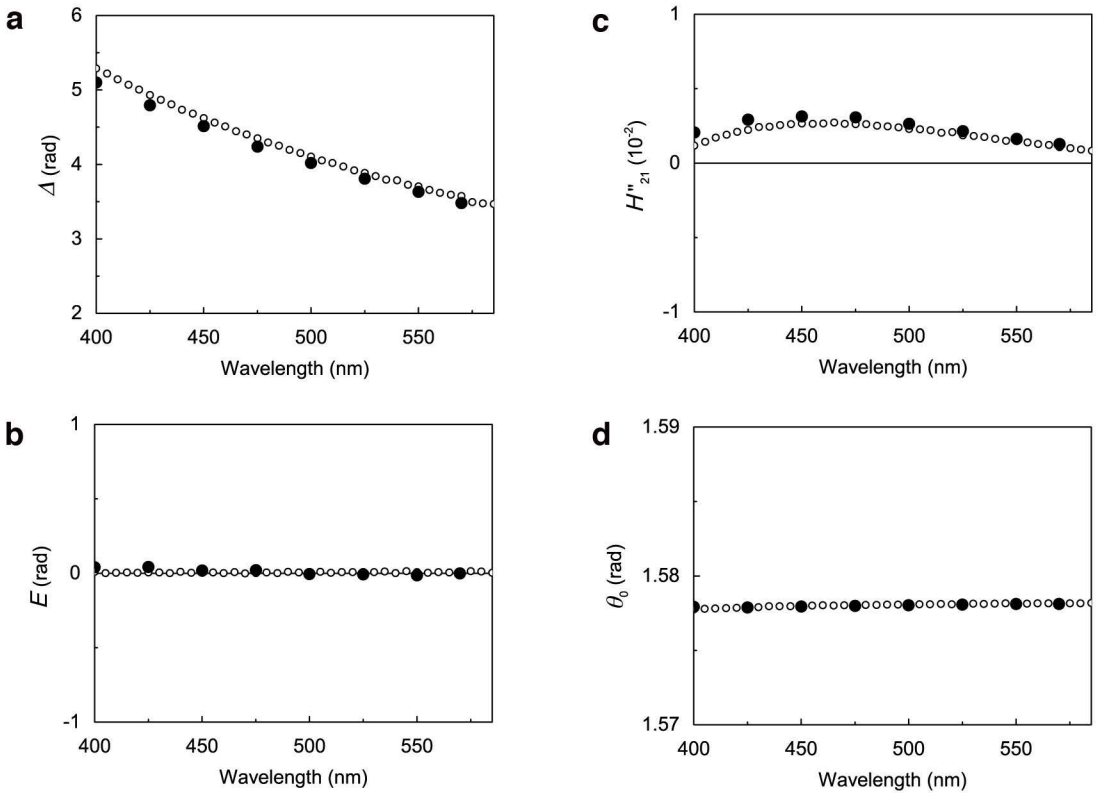

Figure 4.4. Raw experimental results from the analysis of α-quartz plate ($P3_221$) on the (100) face obtained using the G-HAUP (black open circles) and the CCD-HAUP (black solid circles) at 20ºC: (a) Δ, (b) E, (c) $H"_{21}$, and (d) θ_0. Reprinted from "Fast-type High-Accuracy Universal Polarimeter Using Charge-coupled Device Spectrometer" by Takanabe, A.; Koshima, H.; Asahi, T. *AIP Advances* **2017**, in press, DOI: 10.1063/1.4977440,[2] which is an open access article distributed under the terms and conditions of the Creative Commons Attribution (CC-BY) license (http://creativecommons.org/licenses/by/4.0/). Copyright 2017 Author(s).

The systematic error parameters q and δY of the CCD-HAUP measurement determined by least-squares fittings are as follows:

$$q = -3.51\times10^{-4}$$

$$\delta Y = 2.92\times10^{-3}$$

The values of q and δY obtained by least-squares fittings for any other experimental data in this study varied between 10^{-4}–10^{-3} and 10^{-5}–10^{-3}, respectively. In comparison with previous studies,[1,6–8] these values are acceptable.

The k and k' values are obtained by introducing Δ, E, s, t, and the obtained systematic errors to eqs 3.6 and 3.9, as shown in Figure 4.5. Finally CB and CD are determined from eqs 3.12 and 3.13.

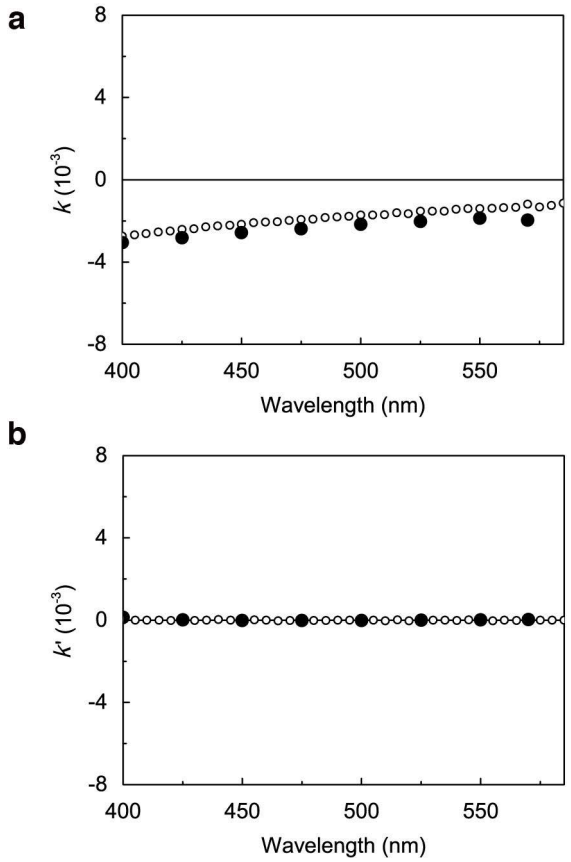

Figure 4.5. (a) *k* and (b) *k'* spectra of α-quartz plate ($P3_221$) on the (100) face measured using with the G-HAUP (black solid circles) and the CCD-HAUP (red open circles). Reprinted from "Fast-type High-Accuracy Universal Polarimeter Using Charge-coupled Device Spectrometer" by Takanabe, A.; Koshima, H.; Asahi, T. *AIP Advances* **2017**, in press, DOI: 10.1063/1.4977440,[2] which is an open access article distributed under the terms and conditions of the Creative Commons Attribution (CC-BY) license (http://creativecommons.org/licenses/by/4.0/). Copyright 2017 Author(s).

Figure 4.6 shows the LB, LD, CB and CD spectra of α-quartz plate ($P3_221$) on the (100) face at 20 ºC measured using with the G-HAUP and CCD-HAUP. The LB value (0.009 at 570 nm) obtained using the CCD-HAUP is also consistent with the previous study (0.009 at 633 nm).[9] The LB and CB values obtained using the CCD-HAUP are almost consistent with those obtained using the G-HAUP. The measuring time of the CCD-HAUP was 1.5 h. On the other hand, that of G-HAUP was 24 h. The results reveal that I could rapidly and simultaneously measure the LB and CB spectra of α-quartz plate ($P3_221$) on the (001) face using the CCD-HAUP system. The measured LD and CD values (Figure 4.6b and d) were zero because α-quartz is transparent in visible region.

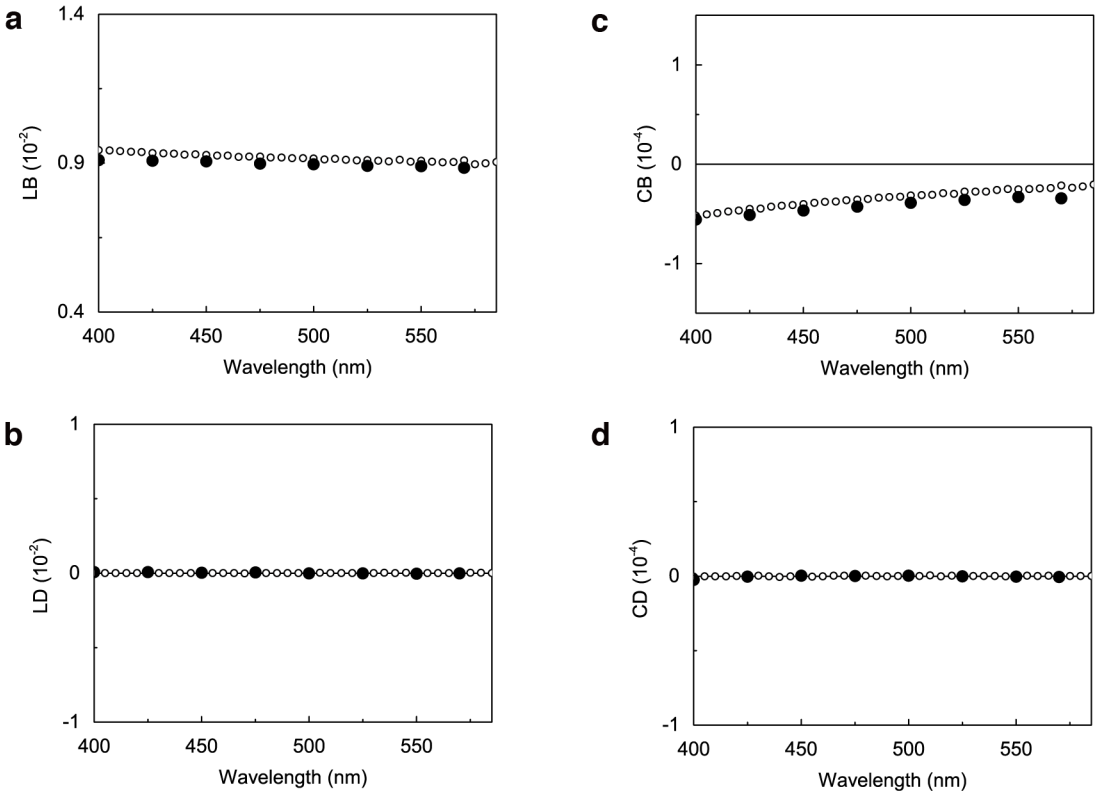

Figure 4.6. Optical anisotropic and chiroptical spectra of α-quartz plate ($P3_221$) on the (100) face: (a) LB, (b) LD, (c) CB, and (d) CD. These properties were measured using with the G-HAUP (black open circles) and the CCD-HAUP (black solid circles). Reprinted from "Fast-type High-Accuracy Universal Polarimeter Using Charge-coupled Device Spectrometer" by Takanabe, A.; Koshima, H.; Asahi, T. *AIP Advances* **2017**, in press, DOI: 10.1063/1.4977440,[2] which is an open access article distributed under the terms and conditions of the Creative Commons Attribution (CC-BY) license (http://creativecommons.org/licenses/by/4.0/). Copyright 2017 Author(s).

4.4.2 Enantiomeric Salicylidenephenylethylamine Crystals

To confirm that the LB, LD, CB and CD can be measured simultaneously using the CCD-HAUP, enol-(*S*)-**1** and enol-(*R*)-**1** crystals were measured. Figure 4.7 shows the raw experimental results (Δ, E, H'_{21}, θ_0) from the analysis of enol-(*R*)-**1** crystal (2.3 μm) on (001) face using with CCD-HAUP and G-HAUP. The data analysis of enol-(*R*)-**1** crystal without UV irradiation is same as described in Section 3.2. The systematic error parameters q and δY determined by least-squares fittings are as follows:

$$q = -1.04\times10^{-4}$$

$$\delta Y = -6.15\times10^{-5}.$$

The k and k' values are obtained by introducing Δ, E, A_{330}, and the obtained systematic errors to eqs 3.6 and 3.9, as shown in Figure 4.8. Finally CB and CD are determined from eqs 3.12 and 3.13, as shown in Figure 4.9.

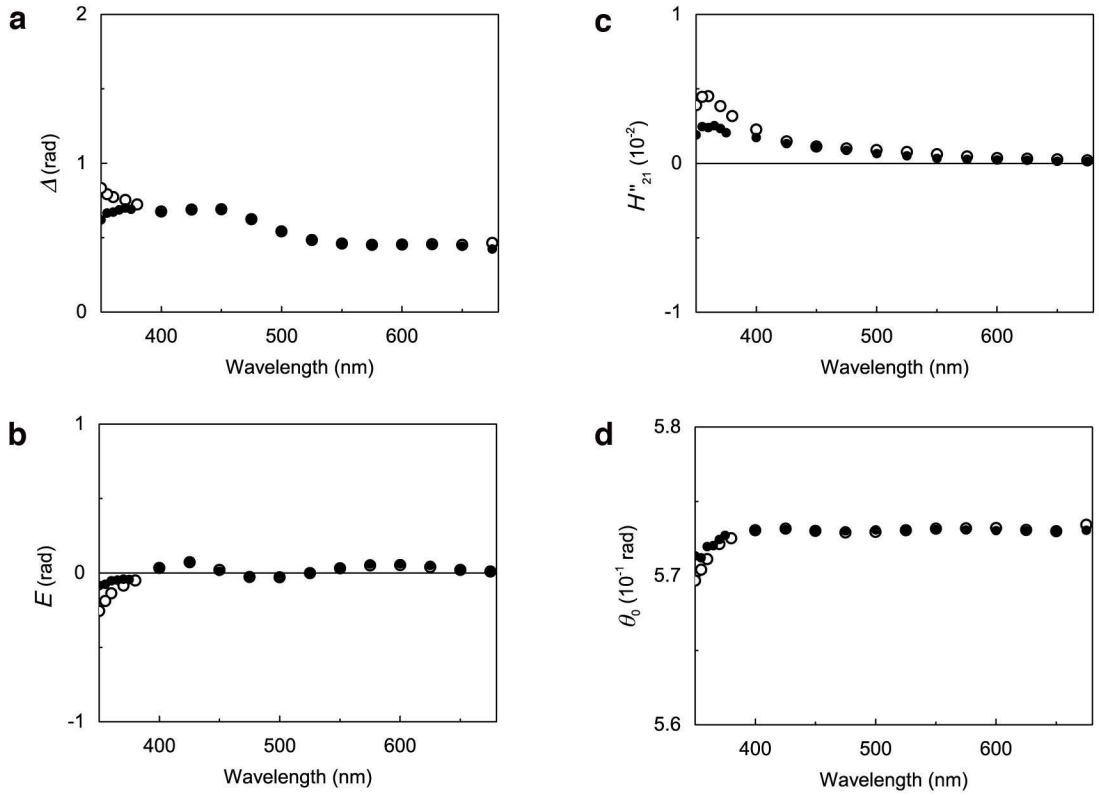

Figure 4.7. Raw experimental results from the analysis of enol-(*R*)-**1** crystal on the (001) face measured using the G-HAUP (black open circles) and the CCD-HAUP (black solid circles) at 20ºC: (a) Δ, (b) E, (c) H'_{21}, and (d) θ_0. Reprinted from "Fast-type High-Accuracy Universal Polarimeter Using Charge-coupled Device Spectrometer" by Takanabe, A.; Koshima, H.; Asahi, T. *AIP Advances* **2017**, in press, DOI: 10.1063/1.4977440,[2] which is an open access article distributed under the terms and conditions of the Creative Commons Attribution (CC-BY) license (http://creativecommons.org/licenses/by/4.0/). Copyright 2017 Author(s).

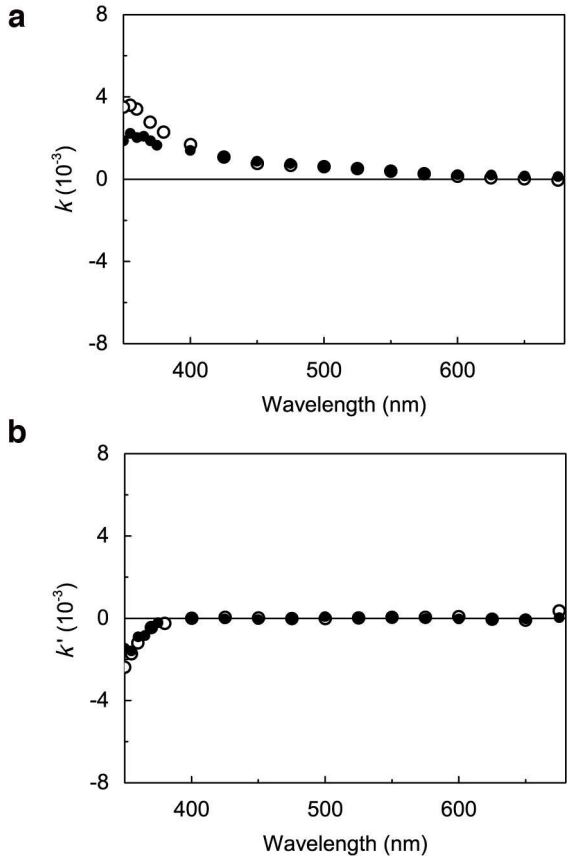

Figure 4.8. (a) *k* and (b) *k'* spectra of enol-(*R*)-**1** crystal on the (001) face measured using with the G-HAUP (black open circles) and the CCD-HAUP (black solid circles). Reprinted from "Fast-type High-Accuracy Universal Polarimeter Using Charge-coupled Device Spectrometer" by Takanabe, A.; Koshima, H.; Asahi, T. *AIP Advances* **2017**, in press, DOI: 10.1063/1.4977440,[2] which is an open access article distributed under the terms and conditions of the Creative Commons Attribution (CC-BY) license (http://creativecommons.org/licenses/by/4.0/). Copyright 2017 Author(s).

Figure 4.9 shows the LB, LD, CB and CD spectra of enol-(*R*)-**1** crystal on the (001) face at 20 ºC measured using with the G-HAUP and CCD-HAUP. The LB and CB values obtained using the CCD-HAUP are almost consistent with those obtained using the G-HAUP above 400 nm. The oscillations are observed in the LB and LD, probably due to the multiple reflections between the (001) and (00$\bar{1}$) parallel planes.[10] The real LB and LD values should be almost constant above 400 nm (0.02 and 0, respectively) by taking into account the multiple reflections, which are in good agreement with those measured using the G-HAUP.[1] Above 400 nm, the sign of the CB is plus and the value is comparable with the data measured using G-HAUP (0.1×10^{-4} at 600 nm). The measuring time of the CCD-HAUP was 1.5 h. On the other hand, that of G-HAUP was 24 h. The results reveal that I could rapidly and simultaneously measure the LB and CB spectra of enol-(*R*)-**1** crystal on (001) face above 400 nm using the CCD-HAUP system.

In UV region, below 400 nm, the LB, LD, CB and CD values obtained using the CCD-HAUP are different with those obtained using the G-HAUP (Figure 4.9). In comparison with Figure 3.7, the LB, LD, CB and CD values obtained using the G-HAUP are correct in the UV region. Although the LD and CD are observed below 400 nm by using the CCD-HAUP, these values are not accurate, because the transmitted light intensity of the CCD-HAUP without sample is very weak below 400 nm (Figure 4.10); less than 5 % of the maximum incident light intensity at 580 nm. Hence, the LB, LD, CB and CD spectra below 400 nm could not be measured accurately by the CCD-HAUP. On the other hand, in the UV region (below 400nm), the transmitted light intensity of the G-HAUP without sample is more than 15 % of the maximum incident light intensity at 470 nm. Hence, the LB, LD, CB and CD spectra below 400 nm obtained by the G-HAUP are accurate even in a large absorption at around 330nm.[1]

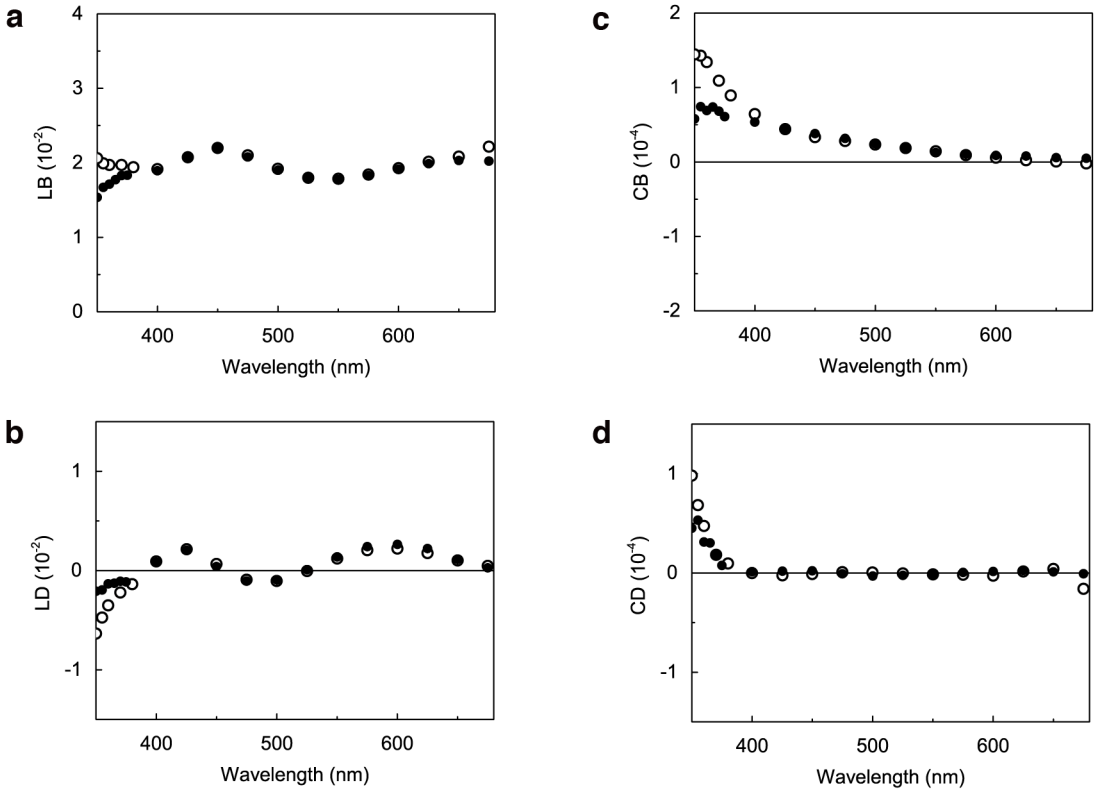

Figure 4.9. Optical anisotropic and chiroptical spectra of enol-(*R*)-**1** crystal on the (001) face: (a) LB, (b) LD, (c) CB, and (d) CD. These properties were measured using with the G-HAUP (black open circles) and the CCD-HAUP (black solid circles). Reprinted from "Fast-type High-Accuracy Universal Polarimeter Using Charge-coupled Device Spectrometer" by Takanabe, A.; Koshima, H.; Asahi, T. *AIP Advances* **2017**, in press, DOI: 10.1063/1.4977440,[2] which is an open access article distributed under the terms and conditions of the Creative Commons Attribution (CC-BY) license (http://creativecommons.org/licenses/by/4.0/). Copyright 2017 Author(s).

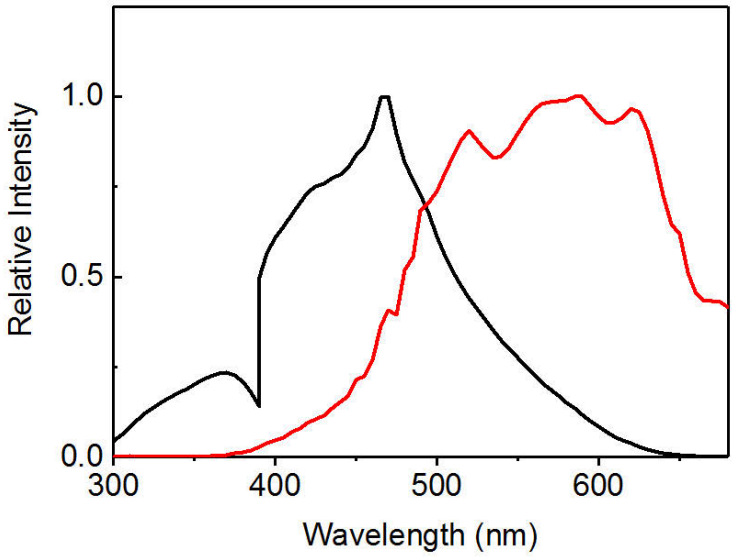

Figure 4.10. Light intensity spectra transmitted through polarizer and analyzer using with the G-HAUP (black solid line) and CCD-HAUP (red solid line). Reprinted from "Fast-type High-Accuracy Universal Polarimeter Using Charge-coupled Device Spectrometer" by Takanabe, A.; Koshima, H.; Asahi, T. *AIP Advances* **2017**, in press, DOI: 10.1063/1.4977440,[2] which is an open access article distributed under the terms and conditions of the Creative Commons Attribution (CC-BY) license (http://creativecommons.org/licenses/by/4.0/). Copyright 2017 Author(s).

Then, I attempted to measure the LB, LD, CB and CD spectra of enol-(*S*)-**1** crystal on the (001) face at 20 ºC using with the CCD-HAUP before, during, and after UV irradiation. UV-LED light (365 nm; UV-400, Keyence) was continuously irradiated from a direction almost vertical to the HAUP light path at low power (5 mW cm^{-2}) to minimize the incidence of UV light to the CCD spectrometer (Figure 3.5). Crystal bending by UV irradiation was prevented by fixing the crystals to the Cu plate with silicone grease.[1] In the CCD-HAUP measurement, I assumed that the thickness of the enol-(*S*)-**1** crystal did not decrease upon UV irradiation within 1.5 h.

Figure 4.11 shows the raw experimental results (Δ, E, H'_{21}, θ_0) from the analysis of enol-(*S*)-**1** crystal (thickness, 5.0 μm) on the (001) face using with the CCD-HAUP and G-HAUP. Before and after UV irradiation, the data analysis of enol-(*S*)-**1** crystal is same as described in Section 3.2. The systematic error parameters q and δY determined by least-squares fittings before and after UV irradiation are as follows:

$$q = -4.49\times10^{-4}$$

$$\delta Y = 9.41\times10^{-4},$$

and

$$q = -2.61\times10^{-4}$$

$$\delta Y = 3.83\times10^{-4},$$

respectively.

Under continuous UV irradiation, the data analysis of enol-(*S*)-**1** crystal is also described in Section 3.2. The systematic error parameters q and δY determined by least-squares fittings are as follows:

$$q = -2.51\times10^{-4}$$

$$\delta Y = 6.90\times10^{-4}.$$

The k and k' values are obtained by introducing Δ, E, A_{330}, A_{460} and the obtained systematic errors to eqs 3.6 and 3.9, as shown in Figure 4.12. Finally CB and CD are determined from eqs 3.12 and 3.13.

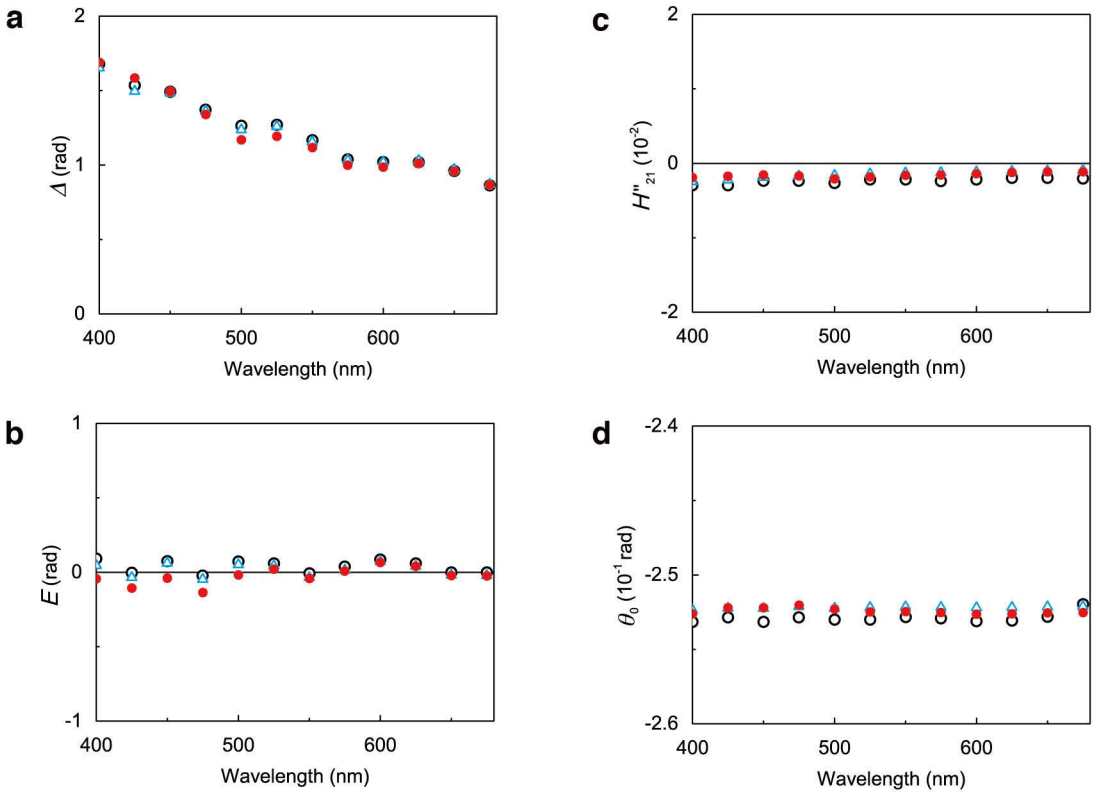

Figure 4.11. Raw experimental results from the analysis of enol-(*S*)-**1** crystal on the (001) face at 20ºC: (a) Δ, (b) E, (c) H'_{21}, and (d) θ_0. These properties were measured with the CCD-HAUP before, during, and after continuous UV light irradiation at 365 nm (black open circles, red solid circles, and light blue open triangles, respectively). Reprinted from "Fast-type High-Accuracy Universal Polarimeter Using Charge-coupled Device Spectrometer" by Takanabe, A.; Koshima, H.; Asahi, T. *AIP Advances* **2017**, in press, DOI: 10.1063/1.4977440,[2] which is an open access article distributed under the terms and conditions of the Creative Commons Attribution (CC-BY) license (http://creativecommons.org/licenses/by/4.0/). Copyright 2017 Author(s).

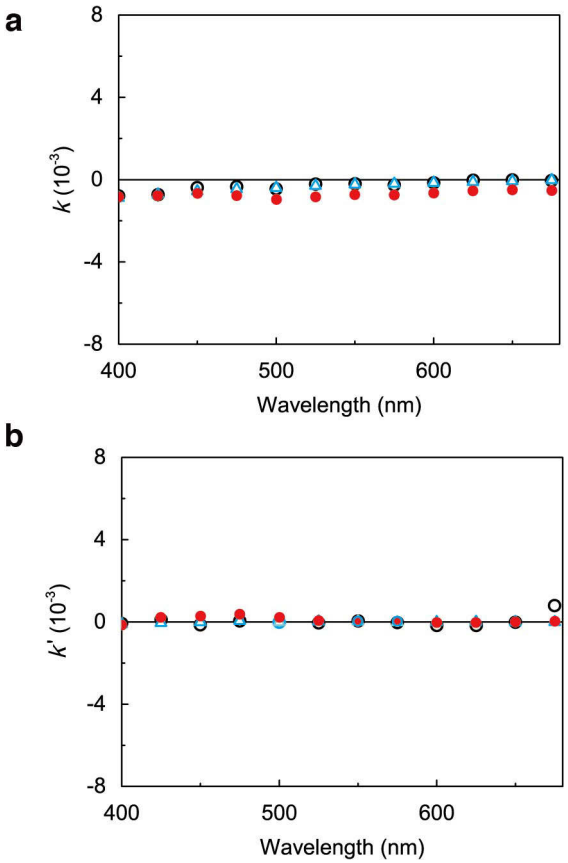

Figure 4.12. (a) *k* and (b) *k'* spectra of enol-(*S*)-**1** crystal on the (001) face. These properties were measured with the CCD-HAUP before, during, and after continuous UV light irradiation at 365 nm (black open circles, red solid circles, and light blue open triangles, respectively). Reprinted from "Fast-type High-Accuracy Universal Polarimeter Using Charge-coupled Device Spectrometer" by Takanabe, A.; Koshima, H.; Asahi, T. *AIP Advances* **2017**, in press, DOI: 10.1063/1.4977440,[2] which is an open access article distributed under the terms and conditions of the Creative Commons Attribution (CC-BY) license (http://creativecommons.org/licenses/by/4.0/). Copyright 2017 Author(s).

Figure 4.13 shows the LB, LD, CB, and CD spectra of both the enantiomeric enol-(*S*)-**1** and enol-(*R*)-**1** crystals on the (001) face before UV irradiation. Although small oscillations are observed in the LB and LD, probably due to the multiple reflections between the (001) and $(00\bar{1})$ parallel planes, the real LB and LD values should be almost constant (0.02 and 0, respectively), which are consistent with those measured using the G-HAUP.[1] The LB and LD spectra between the S and R enantiomeric crystals are coincident (Figures 4.13a and b), because optical anisotropic properties are not related to the chirality of the crystals. The sign of the CB of enol-(*S*)-**1** crystal is minus, which is in a mirror relationship with enol-(*R*)-**1** crystal (Figure 4.13c). The CB value of enol-(*S*)-**1** crystal (0.1×10^{-4} at 600 nm) is in good agreement with that measured using G-HAUP.[1] The baseline is shifted slightly to the positive in the CB spectra, which I consider to be caused by the inaccuracy of systematic error evaluations. The obtained LB, LD, CB, and CD values of enol-(*S*)-**1** crystal before UV irradiation are almost consistent with those obtained using the G-HAUP above 400 nm (Figure 4.14).

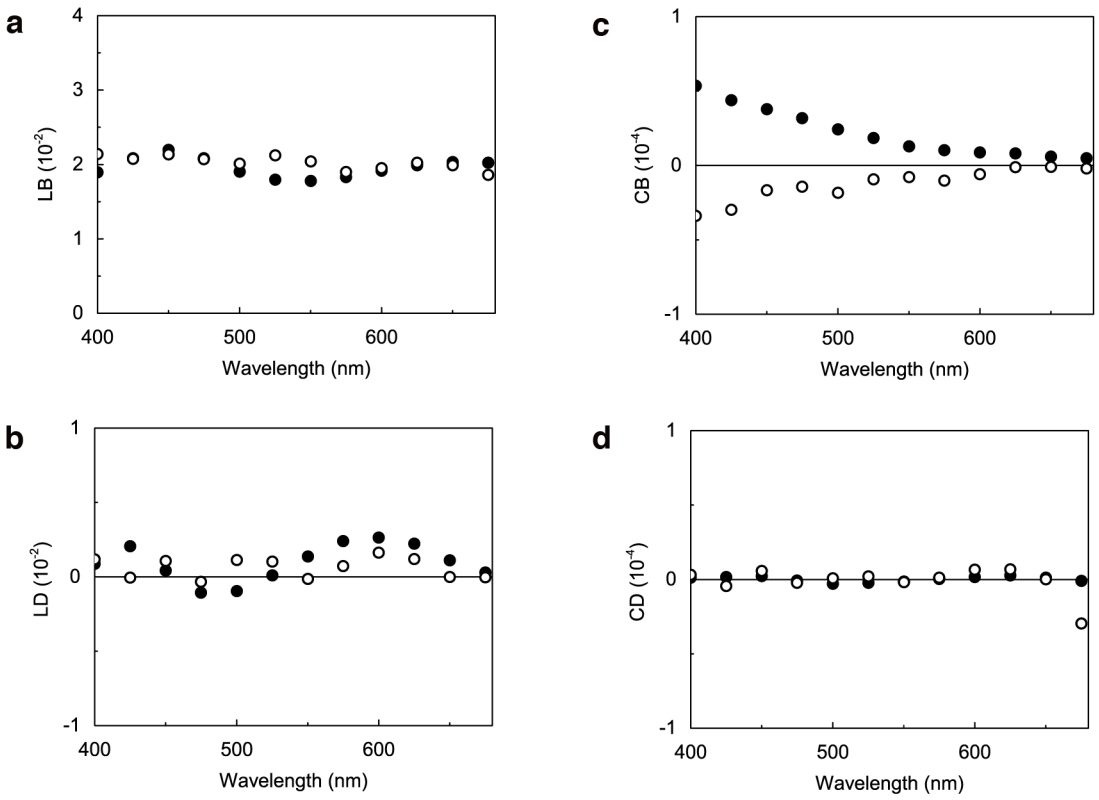

Figure 4.13. Anisotropic optical and chiroptical spectra of enol-(*S*)-**1** (black open circles) and enol-(*R*)-**1** (black solid circles) crystals on the (001) face at 20 ºC: (a) LB, (b) LD, (c) CB, and (d) CD. These properties were measured using with the CCD-HAUP. Reprinted from "Fast-type High-Accuracy Universal Polarimeter Using Charge-coupled Device Spectrometer" by Takanabe, A.; Koshima, H.; Asahi, T. *AIP Advances* **2017**, in press, DOI: 10.1063/1.4977440,[2] which is an open access article distributed under the terms and conditions of the Creative Commons Attribution (CC-BY) license (http://creativecommons.org/licenses/by/4.0/). Copyright 2017 Author(s).

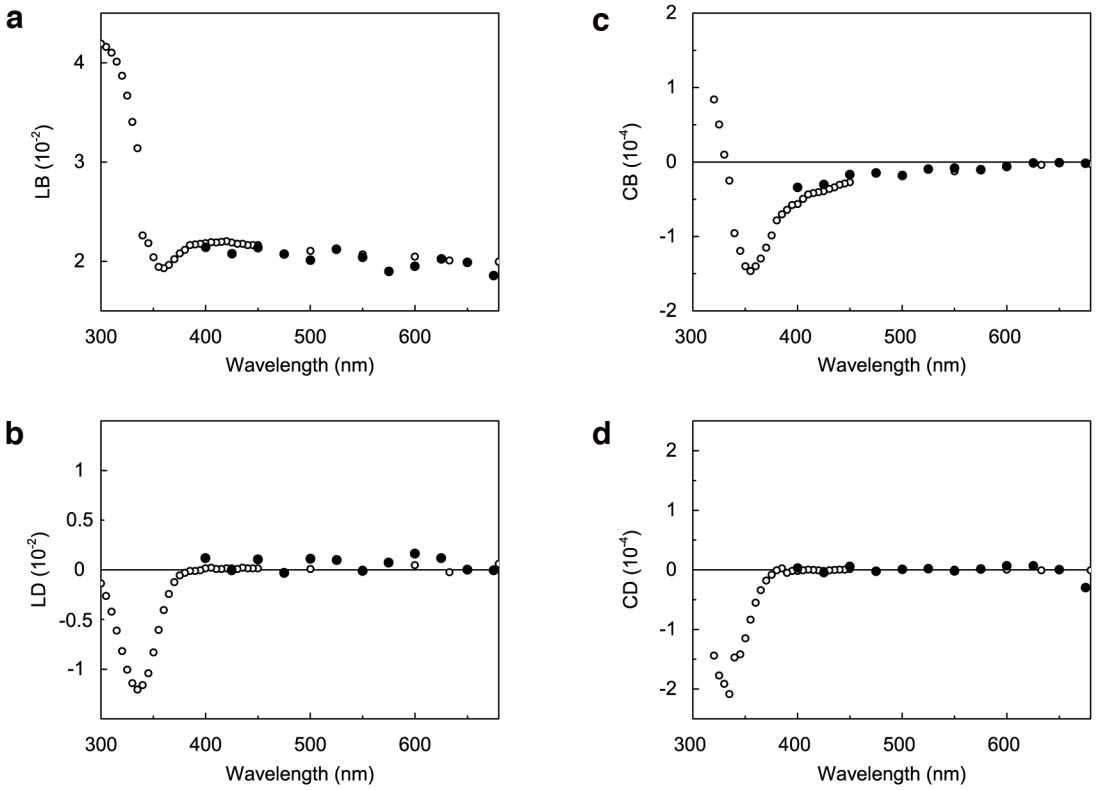

Figure 4.14. Anisotropic optical and chiroptical spectra of enol-(*S*)-**1** crystal before UV irradiation on the (001) face at 20 ºC: (a) LB, (b) LD, (c) CB, and (d) CD. The samples measured using the G-HAUP (black open circles) and the CCD-HAUP (black solid circles) are not same. Reprinted from "Fast-type High-Accuracy Universal Polarimeter Using Charge-coupled Device Spectrometer" by Takanabe, A.; Koshima, H.; Asahi, T. *AIP Advances* **2017**, in press, DOI: 10.1063/1.4977440,[2] which is an open access article distributed under the terms and conditions of the Creative Commons Attribution (CC-BY) license (http://creativecommons.org/licenses/by/4.0/). Copyright 2017 Author(s).

Figures 4.15a and b show the LB and LD spectra of enol-(*S*)-**1** crystal on (001) face at 20 ºC measured using with the CCD-HAUP before, during, and after UV irradiation. Under continuous UV irradiationat 365 nm, the negative *δ*LD peak corresponding to the photostationary state of the product *trans*-keto-(*S*)-**1** appeared at around 460 nm (Figure 4.15d). The *δ*LD value ($-0.18\times10^{-2} \pm 0.02\times10^{-2}$ at 460 nm) measured using with the CCD-HAUP is comparable with the LD value ($-0.15\times10^{-2} \pm 0.02\times10^{-2}$ at 460 nm) measured with the G-HAUP.[1] The *δ*LB spectra exhibited a slight anomalous dispersion of positive, and negative peaks at around 420 and 500 nm with a change in sign at the weak *δ*LD peak (Figure 4.15c). The LB and LD spectra of enol-(*S*)-**1** crystal under continuous UV irradiation were almost consistent with those obtained using G-HAUP above 400 nm (Figure 4.16a and b). The Kramers–Kronig relationship between the LB and LD spectra is satisfied, showing that the LD and LB spectra under weak UV light irradiation were successfully measured by the CCD-HAUP. After stopping UV irradiation, the LD peak and anomalous dispersion of LB disappeared, to return to the initial spectra before UV irradiation.

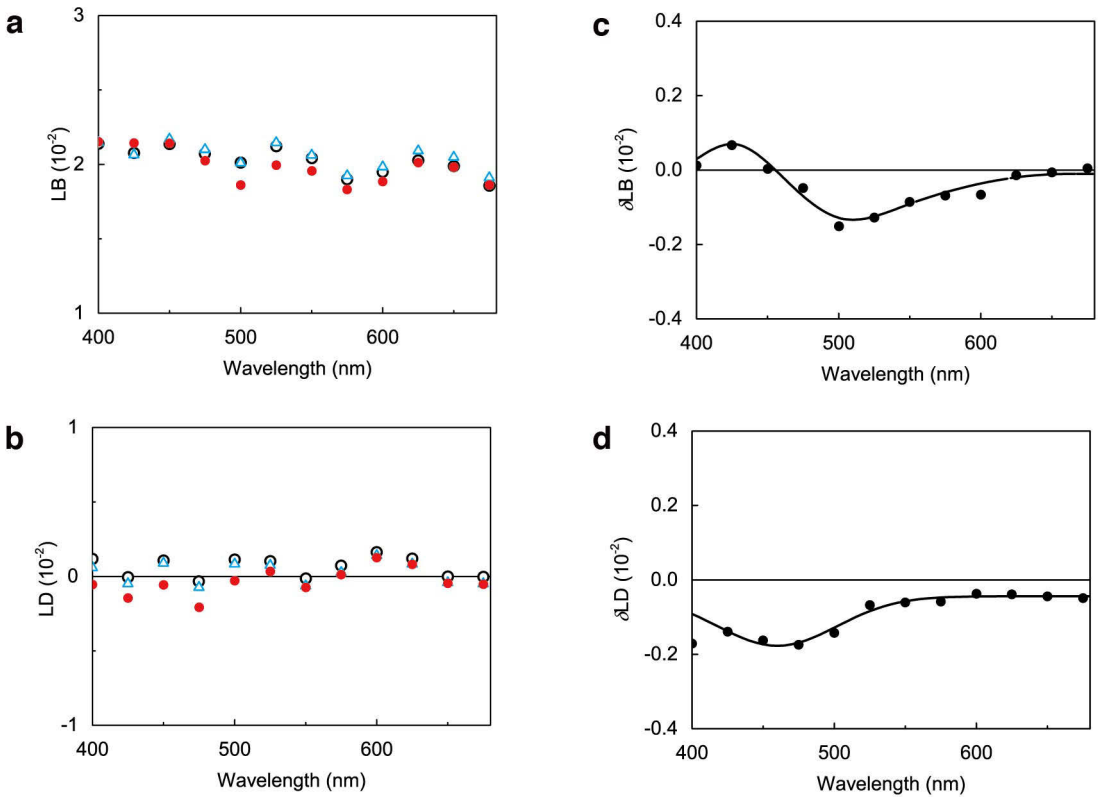

Figure 4.15. (a) LB and (b) LD spectra of enol-(*S*)-**1** crystal on the (001) face measured with the CCD-HAUP before, during, and after continuous UV light irradiation (black open circles, red solid circles, and light blue open triangles, respectively). (c) *δ*LB and (d) *δ*LD present the differences between before and during UV irradiation. The curve line of *δ*LB is served as an eye guide, and that of *δ*LD is fitted by Gaussian functions. Reprinted from "Fast-type High-Accuracy Universal Polarimeter Using Charge-coupled Device Spectrometer" by Takanabe, A.; Koshima, H.; Asahi, T. *AIP Advances* **2017**, in press, DOI: 10.1063/1.4977440,[2] which is an open access article distributed under the terms and conditions of the Creative Commons Attribution (CC-BY) license (http://creativecommons.org/licenses/by/4.0/). Copyright 2017 Author(s).

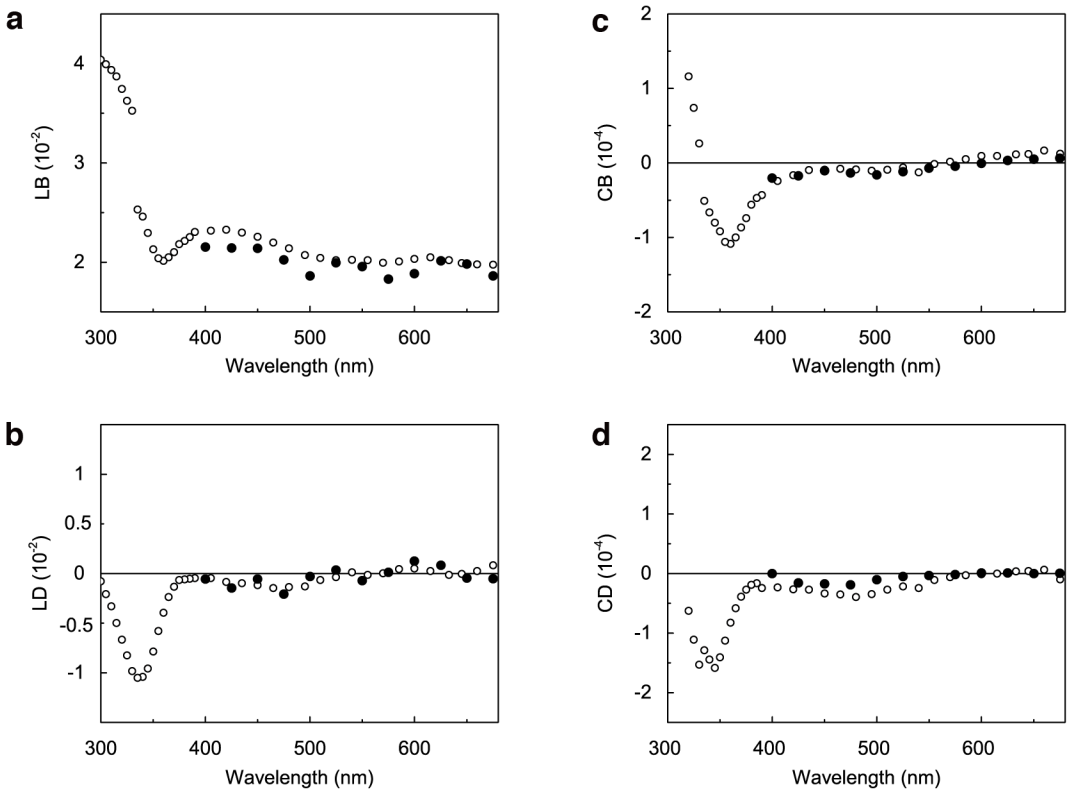

Figure 4.16. Anisotropic optical and chiroptical spectra of enol-(*S*)-**1** crystal under continuous UV irradiation on the (001) face at 20ºC: (a) LB, (b) LD, (c) CB, and (d) CD. The samples measured using the G-HAUP (black open circles) and the CCD-HAUP (black solid circles) are not same. Reprinted from "Fast-type High-Accuracy Universal Polarimeter Using Charge-coupled Device Spectrometer" by Takanabe, A.; Koshima, H.; Asahi, T. *AIP Advances* **2017**, in press, DOI: 10.1063/1.4977440,[2] which is an open access article distributed under the terms and conditions of the Creative Commons Attribution (CC-BY) license (http://creativecommons.org/licenses/by/4.0/). Copyright 2017 Author(s).

Figures 4.17 shows the CB and CD spectra of enol-(*S*)-**1** crystal on the (001) face at 20 ºC measured using with the CCD-HAUP before, during, and after UV irradiation. Under UV irradiation, new small negative CD peak appeared at 460 nm due to the formation of *trans*-keto-(*S*)-**1** crystals (Figure 4.17b). The CB spectra also exhibited anomalous dispersions of negative peak at 500 nm (Figure 4.17a), indicating that the Kramers–Kronig relationship between CB and CD spectra is also satisfied.

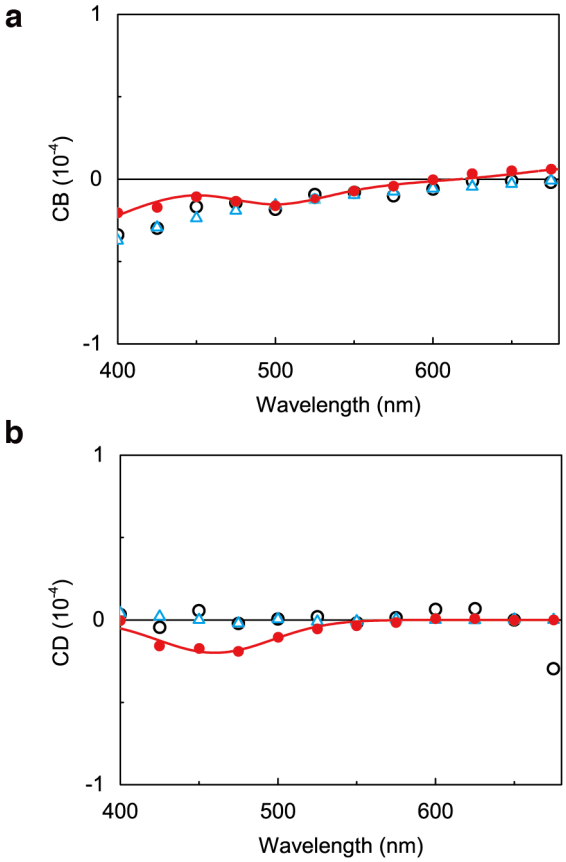

Figure 4.17. (a) CB and (b) CD spectra of enol-(*S*)-**1** crystal on the (001) face. These properties were measured with the CCD-HAUP before, during, and after continuous UV light irradiation at 365 nm (black open circles, red solid circles, and light blue open triangles, respectively). The red solid curve lines are CB and CD under continuous UV irradiation, which are served as an eye guide and fitted by Gaussian functions, respectively. Reprinted from "Fast-type High-Accuracy Universal Polarimeter Using Charge-coupled Device Spectrometer" by Takanabe, A.; Koshima, H.; Asahi, T. *AIP Advances* **2017**, in press, DOI: 10.1063/1.4977440,[2] which is an open access article distributed under the terms and conditions of the Creative Commons Attribution (CC-BY) license (http://creativecommons.org/licenses/by/4.0/). Copyright 2017 Author(s).

The CD value under UV irradiation at 460 nm measured by using the CCD-HAUP was $-0.20\times10^{-4}\pm0.02\times10^{-4}$, which is roughly comparable with that measured using G-HAUP ($-0.44\times10^{-4}\pm0.07\times10^{-4}$).[1] The short measuring time of the CCD-HAUP might contribute to the small standard deviation of the CD value. In contrast, the deterioration of the surface condition of the sample by prolonged UV irradiation for three days might affect the large standard deviation of the CD value obtained by the G-HAUP. The CB values of enol-(*S*)-**1** crystal under continuous UV irradiation were almost consistent with those obtained using G-HAUP above 400 nm (Figure 4.16c). After stopping UV irradiation, the CD peak and the anomalous dispersion of CB disappeared, to return to the initial spectra before UV irradiation.

In the G-HAUP measurement, I had to take into account the decrease in thickness of specimen by prolonged UV irradiation for three days to obtain accurate LB, LD, CB, and CD spectra. The specimen thickness at each wavelength was corrected by dividing the total change in thickness by the number of G-HAUP measurements. In this study, the LB, LD, CB and CD values were successfully measured using the CCD-HAUP on the assumption that the thickness of the enol-(*S*)-**1** crystal did not decrease upon UV irradiation within 1.5 h. The LB, LD, CB and CD obtained by this assumption were almost coincident before and after UV irradiation. By developing the CCD-HAUP, I could overcome the problem that the thickness of the specimen decreases by UV irradiation during the HAUP measurements.

4.4 Conclusions

I have developed a CCD-HAUP, which can carry out fast optical anisotropic and chiroptical measurements of single crystals without any pretreatment, in the visible region and with high accuracy. It has a unique feature that white transmitted lights can be measured simultaneously by using a CCD spectrometer instead of a monochromator and photomultiplier. The CCD-HAUP drastically reduced the measurement time for a data set to only 1.5 h from 24 h required in the G-HAUP. The LB, LD, CB, and CD spectra of single crystals of α-quartz, and chiral photomechanical enol-(*S*)-**1** and enol-(*R*)-**1** before, during, and after UV irradiation were comparable to those measured using the G-HAUP. The developed system is very effective for samples that are susceptible to degradation induced by external stimuli, such as light and heat.

4.5 References

(1) Takanabe, A.; Tanaka, M.; Johmoto, K.; Uekusa, H.; Mori, T.; Koshima, H.; Asahi, T. *J. Am. Chem. Soc.* **2016**, *138*, 15066–15077.

(2) Takanabe, A.; Koshima, H.; Asahi, T. *AIP Adv.* **2017**, in press, DOI: 10.1063/1.4977440.

(3) Tanaka, M.; Nakamura, N.; Koshima, H.; Asahi, T. *J. Phys. D: Appl. Phys.* **2012**, *45*, 175303 (8pp).

(4) Marilyn, J. D. *Appl. Opt.* **1984**, *23*, 1980–1985.

(5) Takanabe, A.; Tanaka, M.; Taniguchi, A.; Yamanaka**,** H.; Asahi, T. *J. Phys. D: Appl. Phys.* **2014**, *47*, 285402 (8pp).

(6) Koshima, H.; Nagano, M.; Asahi, T. *J. Am. Chem. Soc.* **2005**, *127*, 2455–2463.

(7) Nakagawa, K.; Harper-Lovelady, H.; Tanaka, Y.; Tanaka, M.; Yamato, M.; Asahi, T. *Chem. Commun.* **2014**, *50*, 15086–15089.

(8) Asahi, T.; Nakamura, M.; Kobayashi, J.; Toda, F.; Miyamoto, H. *J. Am. Chem. Soc.* **1997**, *119*, 3665–3669.

(9) Kobayashi, J.; Asahi, T.; Takahashi, S.; Glazer, A. M. *J. Appl. Crystallogr.* **1988**, *21*, 479–484.

(10) Hernández-Rodríguez, C.; Gómez-Garrido, P. *J. Phys. D: Appl. Phys.* **2000**, *33*, 2985–2994.

Chapter 5

Summary

The present thesis described the optical activity and optical anisotropy in chiral photomechanical salicylidenephenylethylamine crystals, and changes in these properties accompanied by reaction in the chiral crystals, and the correlation between these properties and the crystal structure.

Chapter 2 described the relationship between photomechanical bending and the calculated crystal structure of enol- and *trans*-keto-(*S*)-**1**. The plate-like crystals of photochromic enol-(*S*)-**1** and enol-(*R*)-**1** caused bending motions with twisting upon UV irradiation, due to shrinkage along the length and width.

Chapter 3 described the optical anisotropic and chiroptical spectra of the chiral photomechanical enol-(*S*)-**1** and enol-(*R*)-**1** crystals on the (001) face before and under continuous UV light irradiation that were simultaneously measured using the G-HAUP. The HAUP measurements were achieved by the careful preparation of thin (< 10 μm) plate-like crystals by gentle sublimation, and by the prevention of crystal bending under UV irradiation by fixing the crystal to the sample plate with silicone grease. The CD spectra of the S and R crystals revealed a negative and positive Cotton effect, respectively at 330 nm, and new peaks appeared at 460 nm under UV light irradiation due to photoisomerization to the R and S *trans*-keto isomers. The magnitudes of CB and CD were around 10^{-4}, i.e., smaller by two orders than those of LB and LD (around 10^{-2}). The Kramers–Kronig relationship held between the LB and the LD, as well as the CB and the CD, before and under continuous UV irradiation. The CB and CD spectra obtained by the HAUP measurements were the opposite

of those measured in the hexane solution, and those simulated by quantum chemical calculation. The dissymmetry parameter (g) value of the crystal along the c axis was around 10 times larger than those in the solution and by calculation. This demonstrated that the dissymmetry parameter could be enhanced by intramolecular and intermolecular interactions in the crystals.

Chapter 4 discussed the development of the CCD-HAUP, and its performance and application. The CCD-HAUP system had the unique feature that white transmitted light across all wavelengths could be measured simultaneously using a CCD spectrometer instead of a monochromator and a photomultiplier. The CCD-HAUP drastically reduced the measurement time for a dataset to only 1.5 h, from the 24 h required for the G-HAUP system. The LB, LD, CB, and CD spectra of single crystals of α-quartz, and enantiomeric enol-(*S*)-**1** and enol-(*R*)-**1** before, during, and after UV irradiation were comparable to those obtained using the G-HAUP. The developed system was very effective for samples that are susceptible to degradation induced by external stimuli, such as light and heat.

Photomechanical motion involves the direct conversion of light energy to mechanical energy; thus, photomechanical crystals are beneficial for energy conversion. Such mechanical crystals can be operated by light irradiation without wire connections. In this thesis, I showed that the chiroptical and optical anisotropic property changes of photomechanical crystals upon UV irradiation could be accurately and simultaneously measured using G-HAUP and CCD-HAUP. It can be concluded that the investigation of the optical activity and optical anisotropy of chiral photomechanical crystals using G-HAUP and CCD-HAUP is indispensable for evaluating chiral photomechanical crystals, to subsequently lead to the diversification of mechanical motion. Further investigation of the optical properties of chiral photomechanical crystals is needed to facilitate the diversification of mechanical motion. For

example, further research on chiral photomechanical crystals that consist of achiral photochromic molecules is required to reveal the relationship between chiral structure and macroscopic deformation.

Directions for future research include improvement of the CCD-HAUP system to extend the measurable wavelength to UV region. Firstly, a high-quality CCD spectrometer that enables the measurement of light intensity in the wavelength range of 200–800 nm needs to be employed. Additionally, the slit width of the CCD spectrometer needs to be broadened. Although a broad slit width causes low resolution, the slit width of the CCD spectrometer should be broadened because the top priority is to detect more light intensity in the UV region. Secondly, the light source must be changed; the current CCD-HAUP employed a 150-W Xenon lamp but the light intensity in the UV region of the CCD spectrometer was poor, even with a low Blaze wavelength (at around 300 nm). Thus, a high-brightness light source should be identified that is suitable for use in the CCD spectrometer. Thirdly, the polarizer and the analyzer should be changed. In the current CCD-HAUP, common Glan-Thompson prisms were employed as the polarizer and the analyzer, however the light transmittance ratio of this prism in the UV region was relatively lower than that in the visible region. To detect the light intensity in the UV region, high-quality Glan-Thompson prisms, which are transparent even in the deep UV region, should be employed.

Future directions for investigation should also involve further shortening the measurement time of the CCD-HAUP to within minutes or seconds. If the measurement of the CCD-HAUP will be completed in minutes or seconds, optical property changes with tracking chemical reactions can be measured. This improvement will provide greater information for evaluating chiral photomechanical crystals, and lead to the diversification of mechanical motion.

Acknowledgements

First of all, I would like to express my sincere gratitude to my supervisor Prof. Toru Asahi. I have been supervised from him since I joined his group in 2011. Although he was always busy with his works, he cut down on his sleep for me to discuss my Ph.D. study. He always gave me a good advice how to conduct my research and write this thesis. I am really glad that I could join his laboratory.

Besides my supervisor, I would like to express my sincere gratitude to the rest of my thesis committee: Prof. Yukio Furukawa, Prof. Hideko Koshima, Associate Prof. Atsushi Shimojima, and Dr. Hiromi Takahashi. I would like to thank them for careful readings and pertinent comments on this thesis. Prof. Yukio Furukawa provided me an opportunity to join the Raman seminar of his team. I could learn the history, principle, and typical experiments of Raman spectroscopy. Prof. Hideko Koshima gave me a lot of her precious time to discuss how to conduct my research and how to write our academic paper and this thesis. I really respect her as one of the best scientific researchers.

I would like to also thank Prof. Takuro Katsufuji and Mr. Hiroaki Ikeda, who provided me an opportunity to attempt to measure dielectric constants.

I am grateful to Dr. Masahito Tanaka in National Institute of Advanced Industrial Science and Technology for enlightening me the first glance of research and borrowing a CCD spectrometer.

I would like to also thank Dr. Hidehiro Uekusa and Dr. Kohei Johmoto in Tokyo Institute of Technology for providing me the data of complicated crystallographic analyses.

I would like to also thank Dr. Tadashi Mori in Osaka University for providing me the data of complicated single molecule DFT calculations.

I would like to also thank Mr. Motoo Shiro for providing me the data of complicated crystallographic analysis.

I would like to also thank Prof. Hisashi Yamanaka and Prof. Atsuo Taniguchi in Tokyo Women's Medical University for providing me an opportunity of a collaborated research.

I would like to also thank to Prof. Miguel A. Garcia-Garibay and Dr. Anoklase Jean-Luc Ayitou. They helped me in all the time of research at UCLA. I will definitely never forget the experiences at UCLA.

I would like to also thank to Dr. Andreas Fischer, Dr. Michael Schmidt, Dr. Stefano Meini, and Dr. Johannes Hoecker. They helped me in all the time of research at BASF SE. I will definitely never forget the experiences at BASF SE.

I am also grateful to Mr. Takahiro Gotoh and Mr. Natsuhiko Sugimura, who helped me in all the time of experiments at Materials Characterization Central Laboratory, Waseda University. Without their precious support, it would not be possible to characterize samples at Materials Characterization Central Laboratory, Waseda University.

I am also grateful to labmates and staffs in Asahi laboratory. I could conduct my Ph.D. study smoothly because I could share the important information with them. I also thank my friends in Waseda University.

Last but not the least, I am really grateful to my father, my mother, my brother and my sister. I could spend a lot of my time to conduct my Ph.D. study with their continuous support. Whenever I was depressed and my thinking was very negative, they always cheered me up. Also I thank my sister's husband, nephew, and niece for their friendly communications. Thank to communications with my sister's nephew and niece, my hardened heart was healed every time.

Research Achievements

Publications

(Academic Papers)

○ 1. Akifumi Takanabe, Hideko Koshima, and Toru Asahi, "Fast-type High-Accuracy Universal Polarimeter Using Charge-coupled Device Spectrometer", *AIP Advances* **2017**, in press, DOI: 10.1063/1.4977440

○ 2. Akifumi Takanabe, Takuro Katsufuji, Motoo Shiro, Hideko Koshima, and Toru Asahi, "Reversible Single-Crystal-to-Single-Crystal Phase Transition of Chiral Salicylidenephenylethylamine", *Crystals* **2017**, *7*, 7

○ 3. Akifumi Takanabe, Masahito Tanaka, Kohei Johmoto, Hidehiro Uekusa, Tadashi Mori, Hideko Koshima, and Toru Asahi, "Optical Activity and Optical Anisotropy in Photomechanical Crystals of Chiral Salicylidenephenylethylamines", *Journal of the American Chemical Society* **2016**, *138*, 15066–15077

4. Akifumi Takanabe, Masahito Tanaka, Atsuo Taniguchi, Hisashi Yamanaka, and Toru Asahi, "Quantitative analysis with advanced compensated polarized light microscopy on wavelength dependence of linear birefringence of single crystals causing arthritis", *Journal of Physics D: Applied Physics* **2014**, *47*, 285402

Presentations

(International, Poster)

1. Akifumi Takanabe, Masahito Tanaka, Kohei Johmoto, Hidehiro Uekusa, Hideko Koshima and Toru Asahi, "LIGHT-DRIVEN TWISTING MOTION OF SALICYLIDENEPHENYLETHYLAMINE SINGLE CRYSTALS", The XXVIth IUPAC Symposium on Photochemistry, Osaka City Central Public Hall, April 2016

2. Akifumi Takanabe, Masahito Tanaka, Kohei Johmoto, Hidehiro Uekusa, Tadashi Mori, Toru Asahi and Hideko Koshima, "High-accuracy Universal Polarimeter Study of Salicylidenephenylethylamine Crystal with Photomechanical Function", The 22nd International Conference on the Chemistry of the Organic Solid State, Niigata, July 2015

3. Akifumi Takanabe, Masahito Tanaka, Motoo Shiro, Hideko Koshima and Toru Asahi, "Chiroptical properties of photomechanical and anisotropic crystals of salicylidenephenylethylamine", 13th Symposium on Chemical Approaches to Chirality, Tokyo University of Science, November 2014

4. Akifumi Takanabe, Masahito Tanaka, Shiro Motoo, Hideko Koshima, and Toru Asahi, "OPTICAL PROPERTIES OF CHIRAL SALYCILIDENEPHENILETHYLAMINE CRYSTALS WITH PHOTOMECHANICAL FUNCTION", The XXVth IUPAC Symposium on Photochemistry, Palais des Congrès in Bordeaux, July 2014

5. Akifumi Takanabe, Masahito Tanaka, Masafumi Matsudomi, Hideko Koshima and Toru Asahi, “Optical properties of salicylideneaniline microcrystals with photomechanical functions”, International Workshop on Green Energy Conversion, Nagano, September 2013

(Domestic, Oral)

1. 高鍋彰文, 小島秀子, 朝日透, “キラル分光装置(HAUP)の迅速化”, 第 25 回有機結晶シンポジウム, 京都大学, 2016 年 9 月

2. 高鍋彰文, 田中真人, 上本紘平, 植草秀裕, 城始勇, 小島秀子, 朝日透, “光屈曲性サリチリデンフェニルエチルアミン結晶のキラル光学的性質”, 日本化学会第 95 春季年会, 日本大学, 2015 年 3 月

3. 高鍋彰文, 田中真人, 上本紘平, 植草秀裕, 城始勇, 小島秀子, 朝日透, “光屈曲性サリチリデンフェニルエチルアミン結晶のキラル光学的性質”, 新学術領域「高次複合光応答」第 2 回公開シンポジウム, 大阪, 2015 年 1 月

4. 高鍋彰文, 田中真人, 城始勇, 小島秀子, 朝日透, “キラルなサリチリデンフェニルエチルアミン結晶の光屈曲とキラル光学的性質”, 2014 年光化学討論会, 北海道大学, 2014 年 10 月

5. 高鍋彰文, 田中真人, 朝日透, “炎症誘発結晶の直線複屈折の定量測定：尿酸一ナトリウム一水和物”, 第 60 回応用物理学会春季学術講演会, 神奈川工科大学, 2013 年 3 月

(Domestic, Poster)

1. 高鍋彰文, 田中真人, 上本鉱平, 植草秀裕, 森直, 朝日透, 小島秀子, “フォトメカニカル機能をもつキラルなサリチリデンフェニルエチルアミン結晶の光学的性質”, 第 63 回応用物理学会春季学術講演会, 東京工業大学大学, 2016 年 3 月

2. Akifumi Takanabe, Motoo Shiro, Hiroaki Ikeda, Takuro Katsufuji, Hideko Koshima, and Toru Asahi, "Thermodynamic phase transition through crystal-to-crystal process of photochromic chiral salicylidenephenylethylamines", 2015 年光化学討論会, 大阪府立大学, 2015 年 9 月

3. 高鍋彰文, 田中真人, 松冨正文, 小島秀子, 朝日透, “フォトメカニカル機能をもつキラルなサリチリデンアニリン結晶の光学的性質”, 第 61 回応用物理学会春季学術講演会, 青山大学, 2014 年 3 月

4. 高鍋彰文, 田中真人, 松冨正文, 小島秀子, 朝日透, “サリチリデンアニリン微結晶の光学的性質とメカニカル機能の関係”, 2013 年光化学討論会, 愛媛大学, 2013 年 9 月

5. 高鍋彰文, 石川和彦, 鈴木俊哉, 田中真人, 朝日透, “結晶誘発性炎症の物理化学的性質：尿酸一ナトリウム一水和物”, 第 59 回応用物理学会春季学術講演会, 早稲田大学, 2012 年 3 月

Others

(Patents)

1. Yoshinori Iketaki, Hideko Koshima, Toru Asahi, Akifumi Takanabe, and Takuya Taniguchi, “OPTICAL DRIVING DEVICE”, WO2016/135775 (2016)

(Awards)

1. Best Poster Award, Akifumi Takanabe, Masahito Tanaka, Motoo Shiro, Hideko Koshima and Toru Asahi, “Chiroptical properties of photomechanical and anisotropic crystals of salicylidenephenylethylamine”, 13th Symposium on Chemical Approaches to Chirality, Tokyo University of Science, November 2014

2. Poster Award, Akifumi Takanabe, Masahito Tanaka, Masafumi Matsudomi, Hideko Koshima and Toru Asahi, “Optical properties of salicylideneaniline microcrystals with photomechanical functions”, International Workshop on Green Energy Conversion, Nagano, September 2013